SISSA - SCUOLA
INTERNAZIONALE
SUPERIORE
DI STUDI AVANZATI
TRIESTE
Strada Costiera 11

ISAS - INTERNATIONAL SCHOOL FOR ADVANCED STUDIES

THESIS FOR THE ATTAINMENT OF THE TITLE OF

"DOCTOR PHILOSOPHIAE"

TOPICS IN THE THEORY OF TWO-DIMENSIONAL ELECTRON SYSTEMS

Candidate :

Dr. Chen Chun-Da

Supervisor :

Prof. Erio Tosatti

Sector : Solid State Physics

Academic Year 1983/84

TRIESTE

CONTENTS

Acknowledgement i

Foreword, and general introduction ii

I. Electronic States in Graphite and LiC_6 and Scanning Tunneling Microscopy on Graphite 1.1

I.A Pseudopotential for Carbon 1.2

I.B Band Structure of Graphite 1.2

I.C Band Structure of LiC_6 . . . . . 1.3

I.D Electronic Surface States on Graphite and Voltage-Dependent Scanning Tunneling Microscopy on Graphite . 1.5

I.E Conclusion 1.6

References 1.7

Table 1 . . . . . 1.8

Figure Captions 1.9

II. Surface State Polarons: An Exemplification for Si(111) 2X1

1. Introduction 1

2. Surface State Polarons in the Buckling Model of Si(111) 2x1 3

2.1 The Buckling Model and its Parameters . . . 4

2.2 Electron Polaron and Hole Polaron 9

2.2.1 Electron Polaron 11

2.2.2 Hole Polaron 13

2.3 Exciton States in the Buckling Model . . . 16

2.4 Excitonic Polaron 19

2.5 Absorption Lineshape 21

3. Surface State Polarons in the π-bonded Chain Model . 24

3.1 The Model and the Parameters 24

3.2 Electron Polaron and Hole Polaron 29

a) Limit of Strongly Localized Polaron . . . 30

b) Polaron Radius 31

c) Polaron Bands 35

3.3 Excitons 39
3.4 Excitonic Polaron 42
3.5 Absorption Lineshape of the π-bonded Dimerized Chain Model 44
4. Experimental Consequences of the Existence of Surface State Polarons 46
4.1 Temperature-dependent Optical Absorption; Strongly Coupling Versus Weak Coupling 46
4.2 Luminescence 50
4.3 Photo-emission 51
4.4 Surface State Polaron Effects in Scanning Tunneling Microscopy 52
4.5 Wigner-Crystallization of Carriers in Surface States 54
5. Concluding Remarks 56
Appendix A 57
Appendix B 59
Table 2.1 62
Table 3.1 63
Table 4.1 64
References 65
Figure Captions 70
III. Fractional Quantized Hall Effect 3.1
A. Survey 3.1
A.1 Introduction 3.1
A.2 The Hamiltonian 3.3
A.3 Choice of Gauge, and One-electron Wavefunction .3.5
A.4 Some Simple Known Facts About H_b 3.7
A.5 Hartree-Fock "Charge Density Wave" (CDW) . .3.10
A.6 Magnetic Wigner Commensurate Super-lattice . .3.11
A.7 Super-lattices in k-space 3.12
A.8 Correlated Jastrow Functions 3.13

A.9 Numerical Approaches 3.14

A.10 Fractional Charge Excitations 3.15

A.11 The 2/5 and 2/7 States 3.16

A.12 Conclusion 3.17

B. Energy Calculation for A Model Wigner Lattice . .3.18

C. Configuration Interaction for Few Electron in the Symmetric Gauge 3.23

C.1 Introduction 3.23

C.2 Outline of the Calculation 3.25

C.3 Center of Mass Angular Momentum: A Good Quantum Number? 3.27

C.4 Results, and Discussions 3.28

D. N electrons Confined onto A Disk 3.29

References 3.31

Figure Captions 3.33

FIGURE CAPTIONS

Fig. 3.1 Ground state energy per particle versus the inverse fractional filling of the lowest Landau level, $m = 1/\nu$. Dot points are our results for the "commensurate"Wigner lattice. Also shown are results of Yoshioka, and Lee [10] (square points), Laughlin [20] (crosses) and Bonsall and Maradudin [11] (solid line). The dashed line drawn through crosses is a guide to the eye only.

Fig. 3.2

a) The ground state energy (solid line) as well as the first excited state energy (dash line), both for per particle, versus total angular momentum for 7, 8, and 9 electron systems with uniform positive background.

b) The ground state energy versus total angular momentum for 7, 8, and 9 electron systems without background. The integers above each point are the corresponding center of mass angular momentum.

c) Energy gap (the first excited energy minus the ground state energy) versus total angular momentum for 8 and 9 electron systems without background.

Fig. 3.3 The average number of electron having specific angular momentum m, $\langle c_m^+ c_m \rangle$, for 8-electron system (a) and 9-electron system (b), with (dash line) and without (solid line) background, at total angular momentum L= 36, 42 and 49, respectively.

Fig. 3.4

a) The ground state energy (solid line) and the first excited state energy (dash line), both for per particle, versus the inverse fractional filling, $1/\nu$, for 3, 4 and 5 electron systems confined onto a disk. Below also shown are the corresponding total angular momentum of the system.

b) The ground state (solid) and the first excited state (dash line) energies, both for per particle, versus electron number (N) for systems confined onto a disk having N_o= 5, 6,..., 16 single-particle states, respectively. And thus the filling factor equals N/N_o.

ACKNOWLEDGEMENTS

I would like to express my gratitude to my supervisor Professor E. Tosatti for his earnest, tireless and patient instructions and for his constant encouragement throughout this research, as well as for his help in the preparation of this manuscript.

I am grateful to Professor A. Baldereschi for his suggestion on the work on graphite and LiC_6 and for his patient, enlightening guidance in that work, as well as his constant encouragement. I am indebted to Professor M. Parrinello for his helpful discussions and advises on Quantum Hall Effect problem. I also wish to express my appreciation for helpful discussions with Dr. A. Selloni and the collaborations with her on surface state polaron and on STM. I thank Dr. A. Nobile for his instructions on computer programming.

All my gratitude also to Professor P. Budinich and Professor L. Fonda for the fellowship grant and for their hospitality at SISSA.

FOREWORD, AND GENERAL INTRODUCTION

The physics of electrons confined to move in restricted geometries, either by anisotropic crystal lattices, or by artifacts such as surfaces, interfaces, inversion layers, etc., has become increasingly important in modern solid state, particularly, if not only, in the field of semiconductors. Often new situations are generated with the conspiracy of low dimensionality, which require a new and separate treatment from their three-dimensional analog.

In the work leading to this thesis I have considered problems in three separate areas, which besides their own specific interest, illustrate three main important questions, namely

(i) One-lectron bands in the very anisotropic layered crystal structures of graphite, and graphite intercalates.

(ii) Electron-phonon coupling for electrons of surface states, whose motion is restricted by the surface to be two-dimensional.

(iii) Electron-electron interaction problems in a two-dimensional system in a magnetic field: the Fractional Quantum Hall Effect.

These three main subjects form the three separate blocks of this thesis work. Each block is self-contained, in that all the introductive as well as conclusive discussion, is given together with the work. In each case, it is interesting to note the vast richness of new situations encountered , and of new results that have been derived by a variety of analytical and numerical approaches. The work on the Quantum Hall Effect is continuing, and the results presented here, though definite, are only preliminary in their interpretation.

1. ELECTRONIC STATES IN GRAPHITE, LiC_6 AND SCANNING TUNNELING MICROSCOPY ON GRAPHITE.

Graphite and graphite intercalation compound (GIC) have potentially important technological application, and they also provide realistic situation for the fundamental study of two-dimension phenomena. As a consequence, renewed interest in the properties of graphite itself has been stimulated in the past several years even though there has been a very large literature on the electronic properties of graphite both experimental and theoretical. New discoveries have come out as the results of recent studies. Holzwarth, Louie and Rabii (HLR) [1] and Posternak, Baldereschi, Freeman, Wimmer and Weinert (PBFWW) [2] have, by very elaborate calculation, recovered and discussed the interlayer state in graphite which was shown (but not interpreted) in the band structure obtained by pseudopotential [3] and cellular [4] methods. There have been new interpretations and discussions about the character of the corresponding interlayer state in LiC_6 [2,5] and also confirmation for that state both in graphite and LiC_6 experimentally by Fauster et al [6]. More recently, Posternak, Baldereschi, Freeman and Wimmer (PBFW) [7] predicted the existence of the electronic surface state in graphite which provides an interpretation of the inverse photoemission result of Fauster et al [6].

The local centrally symmetrical pseudopotential used by Van Haeringen and Junginger [3] was empirically adjusted so as to obtained a reasonable band structure for diamond and silicon carbide. While the simplicity of the pseudopotential method is very attractive, there is, to my knowledge, no local pseudopotential for carbon suitable to deal with graphite has been published. In view of the interest in practical calculations for GIC, it is worth while to have a local pseudopotential for carbon empirically adjusted to obtain a reasonably satisfactory band structure for graphite which has a strongly anisotropic layer structure.

In this part of my thesis, I will present such carbon pseudopotential in sect. 1.A. With this potential, the band structure of gra-

phite and LiC_6, which are presented in sect. 1.B. and 1.C. respectively, have been calculated and some discussion about the character of the interlayer state in LiC_6 is made also in sec. 1.C. Finally the electronic surface state on graphite and Scanning Tunneling Microscopy on graphite are briefly mentioned in sect. 1.D., leaving the details to our paper collaborated with Selloni, Carnevali and Tosatti [8] which is attached in the end of this chapter.

1.A. PSEUDOPOTENTIAL FOR CARBON

To take the advantage of the simplicity of calculation, we are concerned here only with centrally symmetrical local pseudopotential. Almost all screened pseudopotential of "simple" elements, i.e., excluding the transition, rare-earth and the transuranic series, have similar forms. This form can be described as raising parabolically, at least in the neighborhood of q =0, if Sham's screening function is adopted, from a value around $-2/3\ E_{Fo}$, where E_{Fo} denotes the free-electron Fermi bandwith , crossing the q-axis at q_o and arriving its maximum value at q_{max} and finally decaying into zero [9]. q_o roughly equals $(\pi/4)\cdot 2k_F$ almost without exceptional. All these features are preserved in our pseudopotential.

For A-B stacking graphite with lattice parameters a=2.46 A and c=6.71 A, k_F=1.259 a.u., E_F=1.585 Ry and the atomic volume Ω =8.79 A^3 . We adjust the pseudopotential in the functional form to obtain the band structure matching the result of HLR calculation [1]. Special care has been taken for the fitting of energy levels around E_F. The pseudopotential thus obtained is shown in Fig. 1.1 in absolute scale.

1.B. BAND STRUCTURE OF GRAPHITE.

The band structure of graphite has been calculated on plane-wave basis with cut-off kinetic energy of 22.3 Ry (equivalent to 417 plane-waves at Γ point) using our pseudopotential for carbon and with satisfactory

convergency. The result is shown in Fig. 1.2 . Various features of our result are compared with HLR calculation [1] as well as some experimental data [1,10,11] in Table 1. Though the agreement in the lower part of the band structure is poor, the fitting around E_F as well as the general feature of the band structure is fairly good in view of the simple form of our pseudopotential.

The interlayer state which lies above E_F 2.7 ev at Γ point has Γ_1^+ symmetry and its charge distribution at Γ point is concentrated in the region between carbon planes, as shown in Fig. 1.3, wich is in a good agreement with FLAPW result [2].

1.C. BAND STRUCTURE OF LiC_6.

The band structure of LiC_6 has also been calculated using our pseudopotential for carbon and the pseudopotential for Li taken from Cohen and Heine [9]. The lattice parameters are a=2.485 A, c=3.706 A. The cut-off kinetic energy is the same as in the case of graphite, 22.3 Ry (equivalent to 691 plane waves at Γ point), and the convergency is satisfactory.

The result is shown in Fig. 1.4. The whole band is shifted down by an amount of roughly 1 ev(take the top occupied σ-band as representative), with an extra shift of about 1.4 ev for the interlayer state as compared to graphite, relative to the respective Fermi level. HLR [5] and Fauster et al [6] interpreted this extra shift for the interlayer state as an indication of the hybridization between Li(2s) and carbon interlayer state. To investigate this point as well as the character of this state in LiC_6, we have calculated the energy levels at Γ point for A-A stacking graphite with the same carbon layer separation (6.71 A/2) as graphite but the same basal plane parameter (a=2.485 A) as LiC_6, and also for $Li_\alpha C_6$ for α ranging from 0 to 1 (α=0 corresponds to A-A stacking graphite with lattice parameters of LiC_6). The results are shown in the left panel of

Fig. 1.4.

The 10% increase in c-parameter from graphite to LiC_6 and the change in stacking structure should have weak effect on the energy level of σ band whose charge is localized on the carbon plane. The change in the a-parameter is only 1%. We therefore expect that the top occupied σ band at Γ point should vary very little with the above geometry changes and we take this level as a reference. From Fig. 1.4 we notice that:

1) The interlayer level is insensitive to the type of stacking(A-A or A-B) and lies about 7.2 ev above the top band. π band is affected much stronger so thus the Fermi level. Relative to the Fermi level, going from A-B stacking to A-A stacking, apparently the interlayer is shifted down by an amount of $\sim$ 1.2 ev(from 2.7 ev to 1.5 ev above respective Fermi level).

2) The 10% increase in carbon layer spacing affects both the π band and the interlayer state. The interlayer state is shifted down 0.9 ev relative to the top σ band. Since the top occupied π band(the Fermi level) is also shifted down 0.5 ev, the interlayer state is apparently shifted down only by an amount of 0.4 ev, relative to the respective Fermi level.

3) The increase of the component of Li atom affects all the levels. Relative to the case of $Li_{0.6}C_6$, the Fermi level of LiC_6 increases about 0.6 ev. The top σ band increases 0.4 ev, just a little less than the increase of the Fermi level. The top occupied π band increases about 0.25 ev and the interlayer state decreases about 0.25 ev.

From the above investigation we can make some comments:

i) If we ignore the change (0.4 ev) in the top σ band due to the presence of Li atom, going from graphite to LiC_6 the shift of the whole band by about 1 ev with respect to the Fermi level is due to the increase in the Fermi level resulted from the filling of the antibonding π band with Li(2s) electrons.

ii) The extra downward shift of the interlayer level is due mainly to the 10% increase in layer spacing. This is consistent with the character of this state as being a free-electron-like state confined between carbon planes. The intercalation of Li atom does have some contribution to this extra shift, but it can only be a minor cause.

In addition to that, we have also calculated the projection of the wavefunction of this interlayer state at Γ point in $Li_o C_6$, $\psi^{(\Gamma)}_{inter}(r, \alpha=0)$, onto the corresponding wavefunction in LiC_6, $\psi^{(\Gamma)}_{inter}(r, \alpha=1)$, and obtained

$$\left\langle \psi^{(\Gamma)}_{inter}(r, \alpha=1) \middle| \psi^{(\Gamma)}_{inter}(r, \alpha=0) \right\rangle = 0.997 .$$

Because of the spatially extended nature of both the Li(2s) state and the interlayer state and especially because of their large overlap with each other, we expect the Li(2s) state has a considerable amount of contribution to the interlayer state too. But we interpret the extra downward shift for the interlayer state as mainly a consequence of the 10% increase in the carbon layer spacing.

In Fig. 1.5, the charge distribution of the interlayer state at Γ point both for LiC_6 and $Li_o C_6$ are shown.

1.D. ELECTRONIC SURFACE STATES IN GRAPHITE AND VOLTAGE-DEPENDENT SCANNING TUNNELING MICROSCOPY(STM).

PBFW [7] recently predicted the existence of electronic surface states in graphite and interpreted the structure with negligible c-dispersion which lies about 0.1 ev below the bulk interlayer state at Γ point as due to the presence of this surface states.

In the paper [8] collaborated with Selloni, Carnevali and Tosatti, we have done the slab calculation of graphite using our pseudopotential for carbon and recovered the surface state of graphite which lies about

0.1 ev below the interlayer state at Γ point, in good agreement with the experiment[6]. In that paper, we dicussed the application of the STM to surface electronic spectroscopy with an explicit calculation of the voltage-dependent tunneling current for an ideal STM experiment performed on graphite and showed that how surface and bulk electronic states are reflected in the tunneling J-V spectra and that the empty surface states of graphite can be well discriminated against bulk-like structure by considering STM spectra at different tip-surface separation. For details, the paper, which is attached at the end of this chapter for convenience of reference, is referred to.

1.E. CONCLUSION

In this chapter we have fitted a local pseudopotential for carbon which gives band structures for graphite and LiC_6 in a fairly good consistent with elaborately calculated results. We interpret the extra downward shift of the interlayer state in LiC_6 compared with graphite as mainly the result of the 10% increase in carbon layer spacing. We also briefly mentioned the electronic surface state of graphite and the application of STM on graphite which are the subject of our another paper attached in the end of this chapter as reference.

REFERENCES

1. N.A.W. Holzwarth, S.G. Louie, and S. Rabii, Phys. Rev. B26, 5382 (1982).
2. M. Posternak, A. Baldereschi, A.J. Freeman, E. Wimmer, and M. Weinert , Phys. Rev. Lett. 50, 761 (1983).
3. W. Van Haeringen, and H.G. Junginger, Solid State Commun. 7, 1723 (1969).
4. C.P. Mallet, J. Phys. C14, L213 (1981).
5. N.A.W. Holzwarth, S.G. Louie, and S. Rabii, Phys. Rev. B30, 2219 (1984).
6. Th. Fauster, R.J. Himpsel, J.E. Fisher, and E.W. Plummer, Phys. Rev. Lett. 51, 430 (1983).
7. M. Posternak, A. Baldereschi, A.J. Freeman, and E. Wimmer, Phys. Rev. Lett. 52, 863 (1984).
8. A. Selloni, P. Carnevali, E. Tosatti, and C.D. Chen, to be published.
9. See the collection of pseudopotential for "simple" elements by M.L. Cohen, and V. Heine, in Solid State Physics, Vol. 24, ed. by H. Ehrenreich, F. Seitz, and D. Turnbull, Academic Press (1970).
10. W. Eberhardt, I.T. McGovern, E.W. Plummer, and J.E. Fisher, Phys. Rev. Lett. 44, 200 (1980).
11. G. Bellodi, A. Borghesi, E. Guizzetti, L. Nosenzo, E. Reguzzoni, and G. Samoggia, Phys. Rev. B12, 5951 (1975).
12. J.C. Slonczewski, and P.R. Weiss, Phys. Rev. 109, 272 (1958).

TABLE 1. BAND ENERGIES FOR GRAPHITE.

Γ point state	Present results	HLR results[b]	Experiments
bottom σ band	-29.0	-20.8	-20.6[c]
	-28.9	-20.5	
bottom π band	-9.8	-9.1	-8.1[c]
	-7.6	-7.1	-7.2[c]
top σ band	-4.5	-3.4	-4.6[c]
	-4.4	-3.3	
unoccupied	2.7	3.8	4.0±0.5[d]
σ bands	6.0	9.0	9.5[d]
	6.4	9.3	
E_F	0	0	0
bands near E_F[f]			
$E^\circ_2 - E^\circ_3$	0.7	0.7	0.72[e]
$E^\circ_3 - E^\circ_1$	1.0	0.8	0.84[e]
dispersion of interlayer state along Γ-A direction	3.4	2.8	

a. Fermi level chosen as zero of energy; all energies in ev.

b. Only results using Hedin-Lundqvist exchange and correlation potentials are given.

c. Ref. 10.

d. Ref. 6.

e. Ref. 11.

f. Notation of Slonczewski-Weiss. Ref. 12.

FIGURE CAPTIONS

Fig. 1.1 Local pseudopotential for carbon empirically adjusted for graphite.

Fig. 1.2 Band structure of graphite.

Fig. 1.3 Charge-density contour plot for the interlayer (Γ_1^+) state in graphite. Contours are given at multiple of 0.012 el/A^3.

Fig. 1.4 Band structure of LiC_6. The left verticle line denotes the energy levels for Li_oC_6 at c= 6.71 A/2, i.e., the carbon layer spacing of graphite. The left panel shows the energy levels at Γ point for $Li_\alpha C_6$ versus α.

Fig. 1.5 Charge-density contour plots for the interlayer state (Γ_1^+) state in LiC_6 (a) and Li_oC_6 (b). Contours are given at multiples of 0.009 el/A^3.

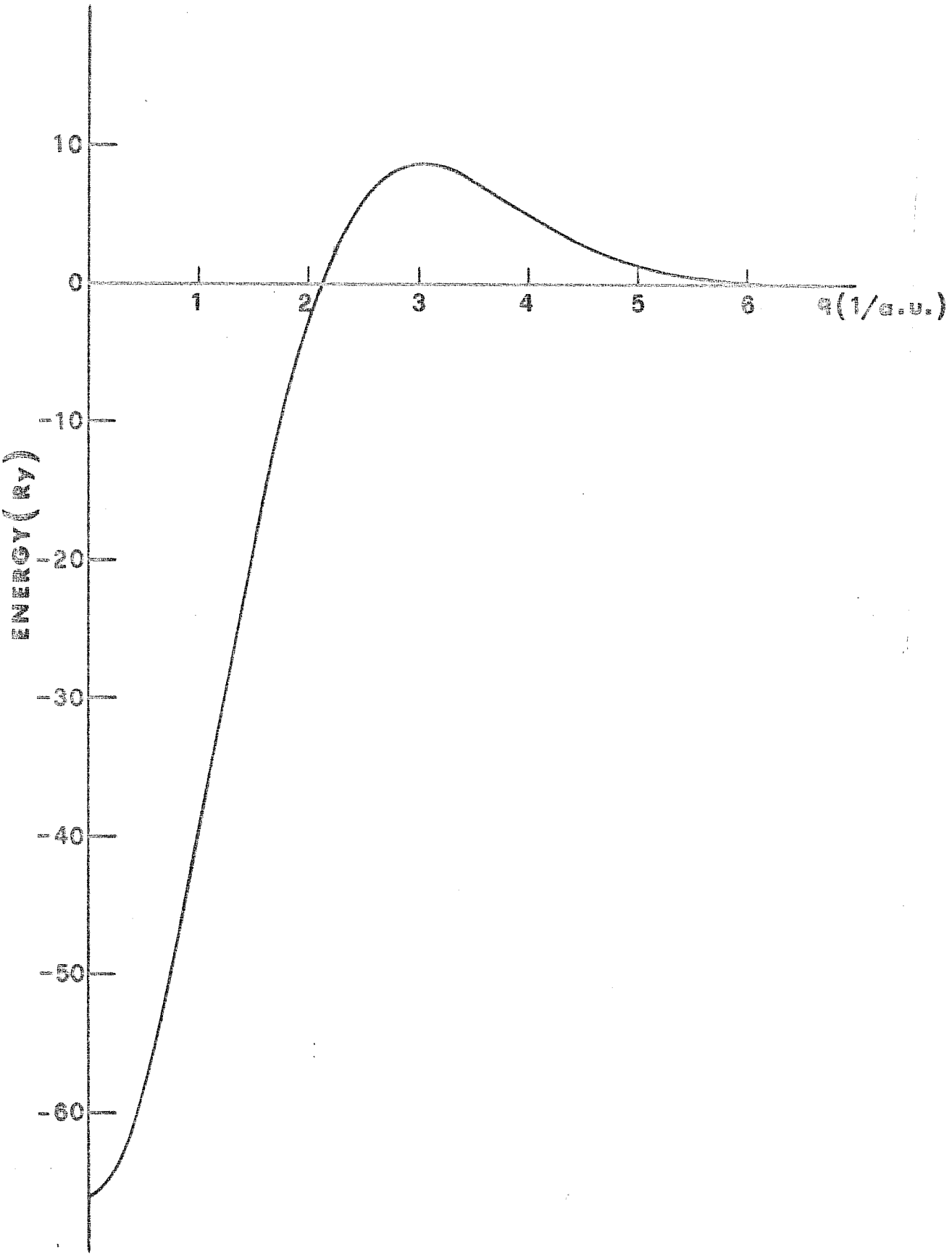

FIG. 1.1
Carbon pseudopotential

Band Structure of
Graphite

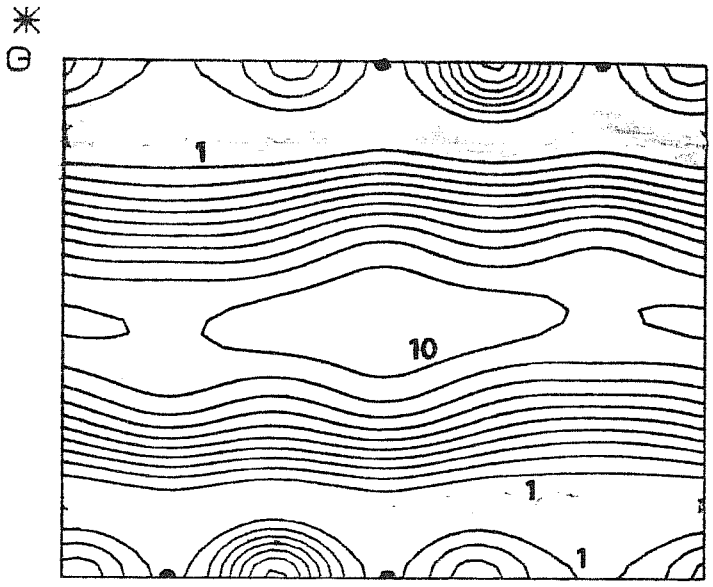

Fig 1.3 graphite

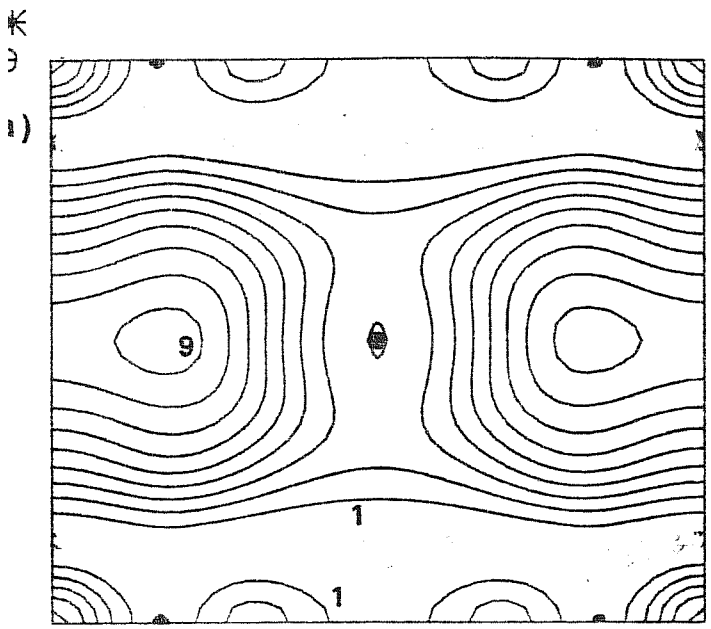

Fig 1.5
LiC6

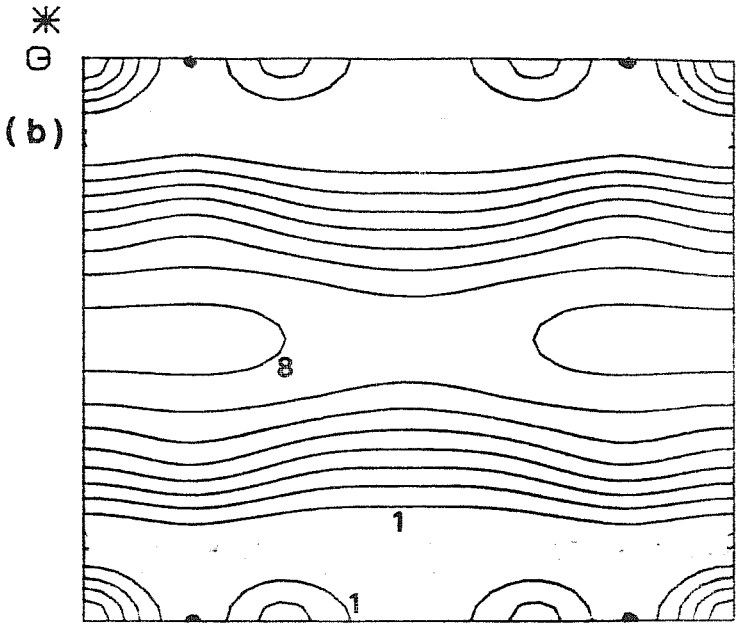

Fig 1.5 (b)
LiC6

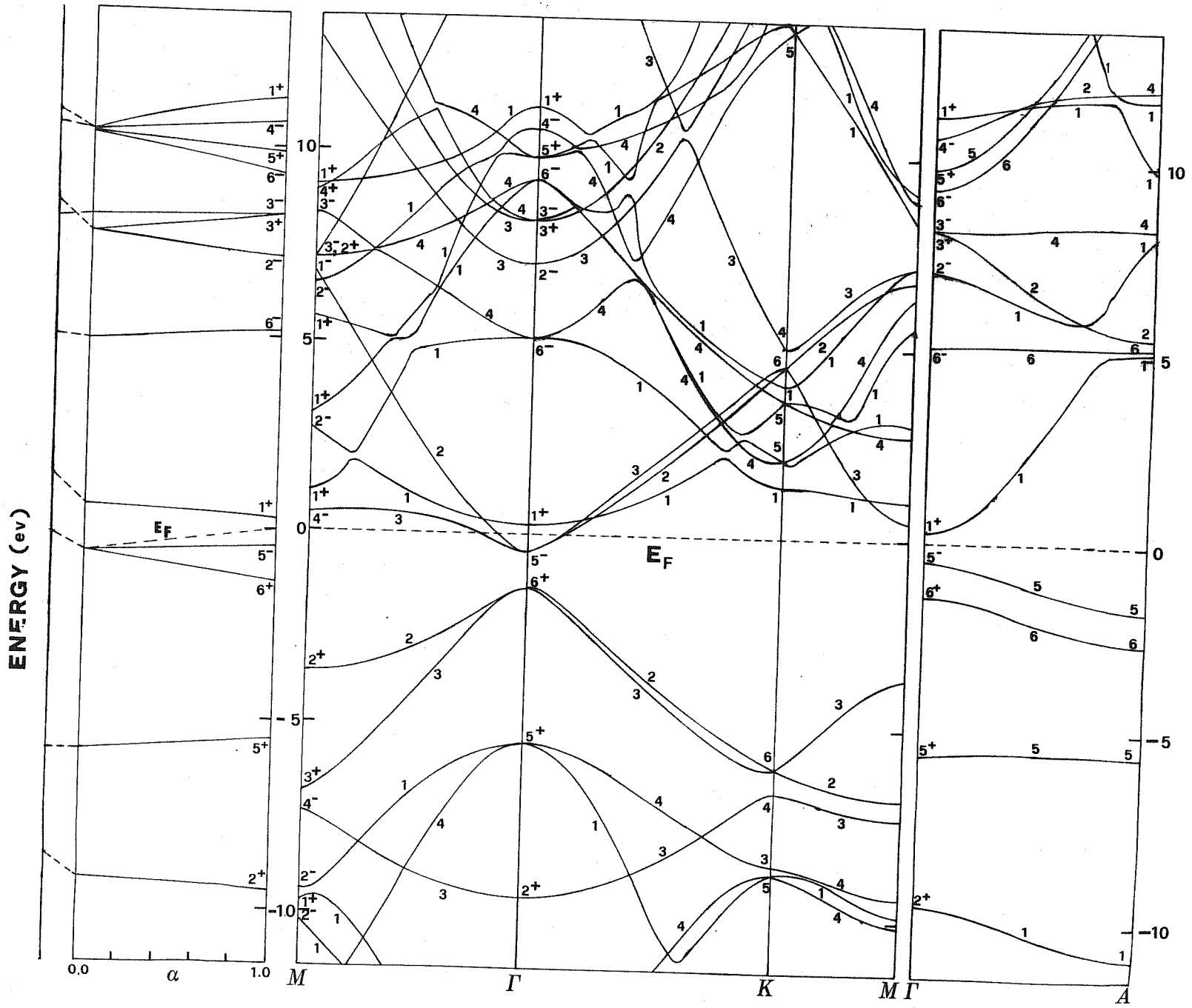
ENERGY (ev)
10
5
0
-5
-10
E_F
0.0
α
1.0
M
Γ
K
M
Γ
A

VOLTAGE-DEPENDENT SCANNING-TUNNELING MICROSCOPY OF A CRYSTAL SURFACE: GRAPHITE

A. Selloni, Dipartimento di Fisica, Universita' La Sapienza, Roma, Italy

P. Carnevali, IBM Rome Scientific Center, Roma, Italy

E. Tosatti and C.D. Chen, International School for Advanced Studies, Trieste, Italy

PACS Index Categories: 73.20.-r, 73.40.Gk

We discuss the application of the scanning tunneling microscope (STM) to surface electronic spectroscopy, with an explicit calculation of the voltage-dependent tunneling current for an ideal STM experiment performed on graphite. We study how surface and bulk electronic states are reflected in the tunneling J-V spectra, and show that empty surface states of graphite can be well discriminated against bulk-like structures by considering STM spectra at different tip-surface separations.

The newly developed technique of Scanning Tunneling Microscopy has been proven to be very useful for the study of surface structures [1]. In usual applications the scanning tunneling microscope (STM) is operated in the so-called constant-tunneling current mode: both the applied voltage V and the tunneling current J are kept fixed while the tip performs a lateral scan over the surface. The resulting surface of constant J, $z = z(x, y)$, is the STM 'real space image' of the surface (z is the vertical position of the tip, while x and y are coordinates in the surface plane). Several theoretical papers have recently appeared, investigating the relationship between the STM images and the surface structure [2–4].

In this note we discuss a different and so far unexploited application of STM, surface electronic spectroscopy. It is intuitively clear that vacuum tunneling into a surface should be stronger when the electron energy is such that it can flow into, or out from, a discrete surface state, or an important surface resonance (even if degenerate with bulk states). We show that the voltage-dependence of the tunneling current can give important information on both filled and empty electronic states. In addition lateral scanning of the tip could be used to obtain a detailed picture of the spatial distribution of each energy-resolved electronic state.

We have chosen to illustrate our idea by direct calculation of the tunneling current J flowing into, or out of, a graphite surface, as a function of an applied voltage V. The point is to show how $J(V)$ is related to the surface electronic structure at energy $E - E_F = V$. Graphite has been chosen as an important test case, because both its atomic and electronic structures are well known. In particular, both localized σ and π states, as well as fairly delocalized interlayer states [5] and recently discovered empty surface states [6,7], coexist within a range of a few eV around the Fermi energy. We suspect it might be technically difficult to achieve such large tunneling voltages over a semimetallic surface. Typical voltages yielding reasonably small currents such as $5 \times 10^{-9} A$ are in the range of $10 mV$ in metal-metal tunneling [1]. However, it is not inconceivable that much higher voltages could be applied, for example, for very short times.

We calculate J using the approach outlined in Ref. 2. Assuming an idealized tip with constant density of states D_t [8], the differential conductivity dJ / dV is proportional to the local density of states of the sample evaluated at the tip position $\mathbf{r} = (x, y, z)$ and at energy $E = E_F + V$,

$$\frac{dJ}{dV} \propto \rho(\mathbf{r};V) = \sum_{nk} |\psi_{nk}(\mathbf{r})|^2 \quad \delta(E_{nk} - E_F - V) \qquad (1)$$

where $\psi_{nk}(\mathbf{r})$ and E_{nk} are the two-dimensional Bloch functions and the corresponding eigenvalues of the semi-infinite crystal.

In the present approach we replace the semi-infinite crystal with a n-layer slab of finite thickness $t = (n-1)c/2$, in a repeated slab geometry, where $c/2 = 3.35$Å is the interlayer spacing in bulk graphite. The width of the vacuum region between adjacent slabs is $2c = 13.42$Å. Four layers are sufficient for the purpose of describing most of the relevant features of $\rho(x, y, z\ ;V)$, but slabs up to 10 layers thick are used, when needed, to investigate finer details.

The graphite slab electronic structure is calculated using a plane wave representation, along with a carbon local pseudopotential [9], empirically adjusted to give a reasonably accurate overall fit of 'ab initio' LAPW results for bulk graphite [5]. Each slab is further encased within a square potential well along z. The well depth, $V_0 = 6.4eV$, is chosen to yield a reasonable value, $\phi = 5eV$, for the workfunction [10]. The width d is empirically adjusted by the requirement that the interlayer surface state should have approximately the same characteristics

as in a full LAPW slab calculation [7]. We find that $d = t + 0.75c$ is a satisfactory value. Fig. 1a shows the energies of the empty surface and interlayer states, calculated at $\mathbf{k} = 0$ for slabs of increasing thickness. Similarly to the finding of Posternak et al. [7], two surface states split off below a band of bulk states. For large thickness the split-off surface states lie about $0.1eV$ below the $\mathbf{k} = 0$ bulk band bottom, a value compatible with the inverse photoemission data [6]. The (x, y) averaged charge density of the surface state for a 10-layer slab is plotted against z in Fig. 1b. The exponential tail into the vacuum corresponds to a decay length $\lambda = 0.63$Å. From this value we estimate $E \sim -1 / (4\lambda^2) \sim 2.4eV$ for the energy of the state relative to the vacuum, which well agrees with the calculated value reported in Fig. 1a.

Our plane wave basis provides a good description of the delocalized interlayer states and empty surface states. On the other hand, many plane waves are required for a good description of the exponential decay of the wavefunction outside the surface. With a 4-layer slab, we have used 705 plane waves (corresponding to a kinetic energy cut-off of $13Ry$) to obtain an exponential decay accurate over five orders of magnitude for the (x, y) averaged valence charge density. A somewhat poorer accuracy is usually obtained close to the 'hollow' site, due to

the relatively low values of the corresponding charge density. Our total valence charge density for a 4-layer slab is shown on Fig. 2, as a function of z, for (x, y) corresponding to 'hollow' (S), 'bridge' (SP), and 'atop' (A) positions. The calculated corrugation at an average distance $z \sim 2$Å from the surface is $0.22 \div 0.27$Å (the uncertainty being related to the above mentioned difficulties at the S site), which compares well with the *He*-scattering values of $0.21 \div 0.29$Å [11].

The use of empirical, not norm-conserving pseudopotentials to study wavefunction properties might be generally questioned [12]. Of course, our reason for using a local pseudopotential is entirely one of convenience, and is only justified as a first approach. However, we stress that in the deep exponential decay region which is of interest for tunneling, the wavefunction is governed entirely by the state energy relative to vacuum, which is reasonably good in our calculation. For example, the energies (relative to vacuum) corresponding to (i) top of the filled σ-band, (ii) π-bonding saddle point, (iii) π-antibonding saddle-point, (iv) surface symmetric (antisymmetric) state, given by a monolayer LAPW as -7.8, -6.9, -3.0, -1.2 (−0.2) eV respectively, are -8.9, -7.6, -3.8, -2.8 (−0.5) eV with our pseudopotential.

The (x, y) average $\bar{\rho}(z;V)$ of the 4-layer slab local density of states $\rho(r;V)$ is plotted against z and for several values of V in Fig. 3. We have chosen values of V which select out successively different graphite states, i.e. top of the σ-states at Γ ($V = -4.eV$), π states close to the Fermi energy ($V = 0$), empty π^* states at the M saddle-point ($V = 1.3eV$) and the empty surface state ($V = 2.5eV$). A much slower decay is obtained for the latter. As a result, starting from a distance $z \sim 2$Å from the surface, $\bar{\rho}$ at $V = 2.5eV$ is already about one order of magnitude larger than all relevant bulk structures. These features, and their consequences on the tunneling current $J(V)$, are made more evident in Fig. 4. Here we show the voltage dependence of the tunneling conductivity for two different distances from the surface. We take $z = 2.5$ and 3.8Å, which are presumably quite small as compared to typical tip-surface separations in present-day scanning tunneling microscopy experiments (estimated values of z are in the range $4 - 10$Å [1-4]). Although the main motivation for our choice of z is simply that our calculated charge density is not well described beyond ~4Å, it is reasonable to believe that no significant new effect can occur between 4 and 10Å. Our results should thus remain very similar at larger distances. Bulk 'resonant' features, such as saddle-point π and π^* states, as well as surface state structures are clearly detectable in the tunneling conductance spectra of Fig. 4 [13]. It is also evident how,

increasing the tip-surface separation, the relative importance of each structure changes, the surface state peak becoming more and more important. It should be noted that the surface to bulk state energy splitting (really of order $0.1 \div 0.2eV$) is artificially increased in a four-layer slab, as shown also on Fig. 1a. One should keep this in mind when extrapolating from the dJ / dV calculated curve of Fig. 4 to the real situation.

So far, we have shown only the (x, y) averaged tunneling conductivity. Fig. 5 illustrates the predicted voltage dependent z-corrugation for constant current of a graphite surface. We note that, while the corrugation is large near the Fermi energy and for the π^* states, it is in fact very small for the surface state, which has a rather plane-wave nature in the (x, y) plane. The maximum height-difference between S and A sites is approximately $\delta z = 0.7 \div 1.0$Å around E_F ($V \sim 0$), $\delta z = 0.2 - 0.3$Å for π^* states ($V = 1.3eV$), and $\delta z = 0.06$Å for the surface state. It is interesting to remark how the corrugation amplitude at E_F is very much different from that of the total valence charge. This example points to the general fact that straight identification of STM maps with surface charge corrugation is not only in principle, but also in practice, clearly mistaken. A

detailed study of the corrugation at the Fermi energy is in progress and will be reported elsewhere.

In conclusion, we have shown that voltage-scanned STM studies of surfaces, and in particular of a graphite surface, should yield much important information on its electronic structure, very difficult so far to investigate with other means.

REFERENCES

1 - G. Binnig, H. Rohrer, Ch. Gerber and E. Weibel, *Phys. Rev. Lett.* **49**, 57 (1982); *Phys. Rev. Lett.* **50**, 120 (1983).

2 - J. Tersoff and D.R.Hamann, *Phys. Rev. Lett.* **50**, 1998 (1983).

3 - N. Garcia, C. Ocal and F. Flores, *Phys. Rev. Lett.* **50**, 2002 (1983).

4 - E. Stoll, A. Baratoff, A. Selloni and P. Carnevali, *J. Phys. C* **17**, 3073 (1984).

5 - M. Posternak, A. Baldereschi, A. J. Freeman, E. Wimmer and M. Weinert, *Phys. Rev. Lett.* **50**, 761 (1983).

6 - Th. Fauster, F. J. Himpsel, J. E. Fischer and E. W. Plummer, *Phys. Rev. Lett.* **51**, 430 (1983).

7 - M. Posternak, A. Baldereschi, A. J. Freeman and E. Wimmer, *Phys. Rev. Lett.* **52**, 863 (1984).

8 - In the opposite limit of a delta-function shaped tip density of states, Eq. (1) would provide directly $J(V)$, rather than dJ / dV.

9 - A. Baldereschi and C.D. Chen, private communication.

10 - The experimental value for the workfunction of graphite is $4.7eV$; see: V.S. Fomenko, *"Handbook of Thermionic properties" (Plenum, New York, 1966).*

11 - W.E. Carlos and M.W. Cole, *Surf. Sci.* **91**, 339 (1980).

12 - D.R. Hamann, M. Schluter and C. Chiang, *Phys. Rev. Lett.* 43, 1494 (1979).

13 - The structure at $V = -0.5eV$ in Fig. 4 appears to be an artifact due to the relatively small number of k points, $N_k = 150$, used for the calculation of $\rho(\mathbf{r},E)$.

FIGURE CAPTIONS

Fig 1. - Fig. 1a shows the energy of surface and interlayer states for graphite slabs of increasing number N of layers. The energy zero is the vacuum level. Dots (triangles) denote symmetric (antisymmetric) surface states with respect to z-reflection symmetry. The ticmark at $E = -2.4eV$ on the left of the figure gives the position of interlayer states in bulk graphite. Fig. 1b shows the (x, y) averaged charge density for the symmetric surface state of a $N = 10$ layer slab. Note that this is a bonding linear combination of surface states on opposite surfaces, which makes it appear slightly more penetrating than the single true surface state is.

Fig. 2 - Valence charge density $\rho_V(x, y, z)$ as a function of z for (x, y) corresponding to: atop (full line), bridge (dashed line) and hollow (dotted line) sites on the surface plane. The inset shows the (x, y) averaged valence charge density. $z = 0$ coincides with a surface plane.

Fig. 3 - z-dependence of $\bar{\rho}$(z,V) for: σ states at V ~ -4.eV, π states close to the Fermi energy, π^* saddle-point states at V ~ 1.3eV and surface states at V ~ 2.5 eV of a 4-layer graphite slab. z=0 coincides with a surface plane. $\bar{\rho}$ is in $\text{Å}^{-3}eV^{-1}$ units.

Fig. 4 - (a): Voltage dependence of the (x, y) averaged tunneling conductivity, given by Eq. (1), for different surface-tip separations. Ticmarks at $V = -4eV$ and $V = +5eV$ refer to σ-states and vacuum level. (b): Calculated band dispersions along ΓK and ΓM for a 4-layer graphite slab.

Fig. 5 - Height-corrugation maps (in Å) in the (x, y) plane for the various states shown on Fig. 3.

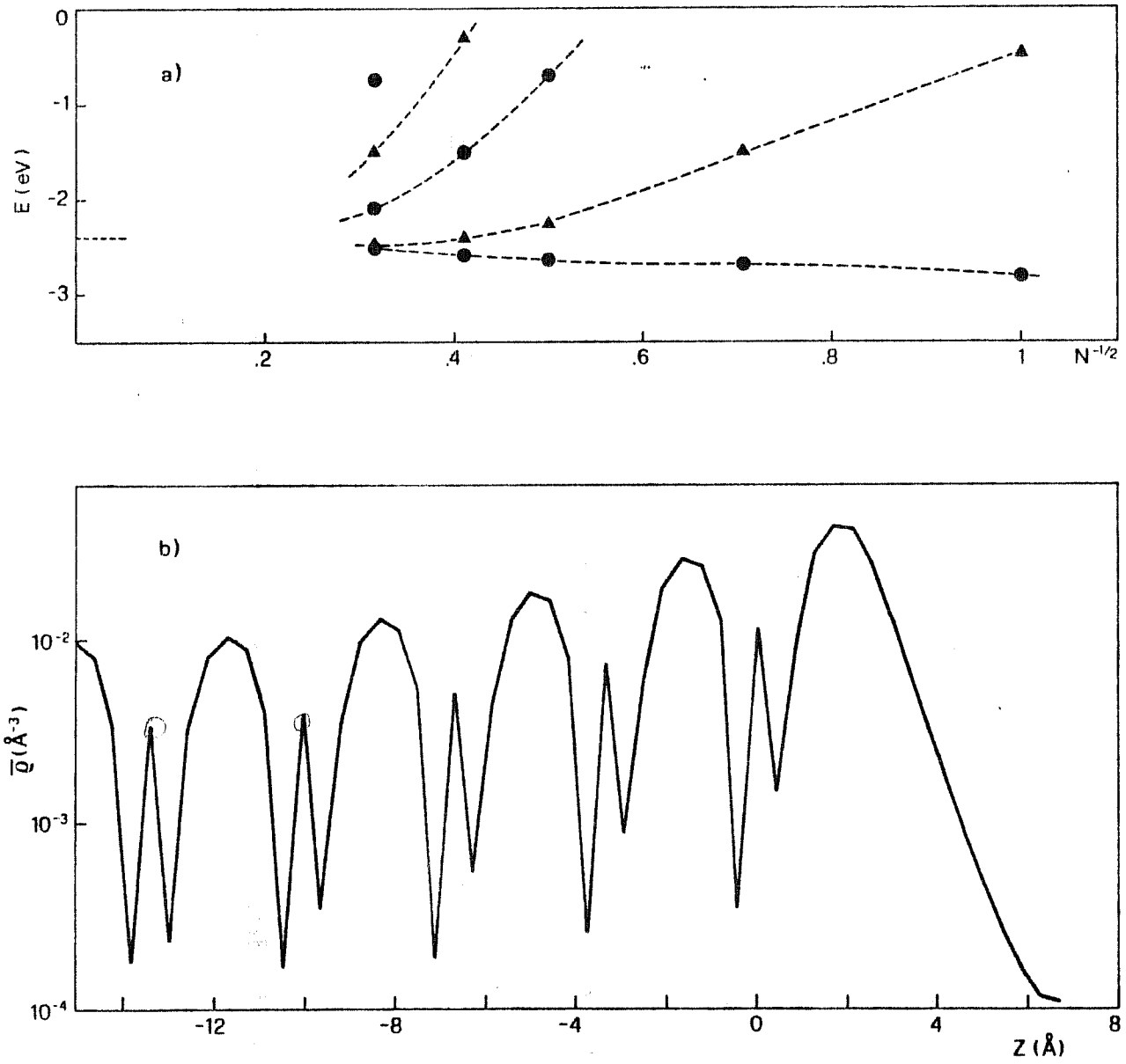
a)
E (eV)
0
-1
-2
-3
.2
.4
.6
.8
1
N^-1/2
b)
ρ̄ (Å^-3)
10^-2
10^-3
10^-4
-12
-8
-4
0
4
8
Z (Å)

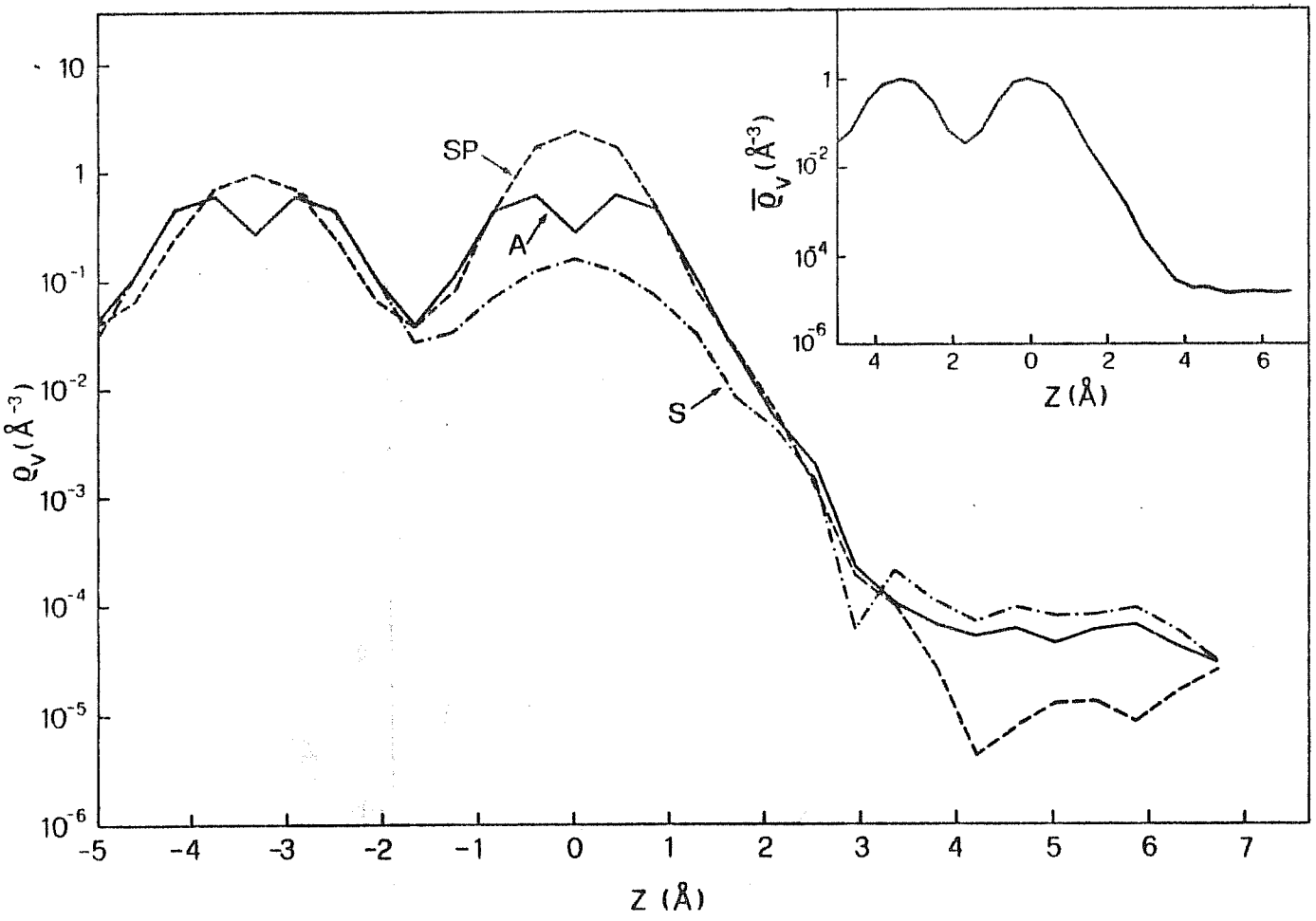
SP
A
S
Q_V (Å^{-3})
Z (Å)
$\overline{Q}_V$ (Å^{-3})
Z (Å)

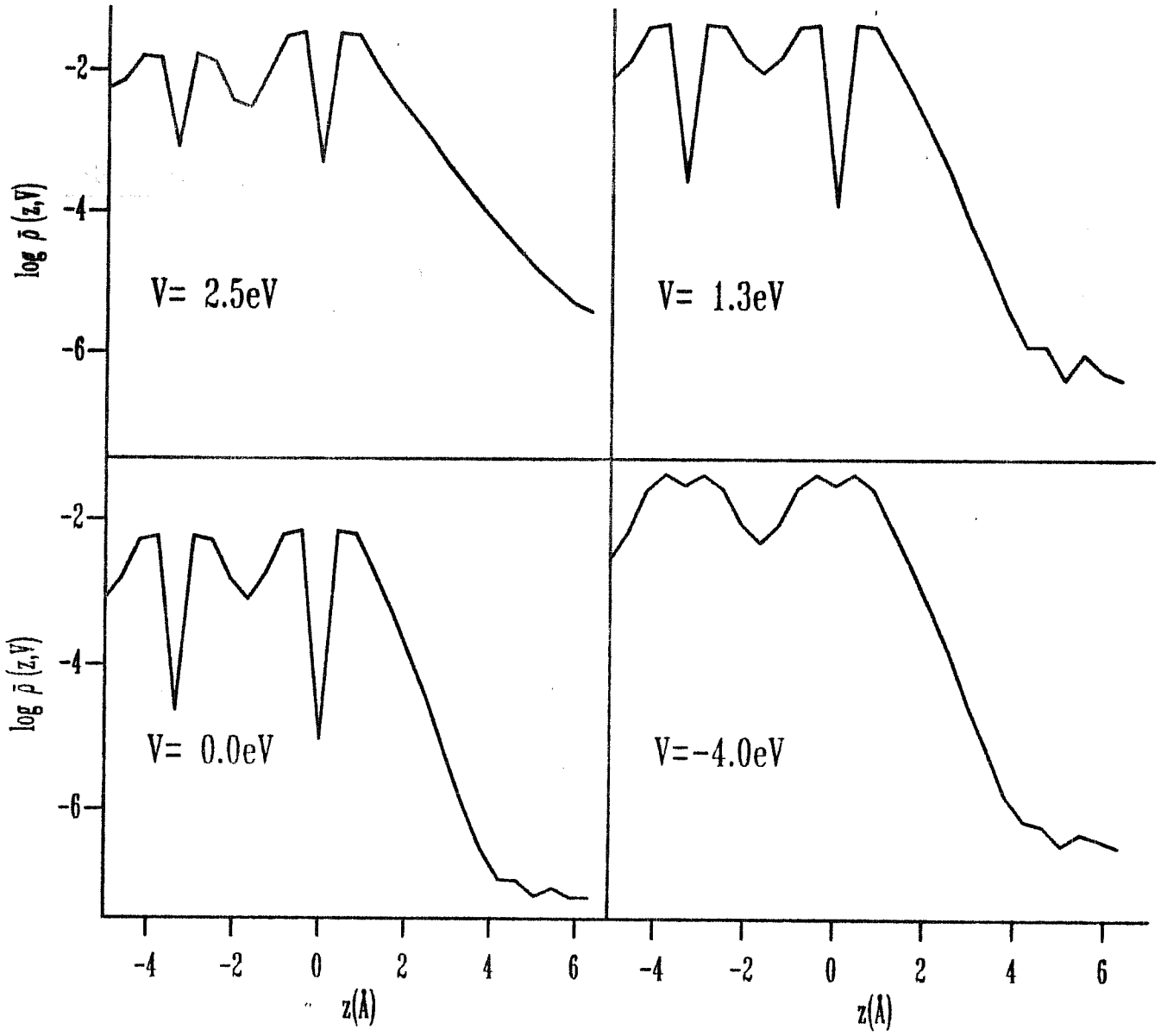

Fig 3

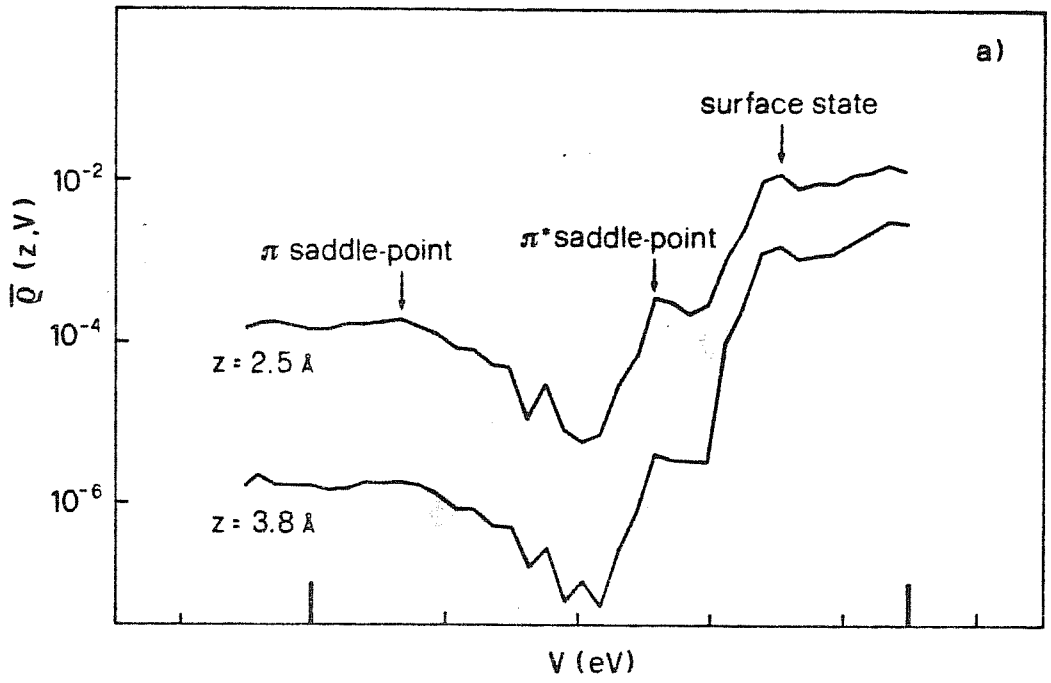
a)
surface state
10^{-2}
10^{-4}
10^{-6}
$\bar{Q}$ (z,V)
π saddle-point
π* saddle-point
z = 2.5 Å
z = 3.8 Å
V (eV)

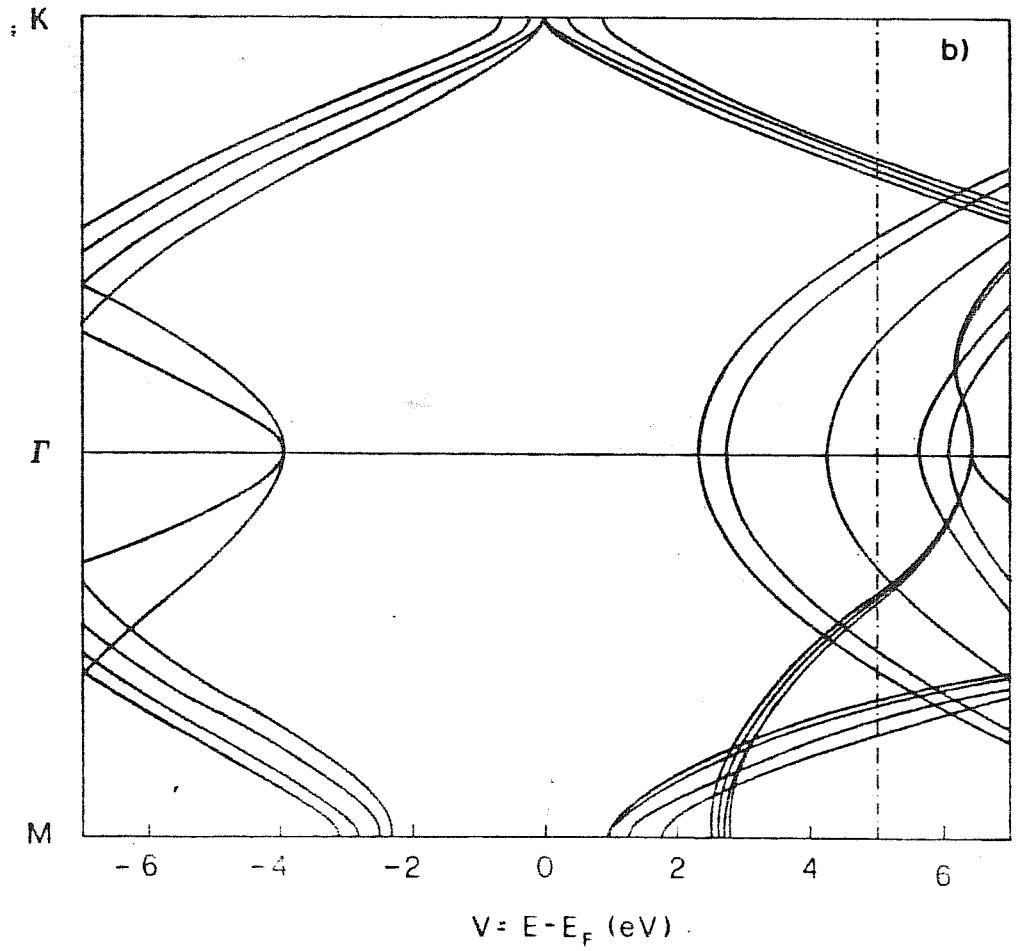
K
Γ
M
b)
-6
-4
-2
0
2
4
6
V = E - E_F (eV)

Fig 4

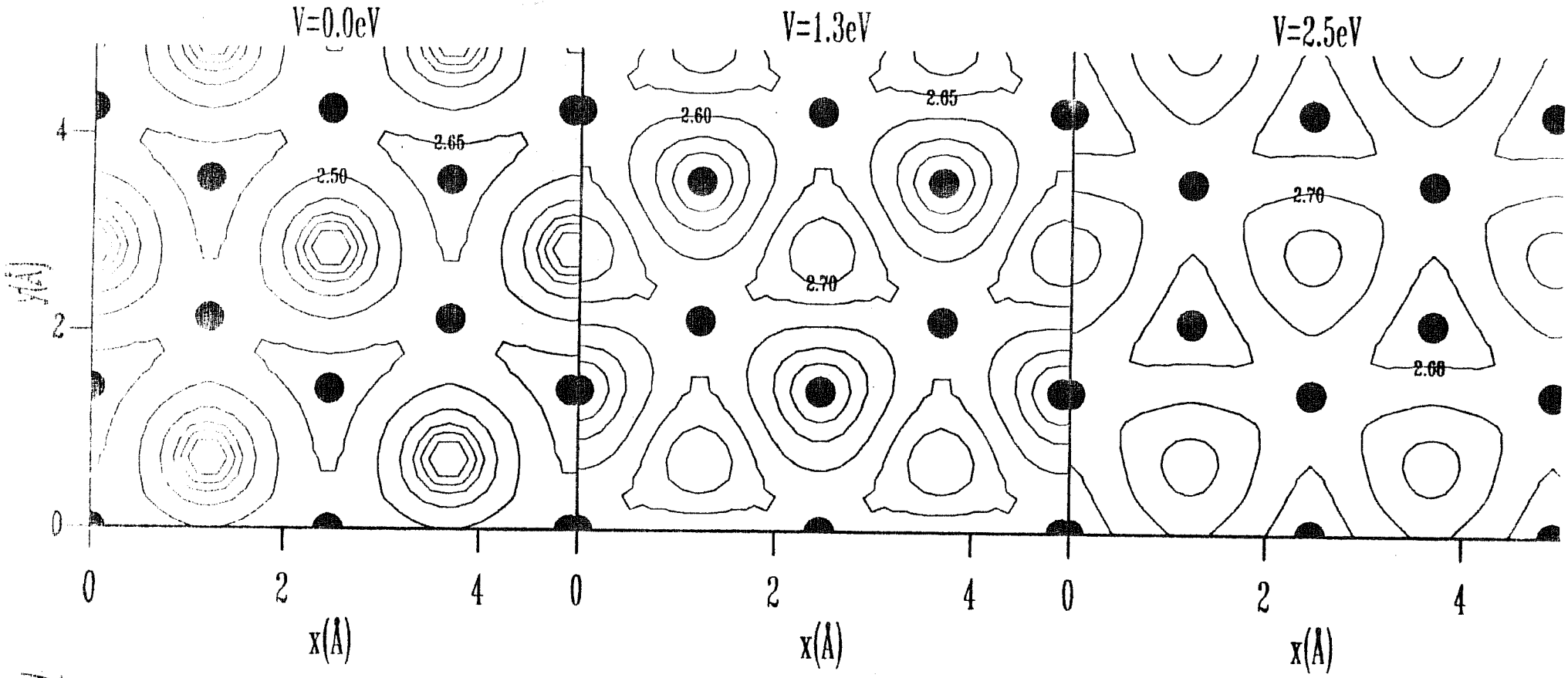
V=0.0eV
V=1.3eV
V=2.5eV
2.50
2.65
2.60
2.65
2.70
2.70
2.68
4
2
0
y(Å)
0
2
4
0
2
4
0
2
4
x(Å)
x(Å)
x(Å)

II. SURFACE STATE POLARONS: AN EXEMPLIFICATION FOR Si(111) 2x1

1. INTRODUCTION

The quantitative experimental detection of surface state energies on clean semiconductor surfaces has become possible in the last decade mostly by means of photo-emission[1] and also optical[2] and energy loss[3] techniques.

At present, these experimental results are being compared with very elaborate self-consistent one-electron calculations[4-8], also in order to learn about the surface geometry, which is generally unknown. The implication is that effects not contained in one-electron calculations, e.g. of the local-density type, can be disregarded, an assumption which is not always obvious. While some work has been devoted towards many-body effects[9-15], lattice reconstruction effects[9-16] and even surface electron-phonon coupling[17], there seems to be no discussion available of polaron effects on surface states.

In this part of my thesis we try to study the polaron effects produced by coupling of the surface state electrons (and holes) to the vibrating surface lattice. For specificity, and also because of its high current interest, we have chosen the clean Si(111)2x1 reconstructed surface as our working example. Since at least two widely discussed reconstruction models - the buckling model[18] and the chain model[19] - are available for the atomic structure of this surface, we have decided to consider both of them. This has been done also in the hope that our predicted behaviour could be sufficiently different for the two cases so as to allow some conclusions to be drawn from a comparison of these predictions with existing or with future experiments. We stress again however that although most numerical calculations carried out in this paper refer to the 2x1 reconstructed Si(111) surface, our scope is much wider. We intend to exemplify the relevant concepts and the main consequences of the more general problem of surface-state polaron, such as one could find, for example, also on a nonreconstructed surface, or on a metal surface.

The structure of this part is as follows. We first construct the model hamiltonian suitable for our purpose and fix the parameters used. This is done in Sect. 2.1. for the buckling model and in Sect. 3.1. for the chain model. Both our model hamiltonians

are strictly one-electron, plus coupling to a surface lattice. While of course electron-electron interactions may often be relevant in a real situation, they are not an essential ingredient of the physical effects we want to describe, and have thus been dropped. Two provisions must however be made in this respect. One is that the one-electron or hole states to be considered must always be energetically close enough to the gap - or the Fermi energy in a metal - that their lifetime, due in effect to electron-electron interactions[20], is long enough for any lattice relaxation to play a role. The second provision is that we will in fact reintroduce some effects of electron-electron interactions when dealing with electron-hole pairs bound to form an exciton. Of course the electron-hole Coulomb attraction is not contained in our hamiltonian and has to be introduced separately, to account for this important feature of the optical spectrum[21,22]. Calculations of such surface state exciton binding energies and wavefunctions are carried out explicitly in Sects. 2.3 and 3.3.

The energy shift and the lattice deformation that occurs when one extra electron - or one hole - is injected in a surface state, otherwise at equilibrium, are calculated for the two models in Sects. 2.2 and 3.2. This state, i.e. a surface state electron (hole) plus its accompanying surface lattice deformation, is what we shall call a surface state polaron.

A surface state polaron will also build up around a bound electron-hole surface pair, i.e. a surface state exciton. This situation, that typically occurs in optical absorption, is of course not just the linear superposition of the polarons of a free electron plus that of a free hole[23-25], and requires separate calculations, which are carried out in Sects. 2.4 and 3.4. The optical absorption itself is calculated - as it is perhaps the most important consequence of surface state polarons of direct experimental relevance - in Sects. 2.5 and 3.5.

The results of Sections 2 and 3 show that surface state polarons can have binding energies easily one to two orders of magnitude larger than in the bulk of the same material. Thus, for example the buckled Si(111)2x1 surface is a strong coupling case with self-trapped electrons and holes -

like in a bulk ionic crystal - while bulk Si is of course a case of weak coupling. Comparison between Sect. 2 and Sect. 3, on the other hand, is useful in that it shows how critically dependent on the detailed surface situation the polaron effects can be, and how they can be handled in each case.

Finally Section 4 is devoted to a discussion of situations where surface state polaron effects will, or might, play an important role. By analogy with known bulk situations, one would expect important consequences on a) transport and b) spectroscopy. Of these, transport is out for a surface state problem: no known evidence has so far been produced for it. One is then left with polaron effects on surface state spectroscopy. The most direct observation of polaron effects is expected in optical absorption from surface states. For increasing coupling strength, the nature of the absorption process goes from band to band - like in a bulk semiconductor - over to Franck-Condon-type, like in a colour centre[26,27]. This aspect is discussed in Sect. 4.1. The corresponding effects expected on luminescence are briefly touched upon in Sect. 4.2, particularly in connection with the contrasting behaviour of the two models investigated. The remaining Sections 4.3, 4.4, and 4.5 are devoted to speculations about possible new experimental consequences of surface state polarons. The ideas exposed in this last part are totally qualitative, and may or may not turn out to be actual quantitative relevance.

2. SURFACE STATE POLARONS IN THE BUCKLING MODEL OF Si(111)-2x1

In this series of Sections 2.1 to 2.5 we proceed to introduce and study polarons in a semiconductor surface state. This will be done in the following sequence. First we introduce a one-electron hamiltonian describing the chosen model, i.e. that of a Si(111)-2x1 buckled surface. Then we study an electron or a hole in a surface state and determine: (a) the form and magnitude of the accompanying lattice distortion; (b) the energy shift (polaron binding) caused by this distortion. Lastly we consider in the same context a surface electron-hole pair and the resulting

optical absorption lineshape, as modified by lattice relaxation.

2.1 The buckling model and its parameters

The surface geometry for the buckling model of Si(111)-2x1 [18] is shown in Fig. 2.1. Alternate $[1\bar{1}0]$ rows of surface atoms are displaced in and out with respect to the "ideal" geometry. The outermost atomic layer of each surface unit cell (a cell is labelled by the index n) contains one raised atom - labelled (n,1) - and one lowered atom - labelled (n,2). Each surface atom carries a dangling-bond (DB) orbital, which we denote $|n, i>$ $(i = 1,2)$. As it turns out[4-9,28], the surface states of Si(111) with energies close to the Fermi level have a very strong DB character. Thus it is reasonable to restrict our attention to DB orbitals in this case. The simplest picture of a DB is a combination of s and p_z wavefunctions, with coefficients which depend on the distance H_{ni} of the atom from the 2nd atomic plane

$$|n,i\rangle = \sqrt{6}\ \frac{H_{ni}}{a}\ |s,i\rangle + \sqrt{1 - 6\left(\frac{H_{ni}}{a}\right)^2}\ |p_z, i\rangle, \quad (2.1)$$

where a is the surface lattice constant ($a = 3.85\text{Å}$). With the choice (2.1), $|n, i>$ is an sp^3 orbital when $H_{ni} = H_o = a/2\sqrt{6}$ (the value for the "ideal" geometry) while it reduces: (a) to a p_z orbital for the fully relaxed case $H_{ni} = 0$; (b) to a pure s orbital when $H_{ni} = 2\,H_o = a/\sqrt{6}$, for then the angle between each pair of back-bonds is $\frac{\pi}{2}$. The DB energy depends on atomic position, in the form

$$\epsilon_i(H_{ni}) = \epsilon_p - \frac{C}{2}\left(\frac{H_{ni}}{a}\right)^2, \quad (2.2)$$

where $C = 12(\epsilon_p - \epsilon_s)$ and ϵ_s and ϵ_p are the s and p atomic energies.

As mentioned in the introduction, we do not intend to include electron-electron interactions in our calculation (except when dealing with the exciton problem). In particular, for instance, the electronic part of the total energy will be simply calculated as a sum of one-electron energies.

The possible relevance of many-body effects in buckling-type models has been discussed to some extent in a few papers[10-15] and found to be important in determining the relative stability of various surface configurations (e.g. paramagnetic vs antiferromagnetic[13]). Our point here is however to start with the simplest possible scheme that would enable us to focus on surface state polarons, a one-electron effect. Thus we just assume in this Section that the buckled non-magnetic surface is the stable ground state configuration of Si(111)-2x1 and describe single-particle properties by the model surface state hamiltonian:

$$H = \sum_{n,i} \varepsilon_i(H_{ni})\, |ni\rangle\langle ni| + t \sum_{\langle ni,mj\rangle} \left[|ni\rangle\langle mj| + h.c. \right], \quad (2.3)$$

where t is the hopping integral and <ni, mj> indicates restriction to nearest neighbours. Here electron-lattice coupling is present through the dependence (2.2) of the on-site energy upon the atom z-coordinate H_{ni}. We wish to underline that this is by no means the only electron-surface lattice coupling mechanism to be expected in a real situation. For example (2.3) does not include the electrostatic coupling (Fröhlich-type[29]) that might quantitatively play a role in this case, since the buckled surface is strongly ionic. Restriction to the coupling (2.3) helps greatly to simplify the problem, while in our view it should not lead to important qualitative errors. Quantitatively we expect (2.3) to underestimate somewhat the coupling strength and thus the polaron binding energies.

For static and uniform buckling, i.e. $\varepsilon_i(H_{ni}) \equiv \varepsilon_i$, (i=1,2) the eigenvalues of (2.3) become

$$E_{\pm}(\underline{k}) = \frac{\epsilon_1+\epsilon_2}{2} + 2t\cos(\underline{k}\cdot\underline{a}_2) \pm \sqrt{\left(\frac{\epsilon_2-\epsilon_1}{2}\right)^2 + \left(4t\cos\frac{\underline{k}\cdot\underline{a}_1}{2}\cos\frac{\underline{k}\cdot\underline{a}_2}{2}\right)^2}, \quad (2.4)$$

where $\underline{k}$ is a vector of the two-dimensional surface Brillouin zone (SBZ) of Fig.(2.1c), and $\underline{a}_1 = \sqrt{3}\, a\hat{x}$, $\underline{a}_2 = a\hat{y}$. The lower and upper signs in (2.4) refer to the

filled (-), or lower band, and to the empty (+), or upper band, respectively. We must now provide an estimate of the parameters t, ϵ_1 and ϵ_2 for Si(111)-2x1. The results of several calculations have shown that the width of the DB bands for the buckling model is quite small, typically a few tenths of an eV [4-5;28]. This is partly due to the large separation between surface atoms, nearest neighbours on the surface being bulk 2nd neighbours, but also to a strong cancellation effect[30]. While the direct hopping has a negative sign, there is an indirect hopping term via second layer atoms that has opposite sign, and slightly larger in magnitude. The latter is large enough to offset the former, but the ensuing cancellation makes the surface band of Si(111) particularly narrow. Assuming thus $t > 0$, the width of the lower band in our model bandstructure is $B_- = 4t$. We take $t = .075$ eV resulting in $B_- = .3$ eV, a value in the range of current estimates. The appropriate value of $(\epsilon_2 - \epsilon_1)$ on the other hand can be determined a posteriori, by requiring that the calculated absorption peak position fits the experimental value[2], $\hbar\omega \sim .45$ eV. This requires, as will be shown later, $\epsilon_2 - \epsilon_1 \sim 1$eV. With these parameters our model bandstructure (2.4) is shown in Fig. 2.2. A useful dimensionless parameter that characterises it is

$$\alpha \equiv \frac{t}{\epsilon_2 - \epsilon_1} \quad , \tag{2.5}$$

which is much smaller than unity in the present case, and will be later used as an expansion parameter.

It is at this point desirable to introduce the Wannier functions of this problem. The Wannier states will be useful in deriving a simple expression for the total energy, and also as good basis functions for the polaron states. The Wannier functions of our model can be expressed as

$$a_{\pm n} = \sum_m \left[c_{1\pm}(n-m)\,|m,1\rangle + c_{2\pm}(n-m)\,|m,2\rangle \right] , \tag{2.6}$$

where the $c_{i\pm}$'s are calculated using the Bloch eigenstates corresponding to (2.4). The general expression for $a_{\pm n}$ is quite involved. However we can

exploit the fact that the "gap" (ϵ_2-ϵ_1) is here sufficiently larger than the bandwidth (4t), and expand to lowest order in α. Then the functions $a_{\pm n}$ take the form

$$a_{-n} = |n,1\rangle + \alpha \sum_{\langle m2,n1\rangle} |m,2\rangle \tag{2.7}$$

$$a_{+n} = |n,2\rangle + \alpha \sum_{\langle m1,n2\rangle} |m,1\rangle \quad , \tag{2.8}$$

where < m2, n1 > (< m1, n2 >) indicates the four nearest neighbours of type 2(1) surrounding the atom (n,1) (or (n,2)). With our value α = .077, the lower (upper) Wannier state is essentially made up exclusively of the DB orbital on atom 1(2), with only 2.2% admixture of atom 2(1). This means of course that the surface is strongly ionic, the electronic charge being almost completely localized on type 1 atoms[31]. The Wannier state energies are

$$\epsilon_{-n} = \epsilon_1 - 4t\alpha \tag{2.9}$$

$$\epsilon_{+n} = \epsilon_2 + 4t\alpha \quad , \tag{2.10}$$

the difference $E_{gn} = (\epsilon_2 - \epsilon_1) + 8\,t\alpha$ being the single-particle gap for localized states.

We now want to determine the T = 0°K static equilibrium positions of the surface atoms corresponding to the hamiltonian (2.3) and the chosen values of the parameters. Thus we minimize the total energy of our model system consisting of 2N surface atoms and 2N surface electrons, if N is the number of surface unit cells. Within the usual Born-Oppenheimer's approximation, the total energy is approximately given by

$$\mathcal{E}_{2N} = \frac{1}{2} \sum_{ni} \gamma \,(H_{ni} - H'_o)^2 + 2 \sum_n \epsilon_{-n} \quad , \tag{2.11}$$

where $H_{ni} - H'_o$ is the displacement of the atom (n, i) from an appropriate reference value H'_o that will be discussed below, and γ is some effective elastic force constant for atomic displacements perpendicular to the surface

plane, therefore simulating the effect of stretching and bending the back-bonds from their equilibrium configuration. In the ground state all unit cells are equivalent, and we normalize our total energy per unit cell,

$$\mathcal{E}(H_1, H_2) = \frac{1}{2}\gamma\left[(H_1 - H_o')^2 + (H_2 - H_o')^2\right] + 2\left(\mathcal{E}_1(H_1) - \frac{4t^2}{\mathcal{E}_2(H_2) - \mathcal{E}_1(H_1)}\right), \quad (2.12)$$

where $\mathcal{E}_1$ and $\mathcal{E}_2$ depend on H_1 and H_2 through (2.2). Minimizing $\mathcal{E}$ with respect to H_1 and H_2 we find

$$H_1^g = \frac{\gamma a^2 H_o'}{\gamma a^2 - (2 - 8\alpha^2)C}, \quad (2.13a)$$

$$H_2^g = \frac{\gamma a^2 H_o'}{\gamma a^2 - 8\alpha^2 C}. \quad (2.13b)$$

Note that $(2-8\alpha^2)$ and $8\alpha^2$ are the fractions of electronic charge on atom 1 and 2 respectively. Eqs. (2.13) show that when the height H_i of an atom increases, so does the electronic charge on it. In fact, this is due to the dehybridization effects contained in (2.1) and (2.2), that cause $\mathcal{E}_i$ to decrease with increasing H_i. In particular it is clear from (2.13) that H_o' would be the atomic position if the DB's were empty. An estimate for the numerical values of the parameters C, γ and H_o' is C = 52.8 eV, γ = 20.4 eV Å^{-2}, H_o' = .65Å, as discussed in Appendix A. With these values the equilibrium positions (2.13) of the buckled surface are H_1^g = .99Å and H_2^g = .66Å.

Since H_1^g, H_2^g minimize the energy (2.12), it follows that substitution of $H_1 = H_1^g + q_1$, $H_2 = H_2^g + q_2$ transforms E in a quadratic form in q_1 and q_2. To lowest order in α the two vibrational normal mode frequencies are

$$\omega_1 \cong \sqrt{\frac{\gamma a^2 - 2C}{M a^2}}, \quad \omega_2 \cong \sqrt{\gamma / M}. \quad (2.14)$$

The corresponding eigenvectors show them to consist essentially of a local vertical vibration of atoms 1 and 2 respectively. We note that the frequency of atom 2 in this approximation is identical to that in the hypothetical "empty" surface ($\hbar\omega_2$ = 55 meV), while that of atom 1 is lowered ($\hbar\omega_1$ = 44 meV) by the presence of 2 electrons.

2.2. Electron polaron and hole polaron

Different techniques are available to handle weak-coupling (WC) polarons and strong-coupling (SC) polarons[32]. Therefore we should first recognize whether our surface-state problem is WC, SC or intermediate. This will be done in the following way.

We start by considering an extra-electron added to the system of 2N surface atoms and 2N electrons. In the absence of coupling to the lattice the excess electron is in a Bloch state of the empty upper band. When the coupling to the lattice is turned on, the electron is subject to two competing tendencies: one towards delocalization, so as to minimize the kinetic energy; local lattice distortions, reducing the electron on-site energy, tend however to favour the localized situation. The strength of the localizing force is measured by the relaxation energy E_R^e which is released when the lattice is allowed to distort around a localized electron[26]. More precisely, E_R^e is the difference between the total energies $\mathcal{E}_{2N+1}$ of the system of 2N atoms and (2N+1) electrons before and after lattice relaxation. If we express the wavefunction ψ_e of the excess electron as a linear combination of empty Wannier states

$$\psi_e = \sum_n c_n \, a_{+n} \quad , \tag{2.15}$$

the energy $\mathcal{E}'_{2N+1}$ is a functional of both the set of atomic coordinates $\{H_{ni}\}$ and the set of coefficients $\{c_n\}$, $\mathcal{E}_{2N+1}(\{H_{ni}\}, \{c_n\})$. Thus the relaxation energy is

$$E_R^e = \mathcal{E}_{2N+1}\left(\{H_{ni}^g\},\{c_n^g\}\right) - \mathcal{E}_{2N+1}\left(\{H_{ni}^e\},\{c_n^e\}\right), \quad (2.16)$$

where the indices 'g' and 'e' label ground and relaxed values respectively. Let us now tentatively assume that we are in a strong coupling situation, so that the Born-Oppenheimer approximation is good. In this case the energy of the relaxed state can be calculated according to the adiabatic prescription: for any given configuration $\{H_{ni}\}$, minimize first $\mathcal{E}_{2N+1}$ with respect to $\{c_n\}$ to determine the adiabatic potential $\mathcal{E}(\{H_{ni}\},\{c_n(H_{ni})\})$, which can subsequently be minimized to determine H_{ni}^e. Even after elimination of the electronic coordinates, the problem of determining the infinite set of atomic coordinates $\{H_{ni}^e\}$ is still generally very difficult. For our SC situation, however, the following approximate procedure turns out to be convenient. We start by assuming that the electron is perfectly localized in a single unit cell, which we call '0':

$$c_n = \begin{cases} 1 & \text{if } n=0 \\ 0 & \text{otherwise} \end{cases}, \quad (2.17)$$

and calculate the value of E_R^e for this test case. This value must be compared with the corresponding kinetic energy B, that is the energy released when the electron, initially localized in one unit cell, is allowed to spread throughout the surface lattice[26]. Here, B is the difference between the upper Wannier state energy, ε_{+0}, and the energy of the bottom of the upper band. If $E_R^e \gtrsim B$, we can consider (2.17) as a sufficiently good guess. If on the other hand, should E_R^e turn out to be noticeably smaller than B, then we must allow the electron to spread over successive shells of empty Wannier states. Eventually, if the linear size of the region in which $\{H_{ni}^e\}$ differs significantly from $\{H_{ni}^g\}$ becomes much larger than the lattice constant, our initial SC assumption (i.e. Born-Oppenheimer) will be invalid, and a different approximation scheme should then be used.

For our buckled surface model, (2.15) with (2.17) turns out to be a good wavefunction for the excess electron, as will be shown below. This could in fact be anticipated, since the hamiltonian matrix element between neighbouring Wannier functions is of order $\alpha << 1$, implying precisely that electron spreading away from the central cell is small.

2.2.1 Electron polaron

The bandwidth B, defined above, must be calculated assuming that the surface lattice is frozen in the ground state equilibrium configuration $H_1 = H_1^g$, $H_2 = H_2^g$, with $H_1^g = .99\mathring{A}$ and $H_2^g = .66\mathring{A}$. The upper band minimum of (2.4) occurs at the $\bar{J}$ point $(0, \pi/a)$ of the SBZ (see Fig. 2.2) and is $(\varepsilon_2 - 2t)$. The corresponding Wannier energy ε_{+o} is given by (2.10), yielding $B = 2t + 4t\alpha$, that is $B = .17eV$ with our choice of the parameters.

The relaxation energy E_R^e is defined by (2.16). However with our choice (2.15)-(2.17) of the electron wavefunction, the total adiabatic energy $\mathcal{E}_{2N+1}$ depends only on the set of atomic coordinates $\{H_{ni}\}$

$$\mathcal{E}_{2N+1}\left(\{H_{ni}\}\right) = \frac{1}{2}\gamma \sum_{ni} (H_{ni} - H_o')^2 + 2\sum_n \mathcal{E}_{-n}\left(\{H_{ni}\}\right) + \mathcal{E}_{+o}\left(\{H_{ni}\}\right) , \quad (2.18)$$

where ε_{-n} is the energy of filled states in cell 'n', while ε_{+o} is the energy of the extra electron in the cell 'o'. As described in Sec. 2.1, the upper Wannier state a_{+o} is basically localized on the atom (0,2), with only a small spread on the 4 nearest neighbours of type 1. This implies however that even with the simplifying assumption (2.17), the lattice relaxation will in principle affect not only the atom (0,2) but also the neighbouring atoms. This, in turn, alters the energies of their (filled) Wannier states. In this way the relaxation can propagate out to successive shells of neighbours. However the relaxation amplitude decreases very quickly with increasing distance from the central site[33]. In this calculation we assume tentatively that there is no relaxation beyond the first shell of type 1 neighbours

of the atom (0,2) (see Fig. 2.8a). Taking into account the equivalence of these four neighbours the relevant energy to be minimized is

$$\mathcal{E}(H_{01}, H_{02}) = \frac{1}{2}\gamma\left[(H_{02} - H'_0)^2 + 4(H_{01} - H'_0)^2\right] + 8\left[\mathcal{E}_1(H_{01}) - 3t\alpha'_e - t\alpha_e\right] + \mathcal{E}_2(H_{02}) - 4t\alpha_e \quad , \tag{2.19}$$

where

$$\alpha'_e = \frac{t}{\mathcal{E}_2(H_2^g) - \mathcal{E}_1(H_{01})} \quad , \tag{2.20a}$$

and

$$\alpha_e = \frac{t}{\mathcal{E}_2(H_{02}) - \mathcal{E}_1(H_{01})} \quad . \tag{2.20b}$$

The new local equilibrium positions for the atom (0,2) and its neighbours are

$$H_{01}^e = \frac{\gamma a^2 H'_0}{\gamma a^2 - C(2 - \alpha_e^2 - 6\alpha_e'^2)}$$

$$H_{02}^e = \frac{\gamma a^2 H'_0}{\gamma a^2 - C(1 + 4\alpha_e^2)} \quad . \tag{2.21}$$

Numerically, the central atom relaxation is quite large: from $H_2^g = .66\mathring{A}$ to $H_{02}^e = .80\mathring{A}$. The corresponding relaxation of the four type 1 neighbours turns out to be in fact negligible, i.e. from $H_1^g = .990\mathring{A}$ to $H_{01}^e = .988\mathring{A}$. This finding confirms the validity of our initial SC assumption. The relaxation energy amounts to $E_R^e = .15$ eV, resulting from an electronic energy gain of .32 eV - due to the outward displacement of the central atom - approximately half-balanced by the necessary elastic cost (-.17eV) [34].

This relaxation energy E_R^e is almost identical to the bandwidth B ($\sim$.17 eV), thus confirming once more that we are dealing with a strong coupling case. We can also calculate the mass renormalization for the excess electron. The renormalization factor is usually expressed as exp (S_e), where S_e is the Huang-Rhys factor[26,27], given in our case (and T = 0°K) by

$$S_e \equiv -2 \langle \chi^g_{vib} | \chi^e_{vib} \rangle = \sum_{i=1,2} \frac{M \omega_i^g \omega_i^e (H_i^g - H_i^e)^2}{\hbar (\omega_i^g + \omega_i^e)} \quad . \tag{2.22}$$

Here χ_{vib} are zero-point vibrational states, ω_1^g and ω_2^g are the vibrational frequencies in the ground state of the system with 2N electrons - given by (2.14) - while ω_1^e and ω_2^e are the corresponding local frequencies in the relaxed state with an extra electron. The latter are calculated by expanding the adiabatic potential (2.19) around the equilibrium positions (2.21), which gives ω_1^e = 44 meV and ω_2^e = 50 meV (against ω_1^g = 44 meV and ω_2^g = 55 meV). The resulting value for the Huang-Rhys factor is S_e = 3.6, which corresponds to a mass enhancement factor exp(S_e) $\sim$ 40 for the excess electron. The original bandwidth B = .17 eV is reduced to a few millivolts, showing that the electron can in fact be considered as immobile, and essentially classical.

2.2.2 Hole polaron

The same approach discussed for the case of an excess electron can be straightforwardly used to evaluate the relaxation energy E_R^h around a localized excess hole. We assume once more that the hole is perfectly localized in a single unit cell, which we call '0'; thus its wavefunction ψ_h reduces to $\psi_h = a_{-0}$, the lower Wannier state of cell '0'. The total adiabatic energy $\mathcal{E}_{2N-1}$ is a functional of only the atomic coordinates $\{H_{ni}\}$ and the relaxation energy can then be expressed as

$$E_R^h = \mathcal{E}_{2N-1}(\{H_{ni}^g\}) - \mathcal{E}_{2N-1}(\{H_{ni}^h\}) \quad , \tag{2.23}$$

where

$$\mathcal{E}_{2N-1}\left(\{H_{ni}\}\right) = \frac{1}{2}\gamma \sum_{ni}\left(H_{ni} - H'_o\right)^2 + 2\sum_{n\neq 0}\mathcal{E}_{-n}\left(\{H_{ni}\}\right) + \mathcal{E}_{-o}\left(\{H_{ni}\}\right) \tag{2.24}$$

In (2.23) the index h is used to label quantities of the hole relaxed state. As discussed in the previous Section, the lattice relaxation can in principle spread over a large region of the surface lattice because the Wannier functions are not strictly "single-site". We assume tentatively that only the central atom (0,1), and its four nearest-neighbours of the type 2 can relax. In this case and taking into account the equivalence of the 4 atoms of type 2 the relevant part of the total energy is

$$\begin{aligned}\mathcal{E}\left(H_{o1}, H_{o2}\right) = \frac{1}{2}\gamma\Big[\left(H_{o1} - H'_o\right)^2 + 4\left(H_{o2} - H'_o\right)^2\Big] \\ + 8\left[\mathcal{E}_1\left(H_1^g\right) - 2t\alpha - 2t\alpha'_h\right] \\ + 8\left[\mathcal{E}_1\left(H_1^g\right) - 3t\alpha - t\alpha'_h\right] \\ + \mathcal{E}_1\left(H_{o1}\right) - 4t\alpha_h \quad ,\end{aligned} \tag{2.25}$$

where

$$\alpha'_h = \frac{t}{\mathcal{E}_2\left(H_{o2}\right) - \mathcal{E}_1\left(H_1^g\right)} \quad , \tag{2.26a}$$

and

$$\alpha_h = \frac{t}{\mathcal{E}_2\left(H_{o2}\right) - \mathcal{E}_1\left(H_{o1}\right)} \quad . \tag{2.26b}$$

In (2.25) $\epsilon_{-a} \equiv \epsilon_1(H_1^g) - 2t\alpha - 2t\alpha_h'$ and $\epsilon_{-b} \equiv \epsilon_1(H_1^g) - 3t\alpha - t\alpha_h'$ are the energies of the lower Wannier functions centered on the atoms denoted as 'a' and 'b' respectively in Fig. 2.3b. Minimization of (2.25) yields the new local equilibrium positions

$$H_{01}^h = \frac{\gamma a^2 H_0'}{\gamma a^2 - C(1-4\alpha_h^2)} \qquad (2.27a)$$

$$H_{02}^h = \frac{\gamma a^2 H_0'}{\gamma a^2 - C(\alpha_h^2 + 6\alpha_h'^2)} \qquad (2.27b)$$

The numerical values of H_{01}^h and H_{02}^h are $H_{01}^h = 1.76\text{Å}$ ($H_1^g = .99\text{Å}$) and $H_{02}^h = .65\text{Å}$ ($H_2^g = .66\text{Å}$). As for the electron polaron the relaxation is strong for the atom in the central site, but almost negligible for the neighbouring atoms, thus supporting the initial SC assumption. Note that the sign of the relaxation for the central atom is opposite with respect to the case of an excess electron. The energy balance consists now of a strong gain of elastic energy (-1.04eV), partially cancelled by an increase of electronic energy (+.66 eV). The resulting value for the hole relaxation energy is $E_R^h = .38$ eV. This must be compared with the value for B_h, the kinetic energy of localization of the hole. B_h is the difference between the energy of the lower Wannier function and the top of the lower band in the undistorted lattice, $B_h = 2t + 4t\alpha = .17$eV in our case. Therefore we conclude that the hole should be self-trapped. This is confirmed by the value of the Huang-Rhys factor S_h for which we find, using an expression analogous to (2.22), $S_h = 8.3$ (the local vibrational frequencies in the relaxed state are now $\omega_1^h = 51$ meV and $\omega_2^h = 55$ meV). The resulting enhancement factor for the hole mass is $\exp(S_h) \sim 4000$, and the hole can thus rather accurately be described as a localized defect.

2.3 Exciton states in the buckling model

As a first step for the calculation of the optical spectrum, in this Section we start studying electron-hole pair excitations - namely exciton states - of our model system of 2N surface atoms and 2N electrons, assuming for the moment that the lattice is frozen in the ground state equilibrium configuration. To this end we need to introduce some effects of electron-electron interactions, so far not present in our calculations. Our model for the exciton consists of an electron transferred from a Wannier state of the lower band - basically localized on an atom of type 1 - to an empty Wannier state centered on a nearest neighbour atom of type 2. The justification for this model is that: (a) this is certainly the lowest (singlet) exciton state, as suggested by the analogy with strongly ionic bulk materials; (b) the dipole matrix element $< a_{-n} | \vec{r} | a_{+m} >$ - determining the strength of optical transitions - is nonvanishing only if a_{-n} and a_{+m} are first neighbouring sites. In our calculation of the exciton binding energy we shall also neglect the terms responsible for the exciton propagation through the surface lattice[21]. In our model these terms - roughly proportional to the square of α in Eq. (2.5) - are very small. In addition, as shown by the results of the next Section, the coupling to the lattice will cause self-trapping of the exciton. With this simplification the singlet exciton binding energy E_{BS} reduces to the sum of the e-h Coulomb and exchange energies[21]

$$E_{BS} = V_c - 2 V_x \quad , \tag{2.28}$$

where

$$V_c = \int d^3r \, d^3r' \; a^*_{-0}(\underline{r}) \, a_{-0}(\underline{r}) \times \frac{e^2}{\epsilon_s |\underline{r} - \underline{r}'|} \, a^*_{+0}(\underline{r}') \, a_{+0}(\underline{r}') \quad , \tag{2.29}$$

and

$$V_x = \int d^3r\, d^3r'\, a^*_{-0}(\underline{r})\, a_{+0}(\underline{r}) \times \frac{e^2}{\epsilon_{bg}\,|\underline{r}-\underline{r}'|}\, a^*_{+0}(\underline{r}')\, a_{-0}(\underline{r}') \,. \tag{2.30}$$

The binding energy of the triplet exciton, instead, is unaffected by electron-hole exchange, i.e. $E_{BT} = V_c$. The surface electron-hole exchange (2.30) is screened by the underlying bulk only, whereas the dielectric screening of the Coulomb attraction (2.29) contains also, in principle, the screening contribution of surface states themselves[35]. However, introduction of this 2-dimensional screening appears to be a minor correction in the present case, where the main interaction to be screened is intra-cell, and will be approximately omitted. On the other hand, we will take care to include it in the π-bonded chain model, where the exciton radius is somewhat larger.

In conclusion, we take the image-charge screening $\varepsilon_s = \varepsilon_{bg} = (\varepsilon_b+1)/2$ for both V_c and V_x, where ε_b is the bulk dielectric constant ($\varepsilon_b \approx 12$ for Si). Using the expansion (2.6) of the Wannier functions in terms of DB orbitals, (2.29) and (2.30) can be expressed in terms of intrasite

$$U_i = \int d^3r\, d^3r'\, |\varphi_i(\underline{r})|^2 \frac{e^2}{\epsilon'_{bg}\,|\underline{r}-\underline{r}'|}\, |\varphi_i(\underline{r}')|^2 ,$$

and intersite

$$V_{ij}(R) = \int d^3r\, d^3r'\, |\varphi_i(\underline{r})|^2 \frac{e^2}{\epsilon_{bg}\,|\underline{r}-\underline{r}'|}\, |\varphi_j(\underline{r}'-\underline{R})|^2 , \qquad i=1,2 \;;\; R \neq 0$$

Coulomb interactions. The intra-site background screening ε'_{bg} appearing in U_i is very hard to evaluate, and we have chosen to make it equal to the intersite screening $\varepsilon'_{bg} = \varepsilon_{bg}$. We evaluate $V_{ij}(R)$ using the point charge approximation

$$V_{ij}(R) \sim \frac{e^2}{\epsilon_{bg} R} ,$$

that is justified by the relatively large distances between surface atoms and by the lateral localization of DB states[4-6]. The intrasite repulsion U_i is evaluated numerically using tabulated atomic wavefunctions[36]. We ignore the different hybridization of the two DB's, and obtain U = 1.9 eV for sp^3 hybrids. This value is in the range of current estimates of the intrasite repulsion for silicon[37].

The exciton binding energy (2.28) can be explicitly written as

$$\begin{aligned} E_{BS} = & -2\alpha^2\beta^2 U + (\beta^4 + 9\alpha^4 + 4\alpha^2\beta^2)\, V\left(\left|\tfrac{1}{2}\underline{a}_1 + \tfrac{1}{2}\underline{a}_2\right|\right) \\ & + 2\alpha^2\beta^2\left[V(|\underline{a}_1|) + V(|\underline{a}_2|) + V(|\underline{a}_1 + \underline{a}_2|)\right] \\ & + \alpha^4\left[3V\left(\left|\tfrac{3}{2}\underline{a}_1 + \tfrac{1}{2}\underline{a}_2\right|\right) + 3V\left(\left|\tfrac{1}{2}\underline{a}_1 + \tfrac{3}{2}\underline{a}_2\right|\right)\right] \\ & + V\left(\left|\tfrac{3}{2}\underline{a}_1 + \tfrac{3}{2}\underline{a}_2\right|\right) , \end{aligned} \qquad (2.31)$$

where α was defined in (2.5) and $\beta^2 = 1 - 4\alpha^2$ (recall that $\underline{a}_1 = \sqrt{3}\,a\hat{x}$ and $\underline{a}_2 = a\hat{y}$, as shown in Fig. 2.1). Numerically we obtain E_{BS} = .55 eV, that is, essentially, the Coulomb interaction between two point charges on nearest neighbour sites. With the same parameters the triplet state binding energy is E_{BT} = .57 eV. The (electron-hole exchange) singlet-triplet splitting obtained here is very small, essentially because it is a contact interaction - i.e. proportional to $|\psi(r_e = r_h)|^2$ - and in our model the electron and the hole belong almost totally to the two different sites, (0,1) and (0,2) respectively, in the cell.

2.4 Excitonic polaron

The presence of a surface state electron-hole pair will also cause a surface lattice distortion, just as a single excess electron or hole does. This relaxation affects the wavefunction of both particles and hence, in principle, also their binding energy. To study this effect we follow the same procedure of Sect. 2.2 for the electron- and hole-polarons, including however the e-h interaction energy $\mathcal{E}_{e-h}$ as essential ingredient of the relevant energy to be minimized:

$$\mathcal{E} = \mathcal{E}_{elastic} + \mathcal{E}_{electronic} + \mathcal{E}_{e-h} \quad . \qquad (2.32)$$

Our model for the exciton is the same studied in Sect. 2.3, that is - basically - a hole on the atom h ≡ (0,1) and an electron on the atom e ≡ (0,2). As in the case of a single electron or hole, we assume that the only atoms which can relax are 'h', 'e' and their respective first neighbours, as shown in Fig. 2.4. The elastic energy is then (neglecting relaxation of atoms like a and b, that are not first neighbours)

$$\mathcal{E}_{elastic} = \frac{1}{2}\gamma\left(h_h^2 + h_e^2 + h_c^2 + 2h_d^2 + 2h_g^2 + h_\ell^2\right) , \qquad (2.33)$$

where we use the simplified notation $h_\nu = H_\nu - H'_o$ and the labelling of the various sites is given in Fig. 2.4. The part of the total electronic energy which can change by relaxation is

$$\mathcal{E}_{electronic} = \varepsilon_{+o} + \varepsilon_{-o} + 4\varepsilon_{-a} + 2\varepsilon_{-b} + 4\varepsilon_{-f} + 4\varepsilon_{-g} + 2\varepsilon_{-\ell} \quad , \qquad (2.34)$$

where ε_{+0} and ε_{-0} are the energies of the upper (centered on 'e') and lower (centered on 'h') Wannier states of cell 'O', while ε_{-a}, ε_{-b}, etc.

are the energies of the lower Wannier states centered on the atoms 'a', 'b' etc. in Fig. 2.4. These Wannier energies have the same meaning and expressions as those given in the previous Sections, e.g.,

$$\mathcal{E}_{+o} = \mathcal{E}_2(H_e) + \frac{t^2}{\mathcal{E}_2(H_e) - \mathcal{E}_1(H_h)}$$

$$+ \frac{2\,t^2}{\mathcal{E}_2(H_e) - \mathcal{E}_1(H_g)} + \frac{t^2}{\mathcal{E}_2(H_e) - \mathcal{E}_1(H_\ell)} ,$$

as can be easily inferred from Fig. 2.4. Finally the electron-hole interaction energy is approximated by a slightly simplified form of (2.31),

$$\mathcal{E}_{e\text{-}h} = 2\,\alpha^2_{e\text{-}h}\,\beta^2_{e\text{-}h}\,U - (\alpha^4_{e\text{-}h} + \beta^4_{e\text{-}h} + 4\,\alpha^2_{e\text{-}h}\beta^2_{e\text{-}h})V(a), \quad (2.35)$$

where $\alpha^2_{e\text{-}h}$ and $\beta^2_{e\text{-}h}$ depend on the atomic coordinates of the atoms 'e' and 'h' through $\alpha^2_{e\text{-}h} = \frac{1}{2}(1-p)$, $\beta^2_{e\text{-}h} = \frac{1}{2}(1+p)$, with

$$p = \left[\, 1 + \frac{4t^2}{(\mathcal{E}_2(H_e) - \mathcal{E}_1(H_h))^2} \,\right]^{-1/2} .$$

Minimization of (2.32) with respect to $\{h_h, h_e, \ldots\}$ - performed numerically - leads to the local equilibrium configuration given in Table 2.1. As in the case of the single-electron and single-hole, there is a strong relaxation of the atoms in the central cell (outward and inward displacements for 'e' and 'h' respectively), while all other atomic positions are substantially unaltered. Note that, due in part to the presence of the electron-hole interaction term in (2.32), the magnitude of the displacement of the atom 'e' (and similarly 'h') is smaller with respect to the single electron (hole) case.

The relaxation energy E_R^{exc} around the localized exciton is obtained as the difference between the values taken by (2.32) before and after the relaxation. The numerical value for E_R^{exc} is $E_R^{exc} = .34$ eV. The effective bandwidth B_{exc} for the exciton motion can be estimated as half of the bandwidth for the single electron or hole, i.e. $B_{exc} \sim .08$ eV in our case. This leads to the conclusion that the exciton polaron - as was the case for the hole polaron - is self-trapped. The energy configuration diagram for the ground and excited states of our model system is sketched in Fig. 2.5. The vertical excitation energy is $\varepsilon_o = E_g^o - E_{BS}^o$, where E_g^o is the local single-particle gap and E_{BS}^o the singlet exciton binding energy in the unrelaxed lattice, numerically $\varepsilon_o = .47$ eV with our parametrization. This energy gives the position of the absorption peak according to Franck-Condon's principle, while E_R^{exc} is the energy released after the optical excitation[26,27]. For the emission process the Franck-Condon energy ε_1 is given by $\varepsilon_1 = \varepsilon_0 - E_R^{exc} - \varepsilon_2$ where ε_2 is the energy of the ground state with distorted lattice configuration (see Fig. 2.5). Using the results of Table 2.1 we can calculate $\varepsilon_2 \approx .12$ which yields $\varepsilon_1 \approx 0$ for the peak of the emission line and correspondingly an extremely large Stokes shift, essentially equal to the Franck-Condon excitation energy. This is indicated in Fig. 2.5 by the minimum of the excited energy curve essentially falling onto the ground state energy curve.

2.5 Absorption line-shape

In the adiabatic and Condon approximation, the normalized line shape function for transitions from the electronic ground state (g) to the exciton state (ex) can be written as[27]

$$I_{g,ex}(E) = I_o \sum_k P_k^g \sum_l |\langle \chi_k^g | \chi_l^{ex} \rangle|^2 \delta(\varepsilon_{ex,l} - \varepsilon_{g,k} - E) , \tag{2.36}$$

where $|\chi_k^g\rangle$ and $|\chi_e^{ex}\rangle$ are the vibrational wave functions for the electronic ground and excited states, with total quantum numbers k and l

respectively. P_k^g is the probability of the state $|\chi_k^g\rangle$ at thermal equilibrium, and I_o is the optical (electronic) squared matrix element.

The phonon frequencies in the ground electronic state are given in Sect. 2.1. In this case, atomic vibrations on sites of type 1 and 2 can be considered as essentially uncoupled, because of the small spread of valence electrons from type 1 atoms to neighbouring sites. The ground state vibronic wavefunctions are

$$|\chi_k^g\rangle = \prod_n \prod_{i=1,2} \chi^{(g)}_{k_{n,i}} (Q_{ni} - H_{ni}^g) \quad , \tag{2.37}$$

where Q_{ni} and H_{ni}^g denote the actual coordinate and the equilibrium position of the atom (n,i) and $\chi^{(g)}_{k_{n,i}}$ is the wavefunction of a harmonic oscillator of frequency ω_i^g and quantum numbers $k_{n,i}$ (with $\sum_{ni} k_{ni} = k$).

When an exciton is created in the cell'0', the vibrational motions of the atoms on which the electron and the hole are centered become coupled through the e-h interaction. For small displacements from the equilibrium configuration the adiabatic potential for the motion of the atoms 'e' and 'h' can be expressed in the form

$$\begin{aligned} \mathcal{E} = {} & \tfrac{1}{2}\gamma_h (Q_h - H_h^{exc})^2 + \tfrac{1}{2}\gamma_e (Q_e - H_e^{exc})^2 \\ & + \delta (Q_h - H_h^{exc})(Q_e - H_e^{exc}) + (\epsilon_2) \end{aligned} \tag{2.38}$$

where the force constants γ_n, γ_e and δ are in principle given by the respective second derivatives of (2.32), evaluated at $Q_h = H_h^{exc}$, $Q_e = H_e^{exc}$. It turns out, however, that H_h^{exc} and H_e^{exc} are so very different from H_{01}^g and H_{02}^g of the ground state, that the true excited state "potential energy" (2.32) which is very nonparabolic, is badly misrepresented, in the neighbourhood of $Q_h = H_{n1}^g$, $Q_e = H_{n2}^g$, by (2.38) if the value of γ_n, γ_e and δ indicated above is used. Strictly speaking, one should determine numerically the true vibronic levels of (2.32), that would no longer be of harmonic-

oscillator type. However, it is clear that we are only interested to know these excited vibronic states in the neighbourhood of $Q_e = H^g_{n1}$, $Q_h = H^g_{n2}$. Locally, these eigenstates will still be similar to harmonic oscillator wavefunctions, however with different parameters. We have found that these wavefunctions are reasonably approximated by the harmonic eigenfunctions of (2.38) where however, different values of the four constants γ'_h, γ'_e, δ' and ε'_2 are used. We use $\gamma'_h = 20.7$ eV/Å^2, $\gamma'_e = 19.5$ eV/Å^2, $\delta' = 3.1$ eV/Å^2 and $\varepsilon'_2 = .24$ eV, which describe reasonably $\mathcal{E}$ of (2.32) in the important region. The corresponding normal mode frequencies are $\hbar\omega_+ = 58.7$ meV and $\hbar\omega_- = 50.2$ meV. The lower frequency mode is characterized by the two atoms "e" and "h" vibrating in phase, while the higher frequency mode has them in opposition of phase. The frequency $\hbar\omega_-$ is close to the frequency characterizing the outward and inward relaxation of the unreconstructed surface in its ground electronic state, as calculated in Sect. 2.1. The other mode appears to be pushed up in energy because it involves changes of the electron-hole interaction energy which itself is large. This is an example of how the presence of an exciton can stiffen the lattice, rather than soften it. The vibrational wavefunctions for the electronic excited state are

$$|\chi^{ex}_{\ell}\rangle = \prod_{n\neq 0} \prod_{i=1,2} \chi^{(g)}_{\ell_{n,i}}(Q_{ni} - H_{ni}) \times \chi^{(+)}_{\ell^+}(Q^+)\, \chi^{(-)}_{\ell^-}(Q^-) \,, \tag{2.39}$$

where Q^+ and Q^- are the normal mode displacements from the equilibrium positions of the 'e' and 'h' atoms.

We have calculated the absorption line shape (2.36) numerically for increasing temperatures, with cut-off $k_{o,i} = \ell^{\pm} = 10$ in the summations over initial and final vibronic states and with an energy resolution $\Delta E = 10$ meV. The results are displayed in Fig. 2.6 in the form of histograms, the vertical lines being approximately the zeros of the δ-function argument in (2.36). The main lines - determining the basic feature of the absorption lineshape - are accompanied by satellites forming a fine structure which becomes increasingly richer with increasing temperature. The lineshape envelope is asymmetrical- Poisson distribution-like - at low temperatures, and evolves slowly

towards a gaussian shape with increasing temperature, as in usual strong coupling situations[27].

At the lowest temperature (T = 2°K) the absorption starts approximately at the energy ε_2' and it has a fine structure due to the slight difference of $\hbar\omega_+$ and $\hbar\omega_-$. The peak of the absorption spectrum occurs at a frequency which is approximately the vertical excitation energy ε_0 = .47 eV of Fig. 2.5.

With increasing temperature the excited vibrational states of the initial electronic configuration give an increasing contribution to the absorption: this produces a tail on the low energy side of the spectrum, while the fine structure sidebands become more numerous and intense with respect to the main sidebands. The total oscillator strength remains constant, being transferred from the high spikes to the low spikes. The lineshape becomes broader and more symmetrical, while there are no detectable shifts of the peak position within the accuracy of our calculations. We shall return to discuss this lineshape in Sect. 4.1.

3. SURFACE STATE POLARONS IN THE π-BONDED CHAIN MODEL

In this Section we shall study surface state polarons for the π-bonded (dimerized) chain model of Si(111)-2x1, recently proposed by Pandey[19]. We follow closely the scheme used in Sect. 2 for the buckling model. In Sect. 3.1 we introduce our one-electron hamiltonian, fix its parameters by requiring a reasonable comparison of the resulting bandstructure with known experimental results, and finally determine the corresponding equilibrium positions (dimerization amplitude) of the surface atoms. In Sect. 3.2 we study polaron states associated with an excess carrier - electron or hole - in a surface state. In Sects. 3.3 to 3.5 we consider an electron-hole pair as created for instance by optical excitation. For this we study first the exciton binding energy and wavefunction in the frozen lattice (Sect. 3.3) and next the coupling of the exciton to phonons (Sect. 3.4). Finally we calculate (Sect. 3.5) the absorption lineshape.

3.1. The model and the parameters

In the π-bonded chain model[19] the surface atoms are each bonded to two other surface atoms and form zig-zag chains along the $[1\bar{1}0]$ direction,

similar to those occuring on the Si(110) surface. An important feature of this geometry is that the surface atoms along a chain are as close as bulk nearest-neighbours ($d_b = 2.35\mathring{A}$) while different chains are quite well separated, their distance being $\sim 6.7\mathring{A}$. Because of this anisotropy the model has a large dispersion[7,8,19] of the DB bands along the chain direction $\bar{\Gamma}\bar{J}$, and flat bands along $\bar{J}\bar{K}$ and $\bar{\Gamma}\bar{J}'$, perpendicular to the chains.

As was done for the buckling model in Sect. 2, we focus only on the atoms of the outermost atomic plane and consider the DB-like states, which we assume mostly p_z in this case. Within this approach, the symmetric chain model originally proposed for Si(111)-2x1 has degenerate bands along $\bar{J}\bar{K}$. To remove this degeneracy we assume that the ground state configuration of the surface is characterized by uniformly dimerized chains, with alternating short (contracted) and long (stretched) bonds[38]. The situation is thus very similar to that of a Peierls-distorted quasi one-dimensional system, particularly to polyacetylene[39]. As shown by Fig. 3.1, the dimerization breaks the reflection symmetry through the xz plane and this gives rise to a finite gap along $\bar{J}\bar{K}$. Contrary to the buckling model, no charge transfer occurs between DB's so that the surface ground state is in this case purely covalent.

To describe the electronic structure of the above model we assume the one-electron hamiltonian to be

$$H = \varepsilon \sum_{n,i} |ni\rangle\langle ni| + \sum_n t_{1,n} \left[|n1\rangle\langle n2| + |n2\rangle\langle n1| \right] + \sum_n t_{2,n} \left[|n1\rangle\langle n-1,2| + |n2\rangle\langle n+1,1| \right] , \tag{3.1}$$

with $|n\,i\rangle$ denoting the i-th (i = 1,2) DB in cell n. Here ε is the DB on-site energy - the same for all DB's - $t_{1,n}$ is the hopping integral between the two DB's connected by the short bond in the cell n, t_{2n} is the hopping integral between the two DB's connected by a long bond in neighbouring cells along a given chain. For uniform dimerization, $t_{1,n} \equiv t_1$ and $t_{2,n} \equiv t_2$,

diagonalization of (3.1) yields the DB's dispersion relations:

$$\varepsilon_{\pm}(\underline{k}) = \varepsilon \pm \left[t_1^2 + t_2^2 + 2 t_1 t_2 \cos k_y a \right]^{1/2}, \qquad (3.2)$$

where the minus and plus signs refer to the filled (-) and empty (+) states respectively. Reasonable values for the band parameters t_1 and t_2 are determined by the following requirements: (a) the valence bandwidth should be $\sim$.8 eV, as suggested by angle-resolved photo-emission[40]; (b) the optical absorption peak should occur[2] at $\sim$ .45 eV. In our calculation the absorption spectrum is inclusive of both the electron-hole interaction, leading to exciton bound states, and of the exciton-lattice coupling, leading to polarons[41]. The exciton-lattice coupling depends strongly on the ratio (t_1/t_2), which is related to the magnitude of the ground state dimerization. Conditions (a) and (b) are well satisfied by taking t_1 = -.9 eV, t_2 = -.45 eV. The resulting surface band structure is shown in Fig. 3.2. It does reproduce fairly well the band dispersions resulting from more realistic calculations for this model[8,19].

We approximate the Wannier functions of our model by simple bonding and antibonding combinations of DB orbitals in the same cell. For negligible overlap between DB's at different sites, we have

$$a_{-n} = \frac{1}{\sqrt{2}} \left(|n1\rangle + |n2\rangle \right) \qquad (3.3)$$

$$a_{+n} = \frac{1}{\sqrt{2}} \left(|n1\rangle - |n2\rangle \right), \qquad (3.4)$$

with energies

$$\varepsilon_{\mp n} = \varepsilon \pm t_{1n} . \qquad (3.5)$$

For the lower (upper) Wannier state the error involved in this approximation

is to neglect an antibonding (bonding) contribution of amplitude $\alpha \equiv (t_2/4t_1) \sim .12$ from neighbouring cells along the chain, more distant cells contributing terms of higher order in α. The Wannier state energies (3.5) on the other hand, need only corrections of second order in α, that can be neglected.

We shall determine the ground state configuration and the electron-lattice coupling by assuming that t_{1n} and t_{2n} depend on bond lengths according to

$$t_{1n} = t_o \exp(-\beta \Delta d_{n1})$$
$$t_{2n} = t_o \exp(-\beta \Delta d_{n2}) \quad , \tag{3.6}$$

where t_o is the hopping integral between DB's at distance d_o (equal to the bulk nearest neighbour distance $d_b = 2.35$ Å), and Δd_{n1} (Δd_{n2}) is the contraction (expansion) of the short (long) bond referred to d_o

$$\Delta d_{ni} \equiv d_{ni} - d_o \quad . \tag{3.7}$$

The functional form (3.6) has been extensively used in surface electronic structure calculations to describe the scaling of tight-binding parameters with distance[28] and is quite reasonable so long as $|\Delta d_{ni}|/d_o << 1$. The values Δd_{n1} and Δd_{n2} are connected by a simple geometrical relationship in our model. With $d_o = 2.35$ Å and $|\Delta d_{ni}| << d_o$, bond angles for uniform dimerization are $\theta \sim 109.5°$ resulting in

$$\Delta d_{n2} = -\frac{1}{3} \Delta d_{n1} \quad . \tag{3.8}$$

This condition, combined with (3.6) and the values of t_1 and t_2, yields the relation between dimerization parameters and hopping integrals

$$\beta \Delta d_{n1} = -\frac{3}{4} \ln (t_1/t_2) \quad , \tag{3.9}$$

numerically $\beta\Delta d_{n1} = -.52$. The hopping parameter for the undimerized chains $t_0 = t_1 \exp(\beta\Delta d_{n1})$ is then determined to be $t_0 = -.54$ eV in our case. This value is in fair agreement with commonly accepted first-neighbour ($pp\pi$) interaction parameters in Si [28].

To calculate the ground state structural configuration of the surface, we consider now the total energy of our system of 2N surface atoms (N is the number of unit cells) and 2N electrons occupying valence band states. Within Born-Oppenheimer's approximation the total energy is

$$\mathcal{E}_{2N} = \mathcal{E}_{latt} + \mathcal{E}_{el}(\{d_{ni}\}) \quad , \tag{3.10}$$

where $\mathcal{E}_{latt.}$ is the lattice (potential) energy and $\mathcal{E}_{el}(\{d_{ni}\})$ is the electronic energy corresponding to the configuration specified by the d_{ni}'s. To evaluate $\mathcal{E}_{latt.}$ we restrict to the dimerization mode - shown in Fig. 3.1 - and describe it in terms of the force constant γ in the approximate form

$$\mathcal{E}_{latt} = \frac{1}{2}\gamma \sum_n \left[(\Delta d_{n1})^2 + (\Delta d_{n2})^2 \right] \quad , \tag{3.11}$$

while the electronic energy is simply

$$\mathcal{E}_{el} = 2 \sum_n \varepsilon_{-n} \quad , \tag{3.12}$$

with the Wannier state energies ε_{-n} given by (3.5). By minimization and with the geometrical constraint (3.9), we find

$$\Delta d_{n1} = \frac{9}{5} \beta t_1 / \gamma \quad . \tag{3.13}$$

We need to estimate the values of the parameters β and γ. The dependence of the total energy on bond-length contraction was recently calculated by Pandey [7] for the symmetric chain model of Si(111)-2x1. His results - in the form of total energy per surface atom - can be parameterized as follows

$$\mathcal{E}_{symm} = const. + \frac{1}{2} K (\Delta d)^2 \quad , \qquad (3.14)$$

where $K \approx 18.5$ eV/Å^2 and Δd is the bond-length contraction/expansion with respect to the calculated equilibrium value, $d_s \approx 2.2$Å. Within our scheme and for small deviations from equilibrium, the total energy per surface atom of the symmetric chain model can be expressed as:

$$\mathcal{E}'_{symm} = const. + \frac{1}{2} (\gamma + \beta^2 t_o)(\Delta d')^2 , \qquad (3.15)$$

where the equilibrium bond-length value - to which $\Delta d'$ is referred - is assumed to be $d_o = 2.35$Å. We ignore the difference between d_s in (3.14) and d_o in (3.15) and require that our parameter $(\gamma + \beta^2 t_o)$ equals the calculated value for K. Combining this condition with (3.9) we get $\gamma = 22.3$ eV/Å^2 and $\beta = 2.7$ Å^{-1}. In the resulting ground state configuration bond-length contractions and expansions are then $\Delta d_1^g = -.194$ Å $\quad \Delta d_2^g = +.065$ Å. For small displacements $q_{ni} = \Delta d_{ni} - \Delta d_{ni}^g$ from equilibrium the total energy increase to second order is

$$\Delta \mathcal{E} = \frac{1}{2} \sum_n \left(\frac{10}{9} \gamma + 2 \beta^2 t_1 \right) q_{n1}^2 \quad . \qquad (3.16)$$

This relation defines the frequency ω_o of the long wavelength 'dimerization mode'

$$\frac{M}{2} \omega_o^2 = \frac{10}{9} \gamma + 2 \beta^2 t_1 \quad , \qquad (3.17)$$

yielding $\hbar\omega_o = .059$ eV with our model parametrization.

3.2 Electron polaron and hole polaron

We consider now an excess electron which, in the absence of coupling to the lattice, occupies a Bloch state of the conduction band. As discussed in Sect. 2.2, the localization or delocalization of this excess electron is roughly determined by the ratio E_R^e/B, where E_R^e is the energy released when

the lattice relaxes around the localized electron while B is the kinetic energy of localization of the electron, $B = |t_2|$ in the present model. If $E_R^e > B$ the electron will be localized. Since electrons and holes are perfectly symmetric in this model, we shall restrict our discussion to electrons. Implicitly all the results will refer also to holes.

We shall also require that the lattice distortions q_{ni} caused by the excess electron satisfy

$$|q_{ni}| << |\Delta d_{ni}^g|$$

where Δd_{ni}^g is the bond-length contraction or dilation in the ground state dimerized configuration. By this restriction we shall automatically exclude from our treatment the possibility of soliton formation.

A) Limit of strongly localized polaron

We first calculate the relaxation energy assuming that the excess electron is perfectly localized in one cell, say cell '0'. We denote by $\{d_{ni}^g\}$ the configuration parameters of the ground state - before the lattice distortion induced by the excess electron - and by $\{d_{ni}^e\}$ those after distortion. Within the adiabatic approximation, the total energy is

$$\mathcal{E}_{2N+1} = \frac{1}{2}\gamma \sum_n \left(\Delta d_{n1}^2 + \Delta d_{n2}^2 \right) + 2 \sum_n \varepsilon_{-n}(d_{n1}) + \varepsilon_{+0}(d_{01}) \quad . \tag{3.18}$$

Since we assume perfect localization, the only bond lengths which change after lattice relaxation are $d_{0,1}$, $d_{0,2}$ and $d_{-1,2}$, with $\Delta d_{02} = \Delta d_{-12} = -\frac{1}{6}(\Delta d_{01} + \Delta d_{-11})$ (see Fig. 3.3). Minimizing $\mathcal{E}_{2N+1}$ with respect to Δd_{01}, we obtain

$$\beta \Delta d_{01}^e \exp(\beta \Delta d_{01}^e) = \frac{9}{10} \beta^2 t_0/\gamma \quad , \tag{3.19}$$

which gives $\Delta d^e_{01} = -.069$ Å and $\Delta d^e_{02} = \Delta d^e_{-12} = +.044$ Å. As shown by Fig. 3.3a the lattice distortion caused by the excess electron is a local reduction of the dimerization with respect to the ground state configuration. This in turn implies a reduction of the lattice potential energy and correspondingly an increase of the valence electron energy, since the bonding energy $|t^e_{10}|$ is decreased. On the whole the relaxation energy is $E^e_R \equiv \mathcal{E}_{2N+1}(\{d^g_{ni}\}) - \mathcal{E}_{2N+1}(\{d^e_{ni}\}) = .14$ eV. This value must be compared with B = .45 eV for the kinetic energy of localization. Since here $E^e_R << B$ we deduce that, unlike in the buckling model of Sect. 2, the excess electron will in this case not stay localized, but will spread to find a configuration energetically more favourable. This is substantially confirmed by the value of the Huang-Rhys factor S^e. The expression for S^e at T = 0°K is $S^e = E^e_R/h\bar{\omega}_o$ [26,27] where $\bar{\omega}_o$ is an appropriate average between ω^g_o - the phonon frequency in the ground state, defined by (3.17) - and ω^e_o, the local value of the phonon frequency in the presence of the excess electron. The local frequency is

$$\omega_o^e = \sqrt{\frac{2}{M}\left(\frac{10}{9}\gamma + \beta^2 t_1^e\right)} \quad .$$

Numerically $\hbar\omega^e_o = .077$ eV, resulting in $S^e \sim 2.1$, a value which indicates an intermediate coupling situation (the mass enhancement is $\exp(S_e) \sim 8$). Note that ω^e_o is larger than the phonon frequency in the ground state.

B) Polaron radius

To account for the spatial extent of the polaron, we now express the wavefunction of the excess electron as a linear combination of upper Wannier states $|n_+\rangle$

$$\psi_e = \sum_n c_n |n_+\rangle \qquad (3.20)$$

with coefficients c_n normalized to unity, $\sum_n |c_n|^2 = 1$. For $\Psi = \psi_e \chi_{vib} \prod_n |n_-\rangle$ the total energy expectation value $\langle\Psi|H|\Psi\rangle$ is

$$\mathcal{E}_{2N+1} = \frac{1}{2}\gamma \sum_n \left(\Delta d_{n1}^2 + \Delta d_{n2}^2\right) + 2\sum_n \left(\varepsilon + t_{1n}\right) + \sum_n \left(\varepsilon - t_{1n}\right)|c_n|^2 + \sum_n t_n \left(c_n^* c_{n+1} + c_n^* c_{n-1}\right), \tag{3.21}$$

where $t_n \equiv -\frac{1}{2} t_{2n}$ is the hopping integral between $|n_+>$ and $|(n\pm1)_+>$. Since we assume that the distortion of the ground state configuration is small, i.e.

$$\Delta d_{ni}^e = \Delta d_{ni}^g + q_{ni} \qquad \text{with} \quad |q_{ni} / \Delta d_{ni}^g| \ll 1 ,$$

we can use

$$t_{1n} = t_1 \left(1 - \beta q_{n1}\right) , \tag{3.22}$$

where $|t_1|$ is the value of the bonding energy in the ground state. For simplicity we shall neglect the dependence of t_n on the cell index by taking $t_n \equiv -\frac{1}{2} t_2$. Since the present situation is one of intermediate coupling, we are in the embarrassing situation that neither the strong-coupling approximations nor the weak-coupling ones are really quantitatively reliable. Another way of putting this, is that in principle we are not allowed any kind of adiabatic approximations, such as: (a) freezing the Δd_{ni}, determining the corresponding c_n, and by substitution into (3.21) obtain the adiabatic potential $\mathcal{E}_{2N+1}$ as a functional of Δd_{ni} alone (good for strong coupling), or (b) freezing the c_n, determining the corresponding Δd_{ni}, and by substitution into the minimum condition of (3.21) with respect to c_n, obtain an equation for c_n alone (good for weak coupling). Rather than going into more elaborate intermediate coupling methods[32], we have chosen to follow route (b) anyway because it is still qualitatively correct, if numerically inaccurate, and also because it has in this case less variational parameters to be determined than the corresponding SC treatment. Freezing first the electronic coefficients c_n, the minimum condition with respect to the lattice coordinates yields

$$q_{n1} = -\frac{1}{2}\,\frac{\Delta d_1^{\,g}}{1+\beta\,\Delta d_1^{\,g}}\,|c_n|^2 \quad , \qquad (3.23)$$

i.e. the excess electron acts to reduce the dimerization magnitude. Substituting into (3.21) we get, to first order in q_{n1}

$$\begin{aligned}\mathcal{E}_{2N+1} = \text{const} &+ \frac{10}{9}\,\gamma\,\Delta d_1^{\,g}\sum_n q_{n1} \\ &- 2\beta t_1 \sum_n q_{n1} \\ &+ \sum_n \left(\varepsilon - t_1 + \beta t_1 q_{n1}\right)|c_n|^2 \\ &- \frac{1}{2}\,t_2 \sum_n \left(c_n^* c_{n+1} + c_n^* c_{n-1}\right) \quad .\end{aligned}$$

By virtue of (3.23) the second and third terms correspond to the elastic gain obtained by "undimerization" and to the related electronic loss in the filled lower band. Using (3.13), we see that these two terms cancel exactly in this case[42], leaving

$$\begin{aligned}\mathcal{E}_{2N+1} = \text{const} &+ \sum_n \left(\varepsilon - t_1 + \beta t_1 q_{n1}\right)|c_n|^2 \\ &- \frac{1}{2}\,t_2 \sum_n \left(c_n^* c_{n+1} + c_n^* c_{n-1}\right) \quad .\end{aligned}$$

We can therefore focus on the motion of the excess electron - the distortion being caused by the electron itself through (3.23) - and ignore from now on the valence electrons. Our treatment now follows closely that of Holstein[43].

The coefficients c_n of the electron wavefunction satisfy the Euler equation generated by the above form of $\mathcal{E}_{2N+1}$

$$\left(\varepsilon - t_{1n}\right) c_n - \frac{1}{2}\,t_2\left(c_{n+1} + c_{n-1}\right) = E\,c_n \quad ,$$

where E is the polaron energy. We use (3.22)-(3.23) to relate t_{1n} to $|c_n|^2$

self-consistently

$$t_{1n} = t_1 + A|c_n|^2 \quad ,$$

$$A \equiv \frac{1}{2}\,\frac{\beta \Delta d_1 g}{1+\beta \Delta d_1 g}\, t_1 > 0 \quad . \tag{3.24}$$

We then obtain

$$\left(\varepsilon_p - A|c_n|^2\right) c_n - \frac{1}{2}\, t_2 \left(c_{n+1} + c_{n-1} + 2c_n\right) = 0 \quad , \tag{3.25}$$

where $\varepsilon_p = (\varepsilon - t_1 + t_2) - E$ is the polaron binding energy referred to the bottom of the upper band at J, $\varepsilon_+(J) = \varepsilon - t_1 + t_2$. Eq. (3.25) can be solved taking $c_n = (-1)^n g_n$ and using the continuum approximation

$$g_{n+1} + g_{n-1} - 2g_n \sim \frac{d^2 g_n}{dn^2} \quad .$$

The bound state solutions ($\varepsilon_p > 0$) have the form[43]

$$g(n-n_o) = \left(\frac{2\varepsilon_p}{A}\right)^{1/2} \operatorname{sech}\left[\sqrt{\frac{2\varepsilon_p}{|t_2|}}\,(n-n_o)\right] \quad , \tag{3.26}$$

where the cell index n_o labels the (infinitely degenerate) set of localized solutions

$$\psi_e(n_o) = \sum_n (-1)^n\, g(n-n_o)\, |n_+\rangle \quad , \tag{3.27}$$

analogous of the upper Wannier states for the problem without coupling. The polaron binding energy can be determined using the normalization constraint $\int dn\, g^2(n) = 1$, which yields

$$\varepsilon_p = \frac{A^2}{8|t_2|} \quad . \tag{3.28}$$

Using A = .49 eV, as given by (3.24), we find ϵ_p = .066 eV. The polaron radius

$$r_p^e = \sqrt{\frac{|t_2|}{2\,\epsilon_p}} \qquad (3.29)$$

is then of the order of $7\mathring{A}$ ($\sim$ 2 surface cells), confirming the intermediate coupling nature discussed earlier on. The envelope function (3.26) is shown in Fig. 3.3b.

C) Polaron Bands

The localized states (3.27) are not yet complete solutions of the polaron problem. Because of the translational symmetry, the true polaron eigenstates should be Bloch functions labelled by $\underline{k}$, the total momentum of the electron and phonon system

$$\Psi_{\underline{k}} = N^{-1/2} \sum_{n_o} e^{ikn_o}\, \psi_e(n_o)\, \chi(n_o) \quad ,$$

where $\chi(n_o)$ is the vibrational wavefunction of the lattice when the electron is in the state $\psi_e(n_o)$. The eigenvalues corresponding to Ψ_k form then a band, whose width is substantially reduced with respect to the bare width $2B = 2|t_2|$, since hopping integrals are multiplied by the overlap between the lattice wavefunctions. One way to determine the polaron band energy is of course to just evaluate the expectation value $E_k = \langle \Psi_k | H | \Psi_k \rangle / \langle \Psi_k | \Psi_k \rangle$. However we prefer to calculate the polaron band dispersion in a different (though, in principle equivalent) way. Using Bloch eigenstates to represent the excess electron wavefunction, we determine the polaron energies E_k by solving the Dyson equation[26,44]

$$E_k = \mathcal{E}_+(k) + \Delta_k(E_k) \quad , \qquad (3.30)$$

where $\Delta_k(E_k)$ is the real part of the electron self-energy, after averaging over the state of the phonon system (at thermal equilibrium). While this procedure is not really more convenient than calculating $\langle \Psi_k | H | \Psi_k \rangle$ in

this case, having established it it will be very convenient later, for the problem of the electron-hole polaron.

We set our total hamiltonian H_{tot} as the sum

$$H_{tot} = H_e + H_L + H' \quad , \tag{3.31}$$

consisting of an electronic part

$$H_e = \sum_{\underline{k}} \varepsilon_+(\underline{k})\, c^+_{\underline{k}}\, c_{\underline{k}} \quad , \tag{3.32}$$

of a lattice contribution

$$H_L = \hbar\omega_o \sum_{\underline{k}} b^+_{\underline{k}}\, b_{\underline{k}} \quad ,$$

and of a coupling term

$$H' = \sum_{\underline{k}\underline{k}'} V_{\underline{k}\underline{k}'} \left(b^+_{-\underline{k}+\underline{k}'} + b_{\underline{k}-\underline{k}'}\right) c^+_{\underline{k}}\, c_{\underline{k}'} \quad . \tag{3.33}$$

In (3.32) c^+_k creates a Bloch electron in the upper band and $\varepsilon_+(\underline{k})$ is the corresponding energy, the lattice being frozen in its ground state configuration. Since we are interested in states close to the band edge along the $\bar{\Gamma}\bar{J}$ direction (see Fig. 3.1), we shall use the simplified dispersion $\varepsilon_+(k) = k^2/2m^*_e$, k being measured relative to the $\bar{J}$ point. We take the effective mass m^*_e to be .57 m_o, as required by our bandstructure (3.2). In the lattice hamiltonian H_L, we have restricted our attention to the optical mode modulating the dimerization along the chains, which is taken to be Einstein-like $\omega_k \equiv \omega_o$, with ω_o given by (3.17). Finally $V_{kk'}$ is evaluated as a function of the derivative of the band energy at k = 0 (point $\bar{J}$ of the SBZ) with respect to the lattice displacements, in the following way[45].

Let us call $\hat{\phi}(n)$ the dimerization amplitude operator in cell n

$$\hat{\phi}(n) = \sum_{\underline{q}} u_{\underline{q}} \left(b^+_{\underline{q}}\, e^{i\underline{q}\cdot\underline{R}_n} + h.c.\right) \quad , \tag{3.34}$$

where $u_q = u_{1q} - u_{2q}$, and u_{1q}, u_{2q} are the displacement amplitudes of atoms 1 and 2 in the chain. In the simplest model of a diatomic chain, we have $u_q = \sqrt{\frac{\hbar}{M\omega_o}} + O(q^2)$. If we call $D = \frac{d\varepsilon_+(k=0)}{d\phi} \cdot L$ the deformation potential, where L is the bond length, the coupling $V_{kk'}$ is obtained as

$$V_{kk'} = D \langle k | \frac{d\hat{\phi}}{dR_n} | k' \rangle = i D (k - k') \cdot u_{k-k'} \qquad (3.35)$$

For our purposes, the presence of the k-dependent interaction $V_{kk'}$ in this formula is rather inconvenient, turning the self-energy calculation into a somewhat extensive numerical problem. For the sake of simplicity, we then replace the true expression (3.35) with a crudely approximate k-independent value

$$V_o = D\, u_o / L \,. \qquad (3.36)$$

The deformation potential is easily derived from the tight-binding energy to be

$$D = -\beta L \left| t_1 + \frac{1}{3} t_2 \right| \,.$$

With our parameter values, $u_o = \sqrt{\frac{\hbar}{M\omega_o}} = 0.095$ au, $L = 4.44$ au, D = 6.6 eV, this yields $V_o = 0.14$ eV. We stress that in view of the large arbitrariness involved in the approximation of replacing $V_{kk'}$ by V_o, our numerical results will have only order of magnitude significance.

Our electron self-energy $\Sigma_k(E)$ satisfies the approximate Brillouin-Wigner equation[26]

$$\Sigma_k(E) \doteq \sum_{k'} |V_{kk'}|^2 \left[\frac{n(\omega_{k-k'}) + 1}{E - \varepsilon_{k'} - \hbar\omega_{k-k'} - \Sigma_{k'}(E - \hbar\omega_{k-k'})} \right. \qquad (3.37)$$

$$+ \frac{n(\omega_{k'-k})}{E - \varepsilon_{k'} + \hbar\omega_{k'-k} - \Sigma_{k'}(E + \hbar\omega_{k'-k})} \Bigg] ,$$

where $n(\omega_k)$ is the phonon thermal occupation number. It is easy to verify that with our approximations , $\omega_k \equiv \omega_o$ and $V_{kk'} \equiv V_o$, $\Sigma_k(E)$ is also independent of k. This allows the explicit evaluation of the sum over k' in (3.37), which of course simplifies a great deal the numerical iterative solution of $\Sigma(E)$. The details of this calculation are given in appendix B. The resulting real and imaginary parts of (3.37), $\Delta(E)$ and $\Gamma(E)$, are plotted in Fig. 3.4 for T = 0°K and T = 300°K. At T = 0°K, the dominant feature of $\Delta(E)$ is the inverse square-root singularity - related to the one-dimensionality of this model -occuring at an energy E* slightly above the unperturbed band edge (the zero of our energy scale). At the same energy E* also $\Gamma(E)$ - which is zero below E* - has an inverse square-root singularity and is then finite and positive at higher energies. In Fig. 3.4 we also show the graphical solution of the Dyson equation (3.30) for a few values of the electron bare energy $\varepsilon_+(k)$. The k = 0 ($\bar{\Gamma}$ point) renormalized electron energy $E_o = \Delta(E_o)$ is -.051 eV, which yields a polaron radius, $r_p^e \sim (2m_e^*|E_o|)^{-1/2}$, of the order of 3 unit cells, in substantial agreement with the results of the previous section. The energy E* defined above is simply $E^* = E_o + \hbar\omega_o$. Because of the singular behaviour of $\Delta(E)$ it is always possible to find a solution of (3.30) in the range $(E_o, E_o + \hbar\omega_o)$, for any value of the bare energy $\varepsilon_+(k)$. The free electron parabola $\mathcal{E}_+(k) = k^2/2m_e^*$ is modified into(a) a lower band, compressed between E_o and $E_o + \hbar\omega_o$; (b) an upper band which exists only for $k > \sqrt{2m_e^*\omega_o/\hbar}$, and tends asymptotically to $k^2/2m_e^*$ for large k. The T = 0°K "polaron band structure" is shown in Fig. 3.5, where both bands - when coexisting - are indicated. Noting that our starting problem has full electron-hole symmetry, all results derived above for electrons, remain valid also for holes, once the sign of all energies is reversed.

At $T \neq 0°K$ also phonon absorption processes contribute to $\Sigma(E)$, as shown by (3.37). The calculated real and imaginary parts of $\Sigma(E)$ at $T = 300°K$ are shown in Fig. 3.4b. At finite T, all singularities are smoothed out because of the finite value of Γ throughout the spectrum. A cutoff wave vector appears, whereby the lower branch of polaron states remains well defined only out to a certain value, as illustrated by the graphical solution of the Dyson equation in Fig. 3.4b. This cut-off wavevector is as small as $\sim .15\ \text{Å}^{-1}$ at $T = 300°K$ while the shift increases gently from 51 meV to $\sim$ 60 meV.

3.3 Excitons

As a preliminary step for the calculation of the optical spectrum, in this Section we study surface state excitons, in particular singlets of total momentum $\underline{k} = 0$. We shall be interested in the way such excitons are affected by coupling to the surface lattice. To this end we must however study first excitons in a frozen lattice. To simplify matters we shall assume the electron and the hole to be on the same chain. One further motivation for this assumption is that the optical cross section for creation of electron-hole pairs on different chains is exponentially small due to the large inter-chain separation.

Using a standard approach[21], we expand the exciton wavefunction in terms of singlet states $\psi(k_e, k_h)$ with an electron in the upper Bloch state k_e and a hole in the lower state k_h

$$\Phi(K=0) = \sum_{k'} c(k')\, \psi(k', k') \quad , \tag{3.38}$$

The coefficients c(k) obey the equation

$$\sum_{k'} \left[\left(\varepsilon_+(k) - \varepsilon_-(k) - E_B \right) \delta_{kk'} + W(k,k') \right] c(k') = 0 , \tag{3.39}$$

where E_B is the exciton binding energy and W(k,k') is the sum of the electron-hole exchange and Coulomb interaction potentials. For vanishing overlap

between Wannier functions of different cells, W(k,k') can be expressed as

$$W(k,k') = N^{-1} \sum_{\underline{l}} e^{i(\underline{k}-\underline{k}')\cdot \underline{l}} \; \omega(\underline{l}) \qquad (3.40)$$

with

$$\omega(\underline{l}) = \begin{cases} 2 \sum_{\underline{m}} X(\underline{m}) - C(0) & \underline{l} = 0 \\ - C(\underline{l}) & \underline{l} \neq 0 \end{cases} .$$

Here

$$X(\underline{l}) = \int d^3r \; d^3r' \; a^*_{+0}(\underline{r}) \, a_{-0}(\underline{r}) \times \frac{e^2}{\varepsilon_{bg} |\underline{r}-\underline{r}'|} \; a^*_{-\underline{l}}(\underline{r}') \, a_{+\underline{l}}(\underline{r}') \qquad (3.41)$$

is the exchange interaction between electron and hole separated by $\underline{l}$, while

$$C(\underline{l}) = \int d^3r \; d^3r' \; |a_{+\underline{l}}(\underline{r})|^2 \times \frac{e^2}{\varepsilon_s |\underline{r}-\underline{r}'|} \; |a_{-0}(\underline{r}')|^2 \qquad (3.42)$$

is the corresponding electron-hole Coulomb interaction. In (3.41) $\varepsilon_{bg} \approx (\varepsilon_b + 1)/2$ is the background screening accounting for bulk polarization effects not directly included in our treatment, while ε_s in (3.42) should also include the screening of DB electrons, $\varepsilon_s = \varepsilon_{bg} + (\varepsilon_{DB} - 1)$[35]. The DB screening is known to be ineffective (i.e. $\varepsilon_{DB} = 1$) at short and large distances[46], but can be significant at intermediate distances, where virtual transitions between DB's can occur.

In order to calculate $X(\underline{l})$ and $C(\underline{l})$, we expand the Wannier functions into DB orbitals, retain only two-centre integral terms and evaluate the Coulomb interaction between charge distributions centered at different sites with the point charge approximation, similarly to what was done in Sect. 2.3

for the buckling model. With the above simplifications the central cell potential W(0) becomes

$$W(0) = \frac{1}{2} U - E_M - \frac{1}{2} V_c (|\underline{R}_{01} - \underline{R}_{02}|) , \qquad (3.43)$$

where U is the intrasite repulsion, $V_c(R) \equiv e^2/\varepsilon_s R$ and E_M is a lattice sum of dipole-dipole-type interactions

$$E_M = V_x (|\underline{R}_{01} - \underline{R}_{02}|) + \sum_{m' \neq 0} \left[V_x (|\underline{R}_{01} - \underline{R}_{m'2}|) - V_x (|\underline{R}_{01} - \underline{R}_{m'1}|) \right] ,$$

with $V_x(R) \equiv e^2/\varepsilon_{bg} R$.

We take U = 1.9 eV, as for the buckling model; the calculated value of E_M is .62 eV, including both intrachain and interchain contributions. We approximate the surface screening function ε_s at distances of 1st, 2nd and 3rd neighbours using the expression suggested by Keldysh[47,48] and based on the macroscopic three layer model. In our case we find ε_s = 15.3, 12.8 and 9.6 for first, second and third neighbours respectively. The resulting exciton potential W(1) along the chain is shown in Fig. 3.6a.

We calculate the exciton binding energy E_B by direct diagonalization of (3.39) over a suitable mesh of k-points along the $\bar{\Gamma}\bar{J}$ direction of the SBZ. The resulting value of E_B is .20 eV, of the same order as other independent estimates for surface state excitons[23,48]. In Fig. 3.6b we show the exciton envelope function in real space

$$d(\underline{\ell}) = N^{-1/2} \sum_{K} c(K) \, e^{i \underline{K} \cdot \underline{\ell}} ,$$

representing the probability amplitude for the electron and hole to be at distance $\underline{\ell}$. Our exciton is mostly localized on nearest and next-nearest neighbour cells with an average radius $r_{exc} \sim 4$ unit cells.

The next higher (singlet) exciton state is found at energy .86 eV, i.e. .16 eV above the lowest singlet and just 4 meV below the upper surface band edge, and is totally insensitive to the details of the central cell potential (e.g. the value of U), as it is appropriate to large radius excitons. In

contrast the energy of the optically inactive triplet exciton (which can be calculated in the same way as the lowest singlet exciton, but excluding the exchange potential from (3.39)) is strongly dependent on the details of the potential in the central cell; in particular large values of U would tend to give a negative triplet excitation energy, thus implying an instability of the ground state against triplet exciton formation (i.e. antiferromagnetism)[49]. With our values of the parameters the triplet binding energy is $\sim$.6 eV, resulting in a positive excitation energy $\sim$.3 eV from the ground state. Interestingly, triplet excitons play an important role also on the buckled surface models. Del Sole and Chadi[13] in particular noted that with large but not unrealistic Hubbard U's the buckled surface was also unstable against formation of triplets, and thus turning into a 2-D antiferromagnet.

3.4 Excitonic polaron

The coupling of the exciton to the lattice in our model is characterized by the polaron radii for the single (unbound) electron and hole being of the same order of the exciton radius in the frozen lattice (see Sects. 3.2 and 3.3). In such cases a strong interference between the electron-hole and the electron-lattice interactions can occur, so that the two terms should be treated simultaneously and on the same footing[23-25]. A similar situation occurred for the buckling model, and actually the electron-hole and electron-lattice couplings were both included in the minimization of the total adiabatic energy (see Sect. 2.4). The approach used for that case however is not convenient for the chain model, essentially because the exciton and polaron states extend over a large number of unit cells. For this reason we use a k-space formulation consistent with the previous part of this Section.

We proceed as in Sect. 3.2.C, replacing the electron Bloch states by exciton states $|k>$, where k denotes the total momentum[26]. We consider only the lowest (singlet) exciton, since the energy separation of the next excited state as well as of the continuum is rather large compared to the phonon frequency. We describe the exciton propagation along the chain by the effective

mass dispersion

$$\varepsilon_k^{exc} = \varepsilon_o^{exc} + \frac{K^2}{2m^*_{exc}} \quad , \tag{3.44}$$

where $\varepsilon_o^{exc} \equiv E_g - E_B$ (= .7 eV with E_g = .9 EV and E_B = .2 eV) is the exciton energy in the frozen lattice, $m^*_{exc} = m^*_e + m^*_h$ ($\sim$1.14 m_o) is the exciton mass and k the total momentum in the chain direction, measured relative to the $\bar{J}$ point where the minimum gap occurs. The exciton hamiltonian - corresponding to (3.32) in Sect. 3.2 - is then

$$H_{exc} = \sum_K \varepsilon_k^{exc} \, |K\rangle\langle K| \quad . \tag{3.45}$$

The lattice hamiltonian H_L is the same as in Sect. 3.2, Eq. (3.33). The coupling of the exciton to the optical dimerization mode is included by adding a term of the form

$$H' = \sum_{kk'} V_{kk'} \left(b^+_{-k+k'} + b_{k-k'} \right) |K\rangle\langle K'| \, . \tag{3.46}$$

Once again we approximate the matrix element $V_{kk'}$ by a constant $V_{exc} \equiv V_{oo} \equiv (\hbar/M\omega_o)^{1/2}\Lambda$, where Λ is the derivative of the exciton energy (at k = 0) with respect to the dimerization amplitude. A simple estimate for Λ -which neglects the dependence of the exciton binding energy on atomic displacements - is

$$\Lambda = \frac{dE_g}{dq_1} = 2\,\frac{d\,|t_1 - t_2|}{dq_1} \quad , \tag{3.47}$$

where q_1 is the length variation of the short bond, while the stretched bond has $q_2 = -\frac{1}{3} q_1$ according to the constraint (3.8). With this approximation $V_{exc} = 2V_o$ (= .28 eV), where V_o is the coupling constant (3.36) for a single electron or hole, and correspondingly the exciton-polaron shift Δ_{exc} is about four times the shift for the electron-polaron or hole-polaron (using (3.37) we find Δ_{exc} = -.21 eV at T = 0°K). We expect this value to be an overestimate, since the choice (3.47) implicitly assumes a complete overlap between the lattice distortions induced by the electron and the hole separately. A correct estimate should probably be intermediate between our value

and that for a large radius exciton (i.e. $r_{exc} >> r_p^e, r_p^h$), for which the polaron shift is just the sum of the shifts for the single (unbound) electron and hole[32] (in that limit $\Delta_{exc} \sim -.1$ eV for our model).

3.5 Absorption lineshape of the π-bonded dimerized chain model

The absorption lineshape is strongly dependent on whether the exciton is in a "free" (weak coupling) or self-trapped (strong coupling) state. Toyozawa's[26] criterion for exciton self-trapping is $V_{exc} >> B_{exc}$, where V_{exc} is the coupling constant defined in Sect. 3.4 and B_{exc} the exciton effective bandwidth. In our case a fair estimate for B_{exc} is $B_{exc} \sim \frac{1}{2}|t_2|$ ($\sim .23$ eV), since $|t_2|$ is the halfwidth of both the hole and the electron bands. This yields $(V_{exc}/B_{exc}) \sim 1$, characterizing an intermediate coupling situation. Accordingly the absorption spectrum is expected to be more complicated than for the limiting situations of WC (lorentzian lineshape) or SC (gaussian lineshape). To calculate the lineshape we use

$$I(E) = \frac{I_0}{\pi} \frac{\Gamma_{exc}(E)}{\left[E - \varepsilon_0^{exc} - \Delta_{exc}(E)\right]^2 + \Gamma_{exc}^2(E)} \qquad (3.48)$$

where $\Delta_{exc}(E)$ and $\Gamma_{exc}(E)$ are the real and imaginary parts of the exciton self-energy, calculated using (3.37). Self-consistency modifies the simple lorentzian shape predicted by lowest order (Rayleigh-Schrödinger) perturbation theory (good for the extreme WC), giving rise to multiple phonon structures which can be interpreted as indirect transitions involving phonon emission and/or absorption. Our calculated absorption spectra at various temperatures are shown in Fig. 3.7. The overall shape of the spectra retains the typical one-dimensional character which is appropriate to our model. It is interesting to note that the energy separation between the various phonon structures approximately corresponds to twice the phonon frequency. The reason why these structures appear is because the transition probability to exciton states of total momentum $k \tilde{=} 0$ - involving an even number of phonons

in our model - is very high, because the density of states of a one-dimensional band is divergent at the edges. The effect of increasing temperature is to broaden and smooth out the structures of the spectra, as usual, as well as to cause shifts towards lower frequencies. The position of the first peak - which should be identified with the peak observed experimentally in ref. 2 is given at various temperatures in Table 3.1.

4. EXPERIMENTAL CONSEQUENCES OF THE EXISTENCE OF SURFACE-STATE POLARONS

This section deals with experimental consequences of the existence of surface-state polarons, as exemplified by the models studied in the previous sections. We will discuss here two classes of effects. The first class consists of effects on optical absorption and luminescence from surface states. The theory of these optical processes in the presence of polaron effects is long understood, and through it we can make, particularly for absorption, detailed predictions on lineshape and temperature dependence. The effects in the second class are new, and constitute a rather more speculative part of this paper. They concern: a) spectroscopic effects that might become visible in angle-resolved surface photo-emission near E_F, and in the new technique of Scanning Tunneling Spectroscopy of Binnig and Röhrer[50]; b) possible Wigner crystallization of surface-state polarons on heavily doped semiconductor surfaces. A quantitative theory of these effects has not yet been worked out at this stage, and we plan to devote some work to it in the future. Nevertheless, it seems of use to present here a first qualitative discussion of these potentially interesting situations.

4.1. Temperature-dependent optical absorption; strong coupling versus weak coupling

The optical absorption calculation for the strong-coupling Si(111)2x1 buckling model has been outlined earlier in Sect. 2. A weak-coupling calculation of optical absorption of Si(111)2x1 in the π-bonded chain model is correspondingly given in Sect. 3.

For strong coupling, the absorption lineshapes are Poisson-like in shape, as in colour centres[27], as exemplified by Fig. 2.6. The fine-structure oscillations in this figure are due to our assumption of narrow δ-function like phonon lines, and may or may not in reality be washed out by finite phonon lifetimes. With increasing T, the peak position approaches more and more closely to the Franck-Condon limit for a "vertical" transition in a configuration

coordinate picture such as that in Fig. 2.5. Like in F-centre absorption[27], this implies a weak to negligible blue-shift with increasing T, associated with a linewidth increasing asymptotically like $\sqrt{T}$. For the actual parameters describing our model of the buckled Si(111)2x1 surface, this temperature dependent shift turns out to be essentially nil, as shown by Fig. 2.6.

In the alternative case of intermediate coupled π-bonded chains, the optical absorption mechanism is more akin to that of bulk Si: transitions occur between the ground state and a fully relaxed excited state. The peak position should shift towards the red, for increasing T, like in bulk Si, due chiefly to the usual Fan[51] mechanism of increasing self-energy with T. This absorption line is (motionally) narrow[26], and all lineshape effects are due to the electronic band dispersion, which is strong in this case.

This contrasting temperature behaviour of the strong-coupling and weak-coupling models is worth considering in more detail, as it may provide a useful clue towards identifying the actual reconstruction mechanism of Si(111).

In addition to the "intrinsic" shifts discussed above - a weak or negligible blue shift for buckling, or a Fan red shift for π-bonded chains - we must consider the concomitant effect of a generally temperature-dependent magnitude of the reconstruction itself. This is the equivalent of lattice expansion in a bulk problem. The T = 0°K reconstruction magnitudes $\phi(0)$, $\phi(0) = H_{2g} - H_{1g}$ for buckling, $\phi(0) = -\Delta d_{1g}$ for the dimerized π -bonded chain, are such as to minimize the total energy E_{tot} at T = 0°K. However as T increases the corresponding minimum of the total free energy F_{tot} will in general be attained at different effective reconstruction magnitudes, i.e.

$$\phi(T) = H_1(T) - H_2(T) \qquad (4.1a)$$

for buckling, or

$$\phi(T) = -\Delta d_1(T) \qquad (4.1b)$$

for π-bonded chain. The state favoured at high T is one that is "softer", both electronically and vibrationally, and thus has a larger entropy (like an expanded crystal in a bulk case)[52]. The free energy depends on the effective magnitude Ø of the reconstruction in a way that can be generally written as an expansion

$$F_{tot} = F_o + c\,\Delta\phi^2 + f\,\Delta\phi^3 + \cdots \,, \qquad (4.2)$$

where $\Delta\emptyset(T) \equiv \emptyset(T) - \emptyset(0)$. The presence of the anharmonic coefficient f implies that the distortion will vary with increasing T, roughly in the form described by Kittel[53]

$$\Delta\phi(T) = -\frac{3f}{4c^2}\,k_B\,T \,. \qquad (4.3)$$

For the case of buckling we obtain from (2.12), at T = 0

$$c_b = \frac{1}{4}\left[\gamma - \frac{C}{a^2} - \frac{64\,t^2a^2}{C(H_1^g + H_2^g)(H_1^g - H_2^g)^3}\right], \qquad (4.4)$$

$$f_b = \frac{16\,t^2a^2}{C\,(H_1^g + H_2^g)\,(H_1^g - H_2^g)^4} \,.$$

For π-bonded chains, similarly at T = 0, we have

$$E_{tot} = \frac{1}{2}\gamma\left(\frac{10}{9}\,\Delta d_1^2\right) + 2\left(\varepsilon + t_o\,e^{-\beta\Delta d_1}\right), \qquad (4.5)$$

whence

$$c_\pi = \frac{5}{9}\gamma + t_1\beta^2 \,,$$
$$f_\pi = \frac{1}{3}\,t_1\,\beta^3 \,, \qquad (4.6)$$

with $t_1 = t_0\,\exp(-\beta\Delta d_1^g)$.

We note that the cubic anharmonicity f has opposite sign in buckling ($f_b > 0$) and π-bonded chains ($f_\pi < 0$). Hence, by (4.3) we expect the reconstruction magnitude $\emptyset$ to decrease with T in the buckling case, and to increase for π-bonded chains. The physical reason for this latter increase is the nonlinearity of the electronic energy gain in (4.5), due in turn to the exponential behaviour of hopping integrals.

In conclusion, the additional energy gap shifts expected from this mechanism are

$$\Delta E_{g,b} = -\frac{C}{2a^2}\left(H_1^g + H_2^g\right)\left(\frac{3f_b}{4C_b^2}\right)k_B T$$

for buckling, and

$$\Delta E_{g,\pi} = \frac{2t_1^2}{\left(\frac{10}{9}\gamma\beta^{-2} + 2t_1\right)^2}\, k_B T$$

for π-bonded chains. With the present values of the parameters, C = 52.8 eV, t = .075 eV, $(H_1^g + H_2^g) = 1.65$ Å, $(H_1^g - H_2^g) = .33$ Å, one can extract an additional temperature-induced red-shift of 1.72×10^{-5} T for the ionic reconstruction, e.g. $\Delta E_{gb} = -5$ meV at T = 300°K. Since the Franck-Condon blue-shift of Fig. 2.6 is in this case negligible, we conclude that the weak red-shift just calculated is all one expects for buckling. On the other hand, with π-bonding parameters of $t_1 = -.9$ eV, $\beta = 2.7$ Å^{-1}, $\gamma = 22.3$ eV Å^{-2} we expect an additional blue-shift of 5.1×10^{-5} T, or $\Delta E_{g\pi} = +15$ meV at 300°K. This amount is not sufficient to offset the large red Fan shift for this case. Table 4.1 summarises the total changes in peak positions expected as a function of T for the two models of Si(111)-2x1. The red shifts predicted for the two cases are almost one order of magnitude different. It seems possible that experimental investigation of this point might bring further information on the actual nature of this reconstruction, which is otherwise still uncertain, since new evidence keeps appearing, which conflictingly points

sometimes towards π-bonded chains[40,54,55], or towards buckling-type reconstructions[56], or neither of the two[57]. The room temperature absorption spectrum of the Si(111)2x1 surface is shown on Fig. 4.1. Its shape seems roughly compatible, after damping is considered, with both the buckling-model result of Fig. 2.6, and the π-bonded chain model of Fig. 3.7. Its temperature-dependence has not yet been studied experimentally. However, very recent polarized-light results[54] seem to yield selection rules which favour the π-bonded chain model.

It is interesting that the T-dependent absorption spectrum measured very recently on a different surface, the Si(111)7x7, shows precisely a red-shifting peak, with a shift of about 40 meV between 15 k and 30°k[58], which is very similar to the predicted π-bonded chain value of table 4.1 for Si(111)2x1.

4.2 Luminescence

The emission behaviour for a weak-coupling and strong-coupling system is very different. For weak coupling, absorption and emission occur at the same frequency. For strong coupling, the emission line is Stokes-shifted by an amount $\sim 2S\hbar\omega_o$ towards the red. If one includes finite carrier lifetimes in a strong case a two-lobed spectrum, like that discussed by Almbladh[59], may also be expected.

No experimental luminescence spectra of Si(111)2x1 are available to date. However, Evangelisti and McGroddy[60] have studied the closely analogous case of Ge(111)2x1 and find no surface luminescence at $\hbar\omega$ larger than 0.2 eV. If this could be simplistically taken as representative of the Si(111)2x1 too, it would imply a Stokes shift larger than 0.3 eV. Our estimated Stokes shift in the buckling model is $\gtrsim$ 0.4 eV, that would suggest exactly this outcome. Hence a careful experimental study of luminescence from Si(111)2x1 can yield crucial information on the actual existence of such surface-Stokes shift.

In the chain model case, however, an alternative explanation for the lack of luminescence could be thermalization of electron-hole pairs created by light into triplet excitons (of much lower energy than the singlets), whose radiative decay is then forbidden, or very weak. Our estimate for the relaxed triplet exciton energy for the π-bonded chain model is $\sim$ 0.1 eV, to be compared with the value $\sim$ 0.45 eV for the relaxed singlet exciton.

4.3 Photo-emission

Valence UPS and XPS studies of surface states on Si(111) have been very numerous - if somewhat confusing[1,40,61] - over the last decade. The view that a photo-emission process must as a rule be assumed to be sudden from the lattice point of view, justifies the complete neglect of all polaron effects - except for a broadening, of the kind discussed by Hedin and Rosengren[62] for a core line - in photo-emission spectra.

There may however be one kind of polaron side-effect, that appears not to have been discussed so far. The reason that makes a photo-emission process generally a fast one is evidently not the high energy of excitation, but rather the short lifetimes of the end products, i.e. the electron and the hole. In particular the hole inverse lifetime increases very fast away from the Fermi level[20]. This suggests, however, that long enough hole lifetime could be achieved when photo-emitting from a narrow energy shell around the Fermi level. The lifetime of a high energy electron, however, will be generally short, if the corresponding wavepacket crosses any amount of bulk. For example, the plasmon mean free path at E = 100 eV is only $\sim$5 Å. If we however consider electrons photo-emitted from a surface state into a final state described by a wavepacket whose trajectory moves away from the surface without scattering further off the electrons of the sample, it might be conceivable to attain a lifetime longer than 10^{-13} sec. If this situation, admittedly rather speculative, were achieved, then in surface photo-emission from a state very near E_F a hole polaron can form, and the hole polaron shift would be transferred to the outgoing electron. Thus the high-energy part of the photo-emission spectrum would not terminate at the "bare" E_F^o, but would extend above it with a tail, or an extra peak, reaching to a higher "renormalized" $E_F = E_F^o + E_{pol}$. For strongly coupled polarons, such as those discussed in Sect. 2., E_{pol} is a measurable quantity of $\sim$ 0.4 eV. The distinguishing feature of this phonomenon should be a very weak k-vector-dependence of the apparent "band" energy close to E_F - reflecting the heavy polaron masses of the strong-coupling case. Rather, the angular photo-emission intensity would go down as one moves away from $k = k_F$, reflecting the localized nature of the hole.

An effect of this kind may already have been observed in photoemission from the chalcogenide layer compounds[63]. It seems possible to envisage a similar explanation for the peak just below E_F seen by Himpsel et al[61], on the Si(111)2x1 surface. In this interpretation of their data, the peak at -0.75 eV would constitute the bare surface state "band". The peak at -0.15 eV would be the "polaron" peak, which is stronger at point $\bar{J}$, in agreement with the fact that the Fermi level of the bare band is closest to E_F at that point. The extracted hole polaron shift of 0.6 eV is of the right order of magnitude for a localized hole, for which our model gave 0.4 eV.

4.4 Surface-state polaron effects in Scanning Tunneling Microscopy

The great usefulness of tunneling of electrons from a sample surface to a metal tip in the study of surface structure has been recently demonstrated experimentally[50]. The tunneling process occurs between electron states on the metal tip and the outermost surface states protruding towards the tip. If V is the voltage drop between the tip and the surface, then tunneling will occur from surface states lying within a depth V from the Fermi surface. Incidentally, this implies that this experimental technique is potentially extremely interesting, when used to study spectra taken as a function of V (positive V would bring information on the filled surface states, negative V on the empty ones). To this date no such study has yet been published, though it seems possible for this technique to develop into a powerful new form of spectroscopy of the surface <u>electron</u> structure (while real-space scanning has already been shown to yield a valuable microscopy of the surface <u>atomic</u> structure).

Surface-state polaron effects may be expected to play an interesting role in the future interpretation of the voltage surface-state spectroscopy suggested above. Let us consider, to start with, the case of V positive, when an electron, originally belonging in a filled surface band, tunnels away from it to flow into the metal tip, leaving a hole in the surface state behind. Two extreme types of situations can be envisaged. If the electron

stripping process is "fast", the lattice has no time to adjust and form a polaron around the hole. Then, the hole energy will be uninfluenced by polaron effects, that can be thus ignored. This is the straightforward analogue of a Franck-Condon transition, such as described for optical absorption, or a photo-emission process. If, on the other hand, the electron stripping occurs slowly enough, the surface lattice will have the time to form a polaron about the hole, whose energy will then be shifted upwards by the amount calculated in the previous sections.

The relevant question is then: how "long" does it take for a surface electron to tunnel from the surface state into the tip? This question, as it turns out, has been rather extensively discussed in the literature, with somewhat variable conclusions. Following Leggett[64], one may define two kinds of times in the problem. One is $\tau_o = \hbar/\Gamma$, with $\Gamma \sim \text{const} \times \exp\left(-d\sqrt{2m\phi/\hbar^2}\right)$, for a barrier of height ϕ and thickness d. Another is $\tau_1 = d\sqrt{m/2\phi}$. The time τ_1 is the "bounce time" over which a successful tunneling event takes place; The time τ_o is the average time one has to wait for a successful attempt, and can clearly be very much longer than τ_1. For d of a few Ångstroms and $\phi \sim 5$ eV, τ_1 is of the order of 10^{-15} sec. We note that this value is about two orders of magnitude shorter than typical lattice readjustment time.

It is at present unclear to us whether the relevant time-scale to discuss possible surface polaron formation during tunneling is τ_0, or τ_1, and this problem will require a separate investigation. The viewpoint that all holes are the result of successful attempts only, each of which lasts the short time τ_1, would lead to the conclusion that polarons have no time to form, and are irrelevant to tunneling. If alternatively we consider that electrons do anyhow leave the surface state, to venture, successfully or not, into the tunneling region with time scale τ_0, then a surface state polaron may be ready around the hole, if $\tau_0 > 10^{-13}$ sec, or not if $\tau_0 < 10^{-13}$ sec. In this case, what appears to be a rather sudden shift of hole energy should show up in the voltage spectroscopy suggested above, as a function of surface-tip distance d, i.e. of current, which depends exponentially upon d.

4.5 Wigner crystallization of carriers in surface states

It is well known that the surface states of semiconductors can be replenished, or emptied of electrons by varying the bulk doping level. In particular, it is known from studies of band bending[65] that on the Si(111)2x1 surface electrons as many as $n \sim 5\times10^{13}$ electrons/cm^2 can be driven into the upper surface state band - or out of the lower surface state band - by strong bulk n-doping - or p-doping. This is quite a large density, and it may not be totally academic to speculate about the state of these excess surface state electrons. A mean distance of the order of 10 Å is already substantially smaller than the average distance of two surface defects on a good quality surface, and so defects can be approximately ignored. In the absence of polaron effects, one would normally expect two-dimensional electrons of this density to be fluid at T = 0. In fact, here, $r_s \sim (m^*/\bar{\varepsilon} a_B \sqrt{\pi n}) \sim 3$ (if $\bar{\varepsilon} \sim 6$ is an effective surface screening, a_B the Bohr radius and a mass $m^* = 1$ is assumed). The effect of strong electron-lattice coupling, however, is that of increasing enormously the effective electron mass. The hole polaron mass for the buckling model of sect. 2, for example, was ~4000. An electron, or a hole, trapped inside a small polaron of this kind is essentially a classical object. Classical 2-dimensional electrons will "Wigner crystallize", neglecting other effects due to long-range fluctuations, all the way from T = 0 up to a melting temperature T_M[66] given approximately by $\Gamma = (k_B T_M)^{-1}(e^2/\bar{\varepsilon})\sqrt{\pi n} \sim 130$. From this, we estimate a melting temperature as high as 25 K. Although residual quantum effects may reduce this temperature, it is nevertheless still substantially higher than 2D melting temperatures seen for electrons on liquid He surfaces[67], of order of 0.4K. In conclusion, we suggest that excess surface state electrons or holes that are responsible for band-bending in a doped semiconductor may be self-trapped polarons, and hence essentially classical objects. As such, they should crystallize at sufficiently low temperature. The crystalline state might become observable experimentally. For example, deformation potentials generate a coupling mechanism between the two-dimensional plasmon-like modes

of this crystal and the Rayleigh wave of the semiconductor. In a way similar to that of electrons on He^{6}, this mechanism would lead to folding of the Rayleigh wave from $K = G = 4\pi\sqrt{n}/2\sqrt{3} \sim 0.5$ $\mathring{A}^{-1}$ back to $k = 0$. In analogy to that case, mixing with the plasmon would make this mode, of frequency as high as 15meV, that would be optically active, and thus observable with either IR absorption or high resolution electron energy-loss.

5. CONCLUDING REMARKS

The main aim of this part has been to introduce the concept, and show the relevance of, polaron effects on electrons that belong in surface states.

This has been pursued by direct study of prototype situations. For this purpose, the 2x1 reconstructed Si(111) surface has been selected, as a system that has received very considerable attention in the past and for which polaron effects, not discussed before, may be of considerable importance. Among the existing models for the reconstructed surfaces, we have chosen the most popular, i.e. buckling, and π-bonded chains. Polaron effects are shown to be very important in either model, and quantitatively more than an order of magnitude larger than in bulk Si, or about as important as in a three-dimensional ionic crystal.

Since strict surface-state transport will probably never be measurable, the main impact of surface state polarons should be on the spectroscopy of surface states. We have concerned ourselves here mostly with optical absorption. A careful polaron study of the electron-hole pairs has been carried out in this light, and a detailed analysis of the absorption lineshape is presented, which also brings out interesting differences between the two reconstruction models. A short discussion at a much more qualitative level is given for surface luminescence, photo-emission, scanning tunneling spectroscopy, as well as for a possible classical crystallization of a dense system of surface state polarons. Our hope is that this paper will stimulate new experimental efforts aimed at elucidating the importance of these polaron effects in surface state spectroscopy.

APPENDIX A

Estimate for the numerical values of the parameters C, γ and H_0' in the buckling model

In order to determine quantitatively the equilibrium values of H_1 and H_2 given by Eqs. (2.13), we must specify the parameters C, γ and H_0'. For C we simply take the value C = 52.8 eV, corresponding to $(\varepsilon_p - \varepsilon_s) = 4.4$ eV, a value introduced empirically by Pandey and Phillips[28] to fit other accurate bulk and surface state calculations. The elastic constant γ and the reference height H_0' are in fact properties of a hypothetical Si(111) surface which a) has no electrons at all in the DB state; b) is ideal, i.e. unreconstructed. We determine them in the following way. Suppose we start with Si(111) in this hypothetical situation. Then "pour in" the 2N surface electrons, while keeping the surface unreconstructed. The total energy change per atom is then

$$\mathcal{E}(H) = \frac{1}{2}\gamma\,(H - H_0')^2 + \varepsilon(H) \quad , \qquad \text{(A1)}$$

where ε is the energy of one electron per DB, $\varepsilon(H) = \varepsilon_p - \frac{C}{2}(\frac{H}{a})^2$. Minimization of (A1) yields

$$H_0 = \frac{\gamma a^2 H_0'}{\gamma a^2 - C} \quad . \qquad \text{(A2)}$$

If we fix $H_0 = .79$ Å, the expected interlayer spacing in the absence of relaxation, then (A2) connects γ and H_0'. For a small uniform displacement Q from equilibrium, the total energy (A1) becomes

$$\mathcal{E}(H+Q) = \text{const.} + \frac{1}{2}\left(\gamma - \frac{C}{a^2}\right)(H_0 + Q - H_0')^2 \qquad \text{(A3)}$$

We can then relate $(\gamma - \frac{C}{a^2})$ to the frequency ω_0 of the surface phonon characterizing the outward/inward relaxation mode of the surface by

$$\frac{1}{2}\left(\gamma - \frac{C}{a^2}\right) = \frac{1}{2} M \omega_0^2 \quad , \qquad \text{(A4)}$$

where M is the atomic mass. We take $\hbar\omega_o$ = 50 meV, a value of the order of a general short wavelength phonon in silicon, and also close to the experimental value of the surface phonon energy observed on Si(111)-2x1 [63]. This yields $(\gamma a^2 - C) \sim 250$ eV, and from (A2) we obtain $H_0' = .65\text{Å}$. Comparison with $H_0 = .79$ Å shows that "pouring in" one electron per DB has produced an <u>outwards</u> surface relaxation. This was of course to be expected, since outwards relaxation of the first layer, by Eqs. (2.1) and (2.2), increases the s-admixture in the DB wavefunction relative to p_z, and ε_s is about 4 eV lower than ε_p.

APPENDIX B - CALCULATION OF THE SELF-ENERGY (3.37)

For $\omega_{k'} \equiv \omega_o$ and $V_{kk'} \equiv V$ (independent of $\underline{k}$ and $\underline{k}'$), Eq. (3.37) can be rewritten in a slightly more convenient form

$$\Sigma(E) = |V|^2 (n_{\omega_o} + 1) \sum_{\underline{k}'} \frac{1}{E - \varepsilon_{k'} - \hbar\omega_o - \Delta(E-\hbar\omega_o) - i\Gamma(E-\hbar\omega_o)}$$

$$+ |V|^2 n_{\omega_o} \sum_{\underline{k}'} \frac{1}{E - \varepsilon_{k'} + \hbar\omega_o - \Delta(E+\hbar\omega_o) - i\Gamma(E+\hbar\omega_o)}, \quad \text{(B1)}$$

where we have taken into account the independence of $\Sigma_k(E)$ on $\underline{k}$ and used $\Sigma(E) = \Delta(E) + i\Gamma(E)$. For our dimerized chain model the sums over $\underline{k}'$ reduce to one-dimensional integrals from $\frac{-\pi}{a}$ to $\frac{\pi}{a}$ along the $\overline{\Gamma J}$ direction of the SBZ. For the simple effective mass dispersion $\varepsilon_k = \frac{k^2}{2m^*}$, these integrals can be carried out analytically. However, before writing down their expressions - which are quite cumbersome - it is convenient to establish a few notations. Separating the real and imaginary parts of $\Sigma(E)$ on the left-hand side of (B1), we can write

$$\Delta(E) = \frac{1}{2} \frac{|V|^2}{\sqrt{\varepsilon_L \hbar\omega_o}} \left[(1 + n_{\omega_o})\, \Delta_1(E) + n_{\omega_o}\, \Delta_2(E) \right]$$

$$\Gamma(E) = \frac{1}{4} \frac{|V|^2}{\sqrt{\varepsilon_L \hbar\omega_o}} \left[(1 + n_{\omega_o})\, \Gamma_1(E) + n_{\omega_o}\, \Gamma_2(E) \right], \quad \text{(B2)}$$

where $\varepsilon_L = \frac{h^2\pi^2}{2m^*a^2}$. Let us next define (i = 1, 2)

$$\varphi_i(E) = \arg A_i(E) \quad , \tag{B4}$$

$$Q_i(E) = |A_i(E)|^{-1} \quad , \tag{B5}$$

$$R_i(E) = \mathrm{Re}\left[A_i^{-1}(E)\right] \quad , \tag{B6}$$

$$I_i(E) = -\,\mathrm{Im}\left[A_i^{-1}(E)\right] \quad , \tag{B7}$$

where

$$A_1(E) = \frac{1}{E - \hbar\omega_0 - \Delta(E-\hbar\omega_0) - i\,\Gamma(E-\hbar\omega_0)} \quad , \tag{B8}$$

and

$$A_2(E) = \frac{1}{E + \hbar\omega_0 - \Delta(E+\hbar\omega_0) - i\,\Gamma(E+\hbar\omega_0)} \, . \tag{B9}$$

We start with $\Gamma_i(E)$, which has a somewhat simpler expression

$$\Gamma_i(E) = \sqrt{\frac{\hbar\omega_0}{Q_i}} \left\{ \sin(\varphi_i/2) \ln \left| \frac{\mathcal{E}_L + 2\sqrt{\mathcal{E}_L Q_i}\cos(\varphi_i/2) + Q_i}{\mathcal{E}_L - 2\sqrt{\mathcal{E}_L Q_i}\cos(\varphi_i/2) + Q_i} \right| \right.$$

$$\left. + 2\cos(\varphi_i/2)\left(\theta_i + \frac{\pi}{2}\right) \right\} \quad , \tag{B10}$$

with

$$\vartheta_i(E) = tg^{-1} \frac{\varepsilon_L - Q_i}{2\sqrt{\varepsilon_L Q_i}\,\sin(\varphi_i/2)} \,. \qquad \text{(B11)}$$

For the two terms contributing to $\Delta(E)$ in (B2) we find

$$\Delta_i(E) = \sqrt{\frac{\hbar\omega_0}{Q_i}} \left\{ \frac{R_i + Q_i}{2I_i} \sin(\varphi_i/2)\, \ln \left| \frac{\varepsilon_L + 2\sqrt{\varepsilon_L Q_i}\cos(\varphi_i/2) + Q_i}{\varepsilon_L - 2\sqrt{\varepsilon_L Q_i}\cos(\varphi_i/2) + Q_i} \right| \right.$$

$$\left. + \frac{\cos(\varphi_i/2)}{\sin\varphi_i} \left[\frac{R_i}{Q_i} \left(\vartheta_i + \frac{\pi}{2}\right) - \vartheta_i^+ - \vartheta_i^- \right] \right\} , \qquad \text{(B12)}$$

where

$$\vartheta_i^{\pm}(E) = tg^{-1} \frac{\sqrt{\varepsilon_L} \pm \sqrt{Q_i}\cos(\varphi_i/2)}{\sqrt{Q_i}\,\sin(\varphi_i/2)} \,. \qquad \text{(B13)}$$

We recall that all terms, such as Q_i, R_i, φ_i, etc. in (B10) and (B12) are functions of E through (B4)-(B7).

The expressions (B2) and (B3) - with (B10) and (B12) - are already in a form which can be easily programmed for a numerical iterative solution, starting for instance from $\Delta(E) \equiv 0$ and $\Gamma(E) \equiv \gamma << 1$ (a small but finite value of γ is of course necessary to avoid divergencies). To test the convergence we monitored the value $\mathcal{J}$ of the integral of the spectral function

$$\mathcal{J} = \frac{1}{\pi} \int dE \, \frac{\Gamma(E)}{(E - \Delta(E))^2 + \Gamma^2(E)} \,.$$

Good convergence ($< 10^{-4}$) usually requires about 20 iterations.

Table 2.1

	H_e	H_h	H_c	H_d	H_g	H_l
Before relaxation	.657	.990	.657	.657	.990	.990
After relax. (exciton)	.727	.860	.658	.658	.990	.990
After relax. (electron)	.801	.988	.657	.657	.988	.988
After relax. (hole)	.653	.765	.653	.653	.990	.990

Vertical distance from the second atomic plane (in Å) of the surface atoms shown in Fig. 2.4, before and after the relaxation following creation of an exciton (with the electron at 'e' and the hole at 'h'). Also given for comparison are the relaxed atomic position for a single electron at 'e' and a single hole at 'h'. For the 'ideal' Si(111) surface, the distance between the first and the second atomic plane is $H_0 = .79$Å.

Table 3.1

T(°K)	2	152	302	452	602
E_o(eV)	.49	.49	.45	.40	.35
Γ_o(eV)	1.5×10^{-5}	9.1×10^{-3}	4.4×10^{-2}	8.8×10^{-2}	.13

Position and halfwidth $\Gamma_0 \equiv \Gamma(E_0)$ of the main peak in the absorption spectrum of the dimerized chain model of Si(111)-2x1 as a function of temperature, as given by Eq. (3.37). In the absence of coupling to the lattice the peak position would be $\varepsilon_0 = .70$ eV. Note that the values of E_0 in this Table do not include the effect of temperature dependence of the reconstruction magnitude, discussed in Sect. 4.1. This additional effect is included in the values reported in Table 4.1.

Table 4.1

$T(^{\circ}K)$	2	152	302	452	602
$\hbar\omega_{peak}$ (eV) (Buckling)	.47(0)	.47(0)	.46(8)	.46(5)	.46(2)
$\hbar\omega_{peak}$ (eV) (π-bonded chains)	.49(4)	.49(8)	.46(5)	.42(3)	.38(0)

Position of the absorption peak as a function of temperature for the buckling and π-bonded chain models of Si(111)-2x1. In both cases the calculated values are inclusive of the lattice dilation effects and coupling to the vibrational modes.

REFERENCES

1. For a review of UPS up to 1980, see D.E. Eastman, J. Vac. Sci. Technol. 17, 492 (1980).

2. G. Chiarotti, S.Nannarone, R. Pastore and P. Chiaradia, Phys. Rev. B4, 3398 (1971);
P. Chiaradia, G. Chiarotti, S.Nannarone and P. Sassaroli, Sol. St. Comm. 26, 813 (1978).

3. J.E. Rowe and H. Ibach, Phys. Rev. Lett. 31, 102 (1973); R. Matz, H. Lüth and A. Ritz, Sol. St. Comm. 46, 343 (1983).

4. M. Schlüter, J.R. Chelikowsky, S.G. Louie and M.L. Cohen, Phys. Rev. B12, 4200 (1975).

5. J.A. Appelbaum and D.R. Hamann, Rev. Mod. Phys. 48, 479 (1976).

6. J.E. Northrup, J. Ihm and M.L. Cohen, Phys. Rev. Lett. 47, 1910 (1981).

7. K.C. Pandey, Phys. Rev. Lett. 49, 223 (1982).

8. J.E. Northrup and M.L. Cohen, Phys. Rev. Lett. 49, 1349 (1982).

9. E. Tosatti, in Festkörperprobleme (Adv. in Sol. St. Phys.) Vol XV, p. 113, H.J. Queisser (ed.), Pergamon/Vieweg, Braunschweig (1975).

10. K. Thoma, Z. Physik B23, 49 (1976).

11. G. Allan and M. Lannoo, Surf. Sci. 63, 11 (1977).

12. C.T. White and K.L. Ngai, Phys. Rev. Lett. 41, 885 (1978).

13. R. Del Sole and D.J. Chadi, Phys. Rev. B24, 1120 (1981).

14. C.B. Duke and W.K. Ford, Surf. Sci. 111, L685 (1981).

15. A. Muramatsu and W. Hanke, Phys. Rev. B27, 2609 (1983).

16. A. Muramatsu and W. Hanke, in "Abinitio calculation of phonon spectra", J.T. Devreese (ed.), Plenum Publishing Co., 1983.

17. F. Guinea and C. Menéndez, Phys. Rev. B27, 1432 (1983).

18. D. Haneman, Phys. Rev. 121, 1093 (1961).

19. K.C. Pandey, Phys. Rev. Lett. 47, 1913 (1981).

20. J.J. Quinn and R.A. Ferrell, Phys. Rev. 112, 812 (1958).

21. F. Bassani and G. Pastori-Parravicini "Electronic states and optical transitions in Solids", Pergamon Press (1975).

22. R. Del Sole and E. Tosatti, Sol. St. Comm. 22, 307 (1977).

23. H. Haken, in "Polarons and Excitons", C.G. Kuper and C.D. Whitfield (eds.), Edinburgh (1962).

24. S.D. Mahanti and C.M. Varma, Phys. Rev. B6, 2209 (1972).

25. M. Rovere and E. Tosatti, Nuovo Cim. 39B, 538 (1977).

26. Y. Toyozawa, in "The Physics of elementary Excitations", Chapt. 7; S. Nakajima, Y. Toyozawa and R. Abe (eds); Sol. St. Sciences vol 12; Springer-Verlag (1980).

27. G. Chiarotti, in "Theory of Imperfect Crystalline Solids", Trieste lectures 1970, IAEA, Vienna (1971).

28. K.C. Pandey and J.C. Phillips, Phys. Rev. Lett. 32, 1433 (1974); Phys. Rev. Lett. 34, 1450 (1975); Phys. Rev. B13, 750 (1976).

29. H. Fröhlich, in "Polarons and Excitons", C.G. Kuper and C.D. Whitfield (eds), Edinburgh (1962).

30. W. Andreoni and E. Tosatti, Proc. 7th Intern. Vac. Congr. & 3rd Intern. Conf. Solid Surfaces, Vienna (1977), ed. by L. Dobrozemski et al, p. 591.

31. It should be noted however that the ionic charge transfer would not be quite so large had intra-atomic electron-electron repulsions been considered. This is an artifact of the one-electron hamiltonian (2.3), which for the present purposes does not have any negative consequence.

32. As a general reference see e.g. C.G. Kuper and C.D. Whitfield (eds): Polarons and Excitons, Edinburgh (1962).

33. This decay is actually exponential, at least in a simple model like ours, where all vibrational frequencies are finite (Einstein-like).

34. This balance is qualitatively very similar to that of a Jahn-Teller distortion h, where the total energy has a form $E = -\alpha h$(electronic) + βh^2(lattice). In this case exactly half the electronic gain is absorbed by the lattice distortion.

35. See e.g. W. Kohn, in "Lectures in Theoretical Physics", ed. by R. Balian and C. De Witt, (Gordon and Breach, 1967).

36. E. Clementi and C. Roetti, Atomic Data and Nuclear Data Tables, 14 (1974).

37. M. Schlüter, Proceedings of the International School "E. Fermi" of Varenna ed. by F. Bassani, F. Fumi and M. Tosi (1983), to appear.

38. K.C. Pandey, Phys. Rev. B25, 4338 (1982). Recent measurements of the surface reflectivity of Si(111)2x1 using polarized radiation seem actually to favour a symmetric (probably somewhat buckled) chain configuration rather than the dimerized (asymmetric) one discussed in this paper (see Ref. (54)). Polaron effects, however, are expected to be qualitatively similar for the two cases. In particular, also the buckled chain is an intermediate coupling situation.

39. W. P. Su, J.R. Schrieffer and A.J. Heeger, Phys. Rev. B22, 2099 (1980).

40. R.I.G. Uhrberg, G.V. Hansson, J.M. Nicholls and S.A. Flodström, Phys. Rev. Lett. 48, 1032 (1982).

41. Actually, the strong analogy with polyacetylene raises the question of whether soliton could occur on this π-bonded chain model[39]. We have chosen not to pursue the issue of solitons in this paper. Should the π-bonded dimerized chain model be definitely established for the Si(111)-2x1 surface, this issue might well be worth taking up again.

42. This fact follows generally for any situation where the energy change is of the form $\Delta E = \alpha_1 d + \alpha_2 d - \frac{1}{2}\gamma d^2$ where $\langle \Delta E \rangle_{min} = \frac{2\alpha^2}{\gamma} + \frac{2\alpha^2}{\gamma} - \frac{2\alpha^2}{\gamma}$ if $\alpha_1 = \alpha_2 \equiv \alpha$. Hence exact cancellation between the filled band contribution and the elastic term is expected to occur for example, also in the case of polyacetylene, which has a similar band structure.

43. T. Holstein, Ann. Phys. 8, 325 (1959).

44. L. Hedin and S. Lundqvist, in Sol. St. Phys. vol. 23, p. 1: edited by F. Seitz, D. Turnbull and H. Ehrenreich; Academic, New York (1969).

45. C. Kittel, "Quantum Theory of Solids", John Willey & Sons, Inc., New York-London (1963).

46. T. Ando, A. Fowler and F. Stern, Rev. Mod. Phys. 54, 437 (1982).

47. L.V. Keldysh, JETP Lett. 29, 653 (1979).

48. R. Del Sole and A. Selloni, to be published.

49. In this respect it is interesting to note that the resulting "triplet" exciton condensate" would be an insulator with negligible dimerization, with strong analogy with the state suggested by A. Ovchinnikov et al., Usp. Fiz. Nauk, 108, 81 (1972) (Sov. Phys. Usp. 15, 575 (1973)), for polyacetylene and other 1-D chain systems. It is not clear to us whether the question of triplet excitons has been investigated at all in polyacetylene.

50. G. Binnig H. Rohrer, Ch. Gerber and E. Weibel, Phys. Rev. Lett. 49, 57 (1982); Phys. Rev. Lett. 50, 120 (1983).

51. H.Y. Fan, Phys. Rev. 82, 900 (1951).

52. V. Heine and J.A. Van Vechten, Phys. Rev. B13, 1622 (1976).

53. C. Kittel,"Introduction to Solid State Physics" (John Wiley & Sons, Inc. 1976), Ch. 6.

54. P. Chiaradia, A. Cricenti, S. Selci and G. Chiarotti, to be published; R. Del Sole and A. Selloni, to be published.

55. R.M. Tromp, L. Smit and F.J. van der Veen, Phys. Rev. Lett. 51, 1672 (1983).

56. R. Feder, Solid State Commun. 45, 51 (1983).

57. H. Lui, M.R. Cook, F. Jona, and P.M. Marcus, Phys. Rev. B28, 6137 (1983).

58. J.E. Demuth, B.N.J. Persson, and A.J. Schell-Sorokin, Phys. Rev. Lett. 51, 2214 (1983).

59. C.O. Almbladh, Phys. Rev. B16, 4343 (1977).

60. F. Evangelisti and J. McGroddy, Solid State Commun. 25, 1157 (1978).

61. F.J. Himpsel, P. Heimann and D.E. Eastman, Phys. Rev. B24, 2003 (1981); F. Houzay, G. Guichar, R. Pinchaux, G. Jezequel, F. Solal, A. Barski, P. Steiner, and Y. Petroff, Surface Sci. 132, 40 (1983).

62. L. Hedin and A. Rosengren, J. Phys. F7, 1339 (1977).

63. G. Sawatzky, priv. commun.; D.K.G. de Boer, thesis, University of Groningen (1983).

64. A.J. Leggett, Progr. Theor. Phys. Suppl. 69, 80 (1980); see also the later discussion of M. Büttiker and R. Landauer, Phys. Rev. Lett. 49, 1739 (1982).

65. F.G. Allen and G.W. Gobeli, J. Appl. Phys. 35, 597 (1964).

66. R.C. Gann, S. Chakravarty and G.V. Chester, Phys. Rev. B20, 326 (1979).

67. C.C. Grimes and G. Adams, Phys. Rev. Lett. 42, 795 (1979).

68. H. Ibach, Phys. Rev. Lett. 27, 253 (1971).

FIGURE CAPTIONS

Fig. 2.1 Geometrical arrangement of surface atoms for the buckling model of Si(111)-2x1. Black dots and empty circles represent raised and lowered first-layer atoms respectively.

(a) Top view; a = 3.85 Å is the surface lattice constant along the $[1\bar{1}0]$ direction.

(b) Side view; H_1 and H_2 are the vertical distances of the raised and lowered atoms from the second atomic plane (not in scale).

(c) The surface Brillouin zone.

Fig. 2.2 Surface-state energy bands for the buckling model of Si(111)-2x1, with $(\varepsilon_2 - \varepsilon_1) = .98$ eV and t = .075 eV. The zero of the energy scale is the midgap energy.

Fig. 2.3 Surface atoms involved in the relaxation following injection of a) an excess electron in (0,2); b) an excess hole in (0,1). The figures in square brackets denote the electron (hole) wave function square amplitude at the various sites after relaxation.

Fig. 2.4 Surface atoms involved in the relaxation following creation of an exciton, with the hole localized at 'h" and the electron at 'e'.

Fig. 2.5 Qualitative energy-configuration diagram for the ground state and the lowest singlet exciton of our buckling model of Si(111)-2x1. $\varepsilon_0 = .47$ eV is the position of the absorption peak according to Franck-Condon's principle, $E_R^{exc} = .35$ eV is the energy released after optical excitation, $\varepsilon_1 \approx \varepsilon_0 - (E_R^{ext} + \varepsilon_2) \approx 0$ is where the luminescence line should be.

Fig. 2.6 Normalized absorption lineshape at various temperatures for the buckling model of Si(111)-2x1, in the Condon approximation. The width of each line of each line of the histogram is E = 10 meV. The modulations

are due to two different vibrational frequencies of the excited state ($\hbar\omega_+$ = 59 meV and $\hbar\omega_-$ = 50 meV), as discussed in the text. Note that before these calculated lineshpaes can be compared with experiments, the additional rigid red shift due to T-dependence of the reconstruction magnitude discussed in Sect. 4.1 must be considered.

Fig. 3.1 Atomic arrangement in the surface plane for the π-bonded chain model of Si(111)-2x1 (top view):

(a) the symmetric chain model, where (n,i) is the i-th atom in the n-th unit cell and a = 3.85 Å;

(b) the dimerized chain model (for clarity of the figure the dimerization is strongly magnified);

(c) atomic displacement pattern for the 'dimerization mode';

(d) the surface Brillouin zone.

Fig. 3.2 The surface bandstructure of the dimerized chain model of Si(111)-2x1, with t_1 = -.9 eV and t_2 = -.45 eV. The zero of the energy scale is the midgap energy, i.e. the surface Fermi level.

Fig. 3.3

(a) Qualitative picture of the lattice distortions caused by a strongly localized excess electron for the dimerized chain model.

(b) Electron-polaron envelope function g_n, Eq. (3.27); n is the cell label along a given chain; g_n is symmetric for n → (-n).

Fig. 3.4 Real (Δ) and imaginary (Γ) parts of the electron and hole self-energies, Eq. (3.37):

(a) at T = 0°K and (b) at T = 300°K. The zero of the energy scale is here the bottom of the conduction band at $\bar{J}$ (on top of the valence band for the hole). The intersections between the lines $E - \varepsilon^0(k)$ and $\Delta(E)$ give the solutions of the Dyson equation (3.30).

Fig. 3.5 Polaron bands along the chain direction $\overline{\Gamma J}$, obtained by solution of the Dyson equation as shown in Fig. 3.4:
(a) at T = 0°K; (b) at T = 300°K. The dashed lines are the bare bands, before coupling to the lattice. The solid lines show the first, sharp, polaron band. The shaded area is centered about the mid-point of the second, broad polaron band, its width reflecting the corresponding energy width 2Γ.

Fig. 3.6
(a) (Inverted) electron-hole interaction potential for singlet excitons along the chain direction using: U = 1.9 eV, ε_{bg} = 6.5 and DB screening evaluated according to the macroscopic three-layer model (see text).
(b) Envelope function for the lowest singlet exciton.

Fig. 3.7 Absorption spectrum of the dimerized chain model at various temperatures, calculated according to (3.48). Note that before these calculated lineshapes can be compared with experiment, the additional rigid blue shift discussed in Sect. 4.1 must be considered. The origin of the oscillations is described in the text.

Fig. 4.1 Room temperature optical absorption of the Si(111)2x1 (after Chiaradia et. al, ref.(54)).

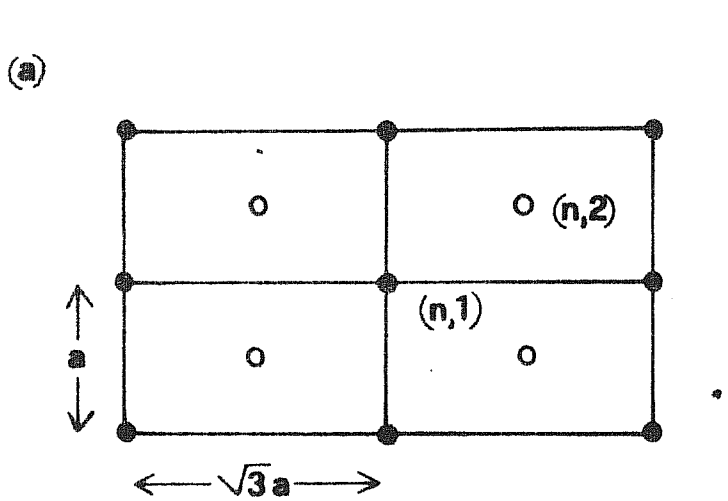

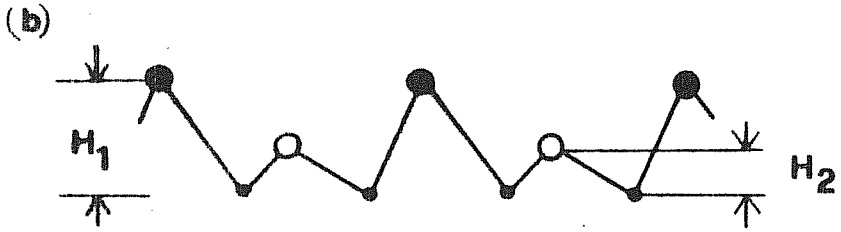

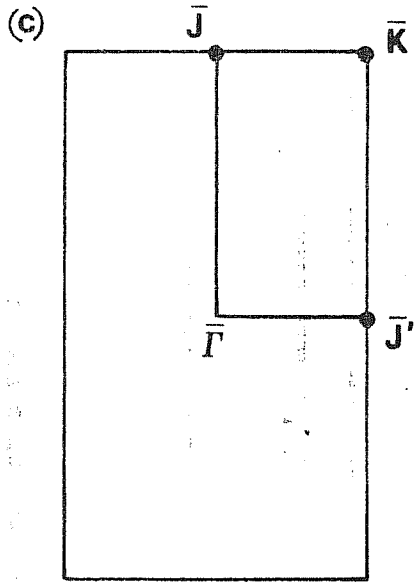

CHEN, Sellom, Jozetti Fig 2.1

CHEN, Selloni, Tosatti Fig 2.2

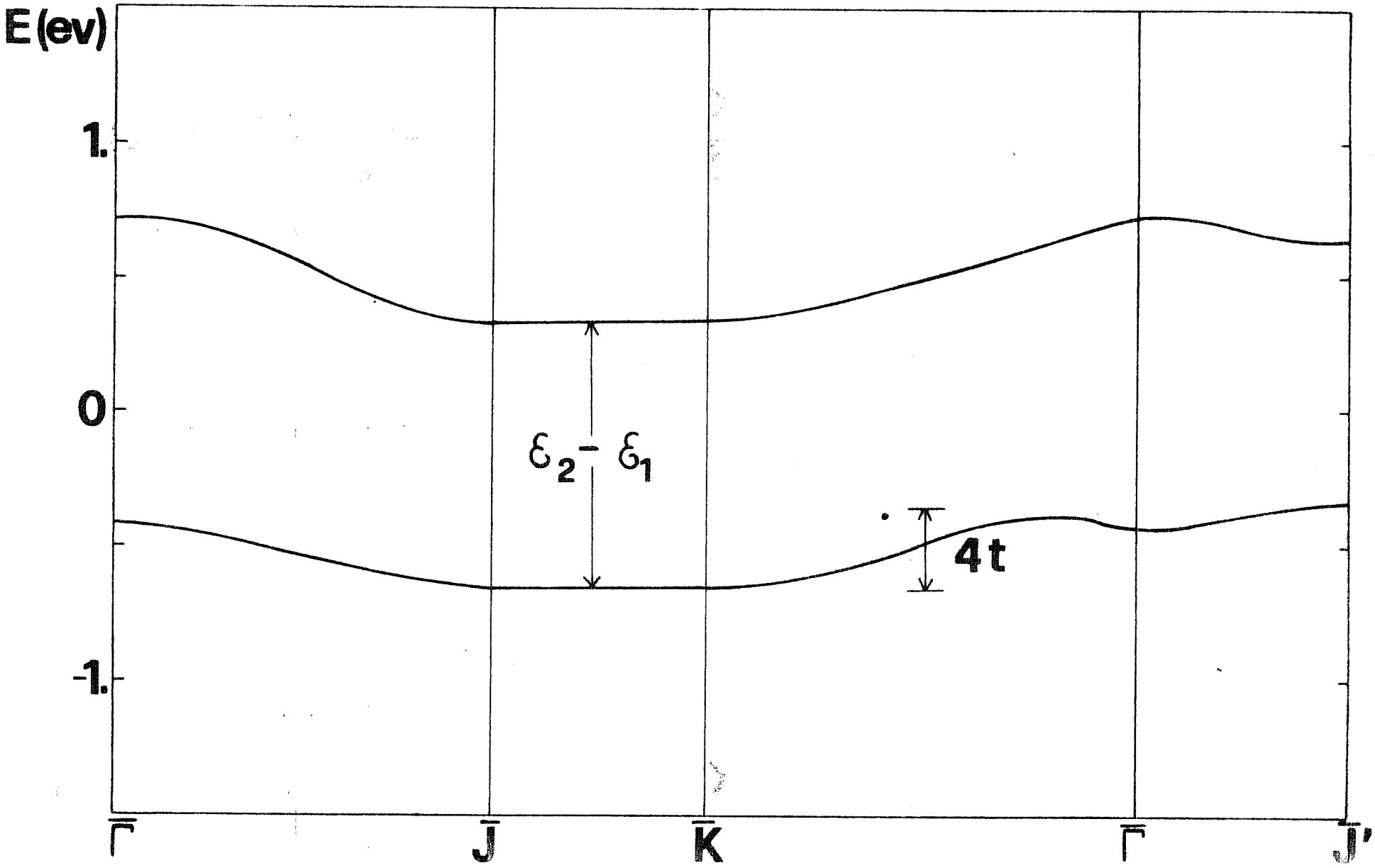

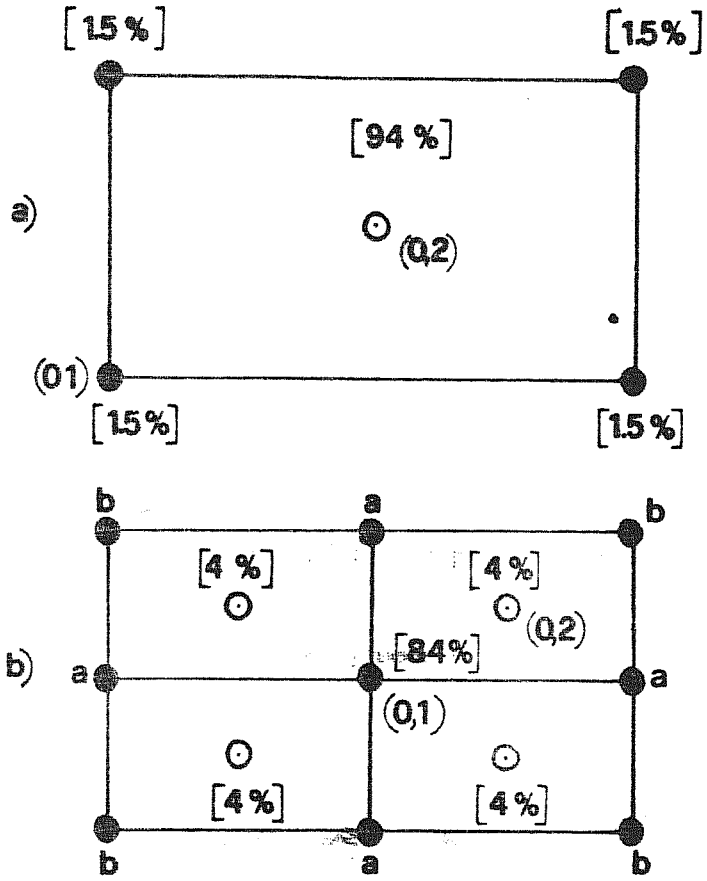

CHEN. Sellom. Tozatti Fig 2.3

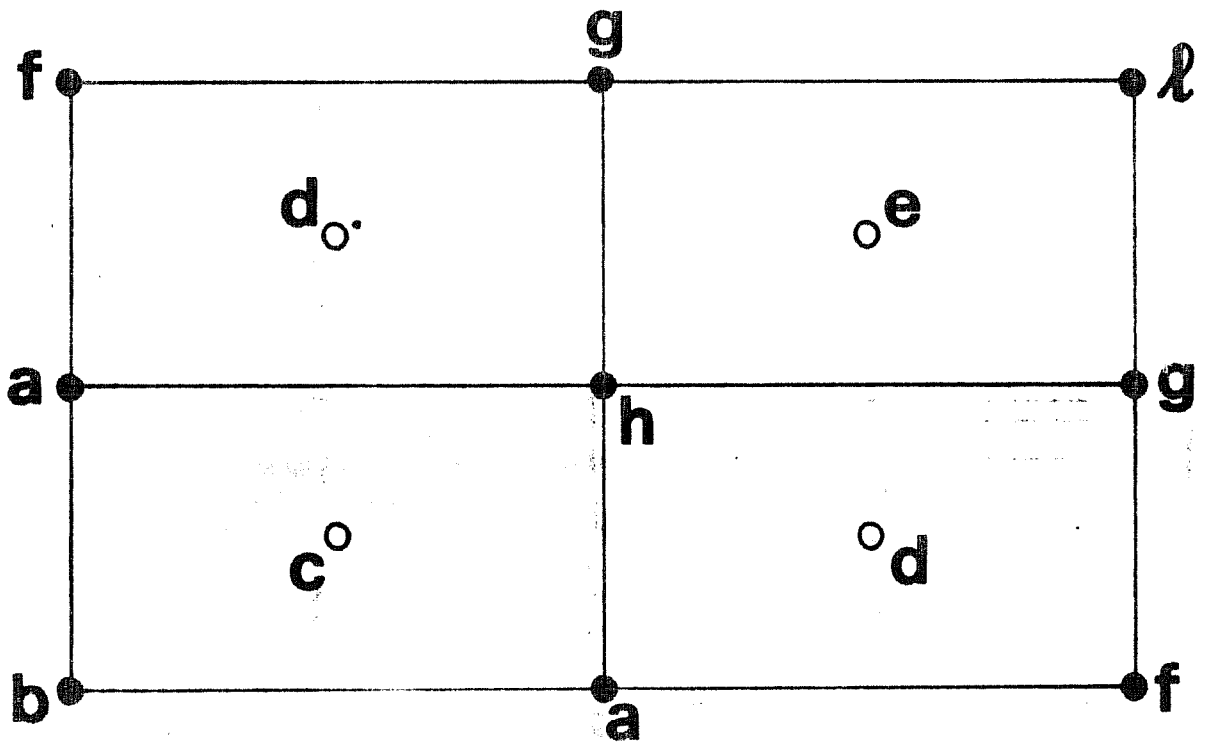

Chen. Sellon. Tozatti Fig 2.4

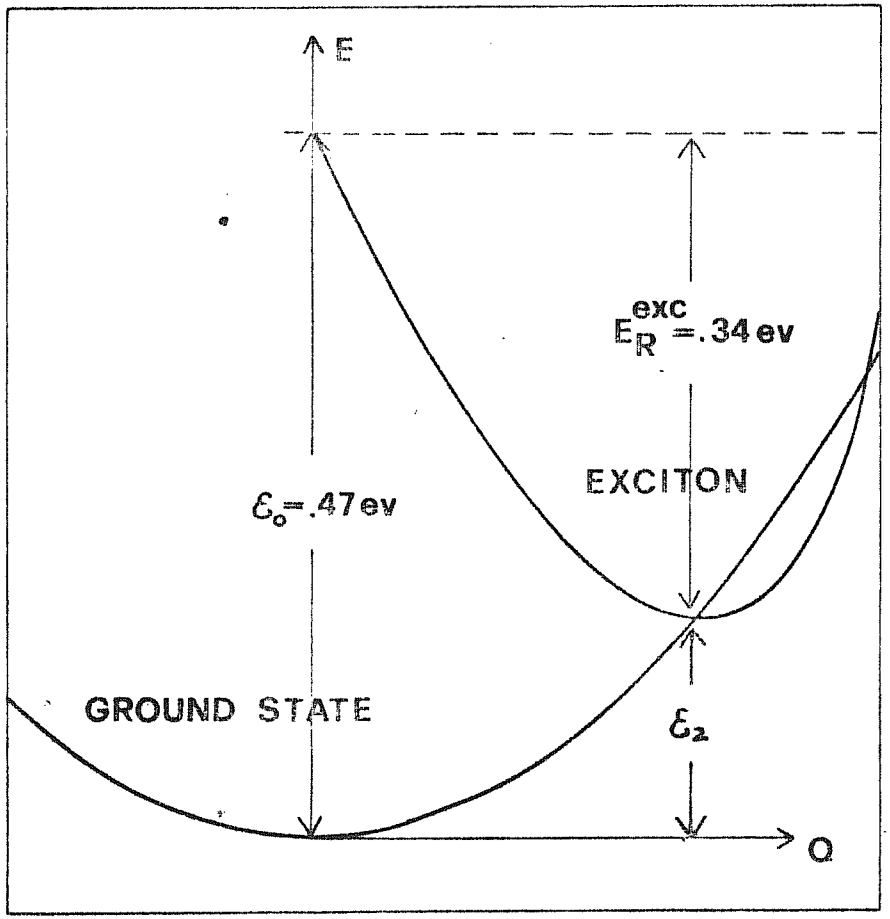

Chen, Sellon, Jortner
Fig 2.5

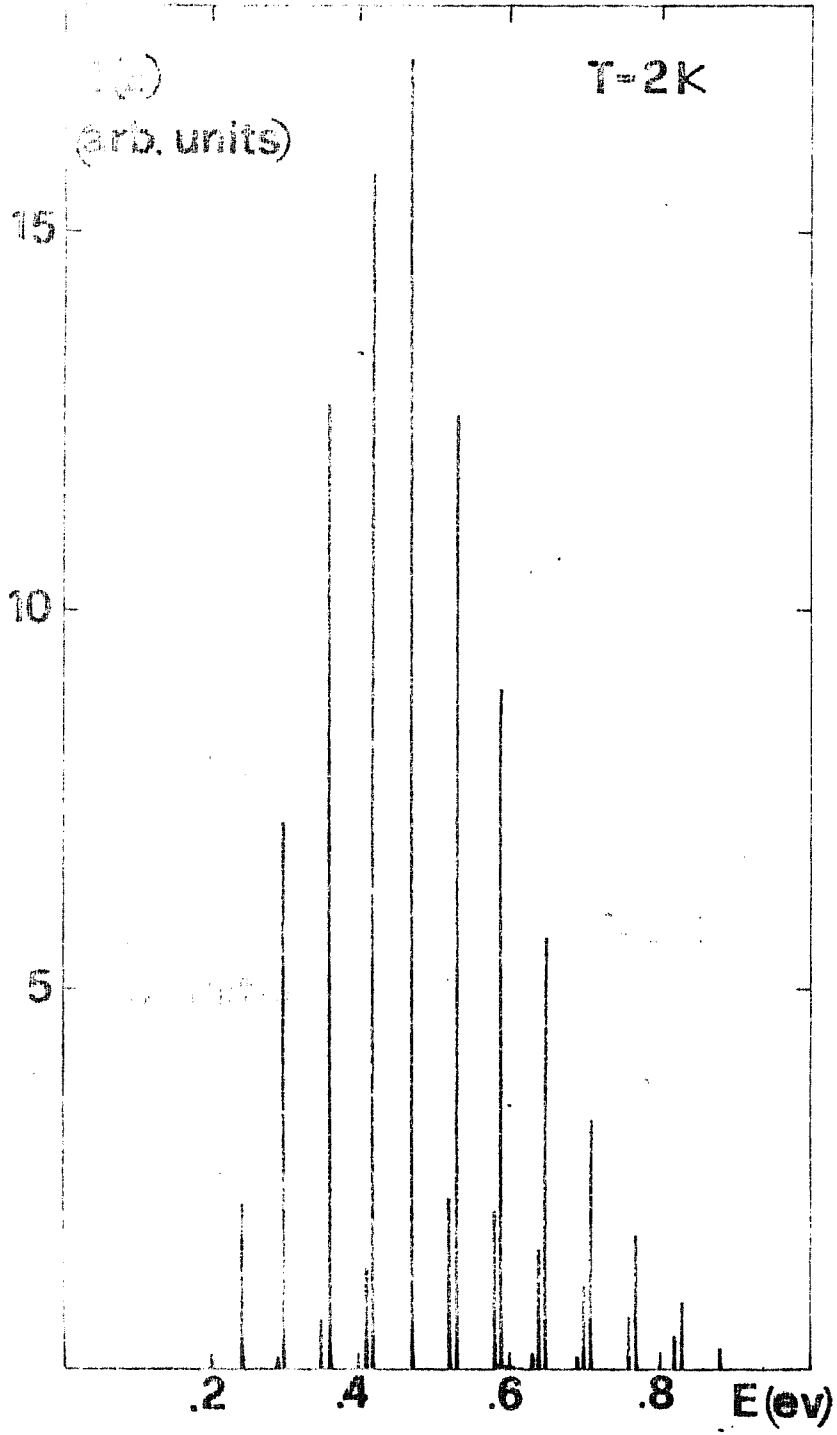
I(E)
(arb. units)
T=2K
15
10
5
.2
.4
.6
.8
E(ev)

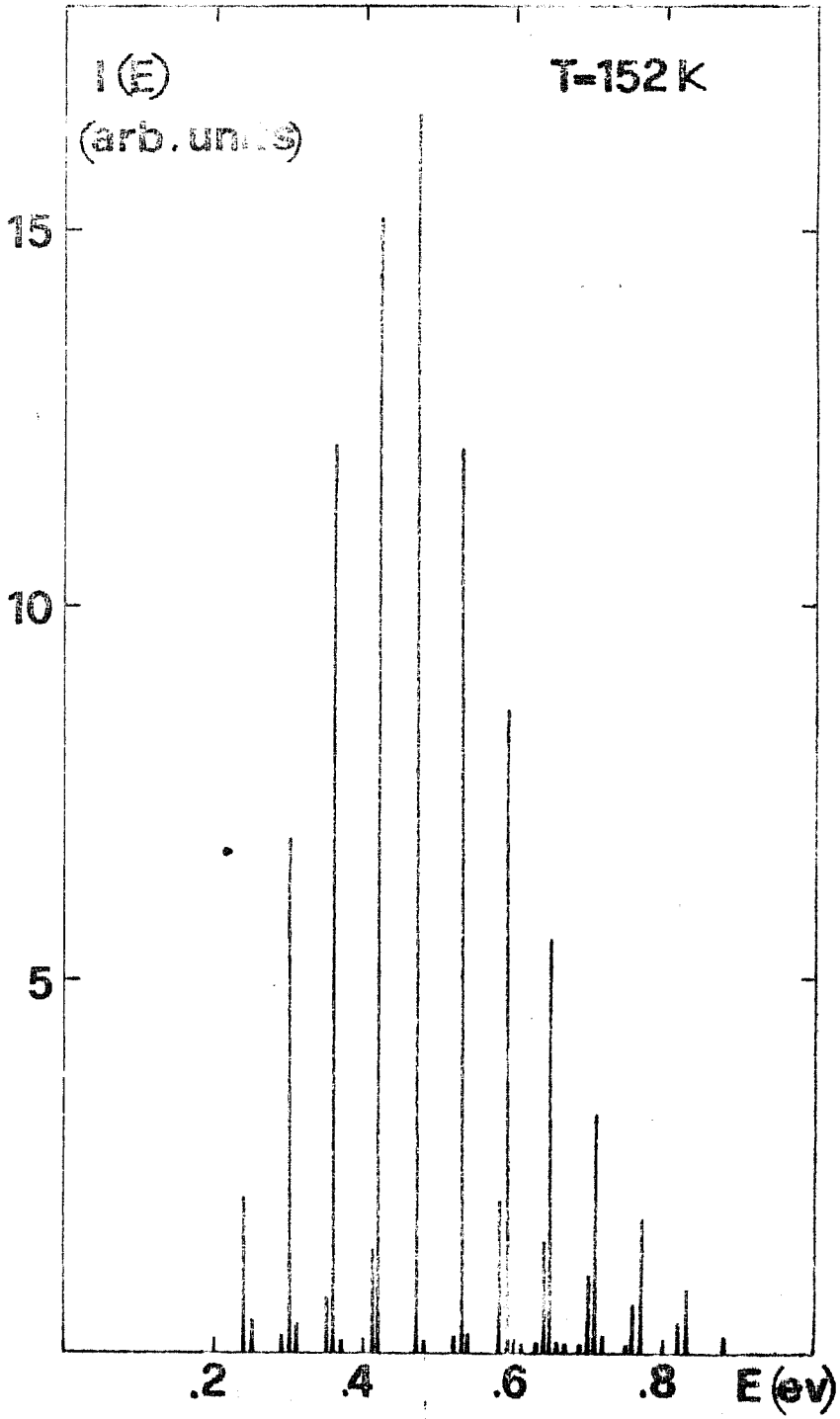
I(E)
(arb. units)
T=152K
15
10
5
.2
.4
.6
.8
E(ev)

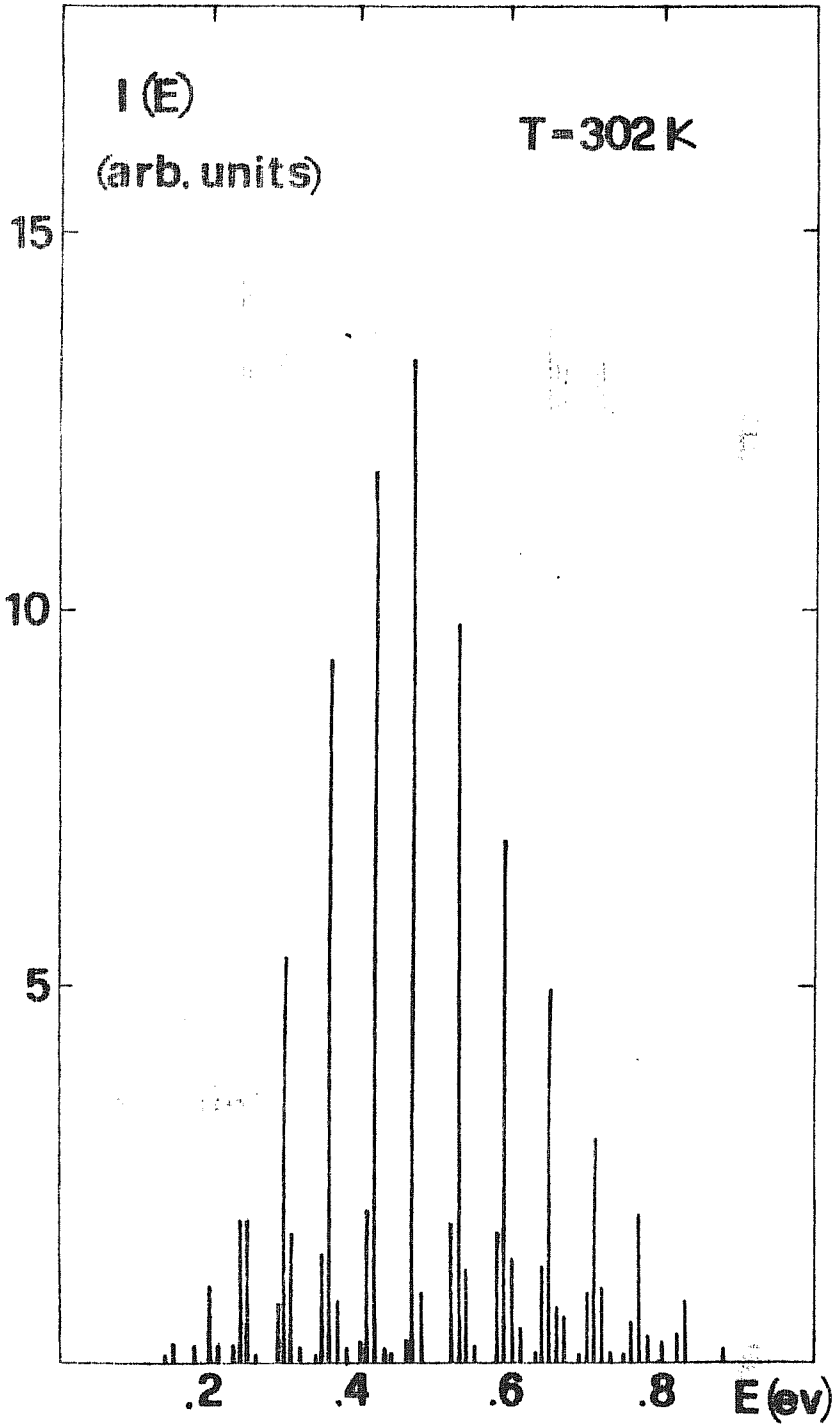

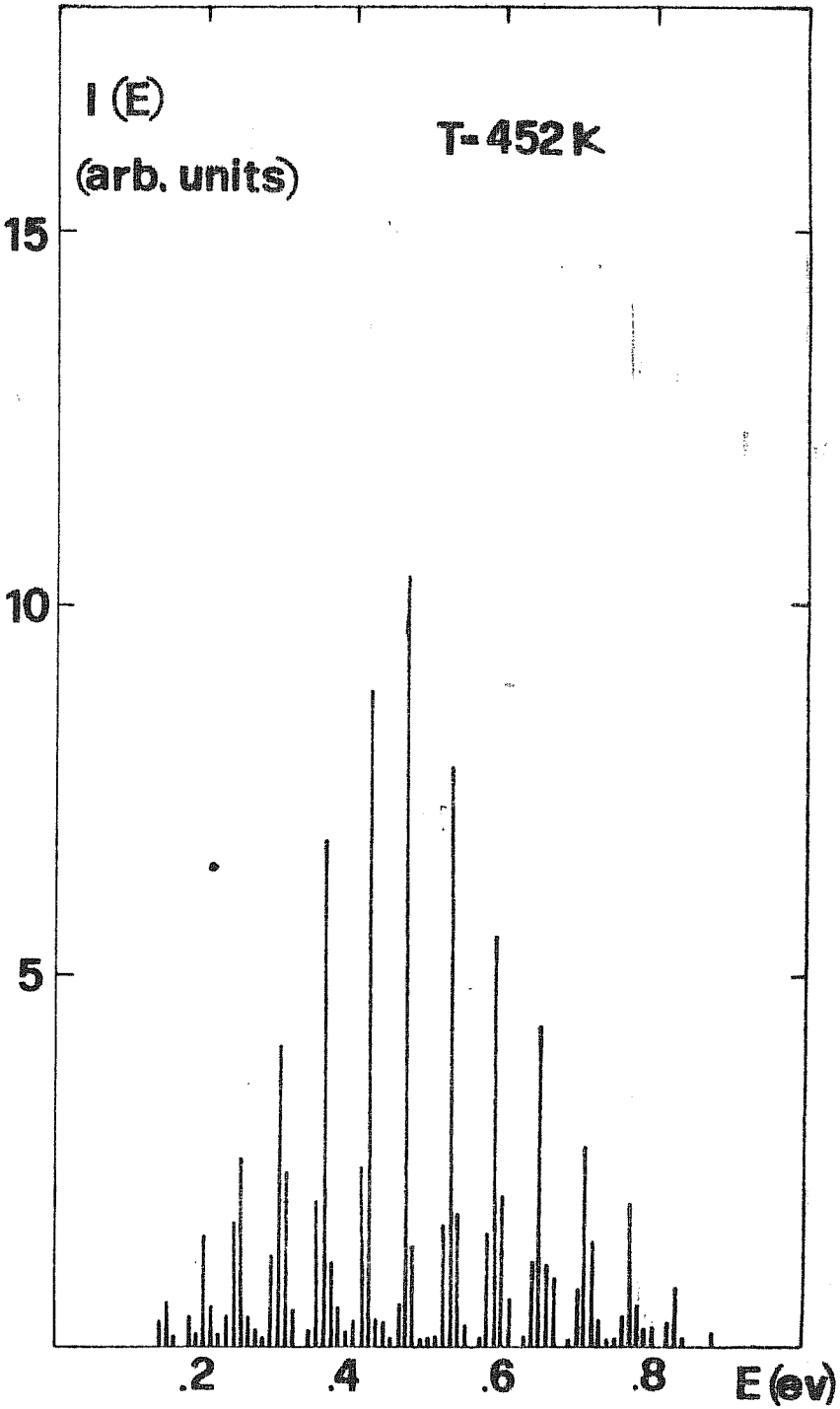

Clean Pt(100), Fig. 2.6

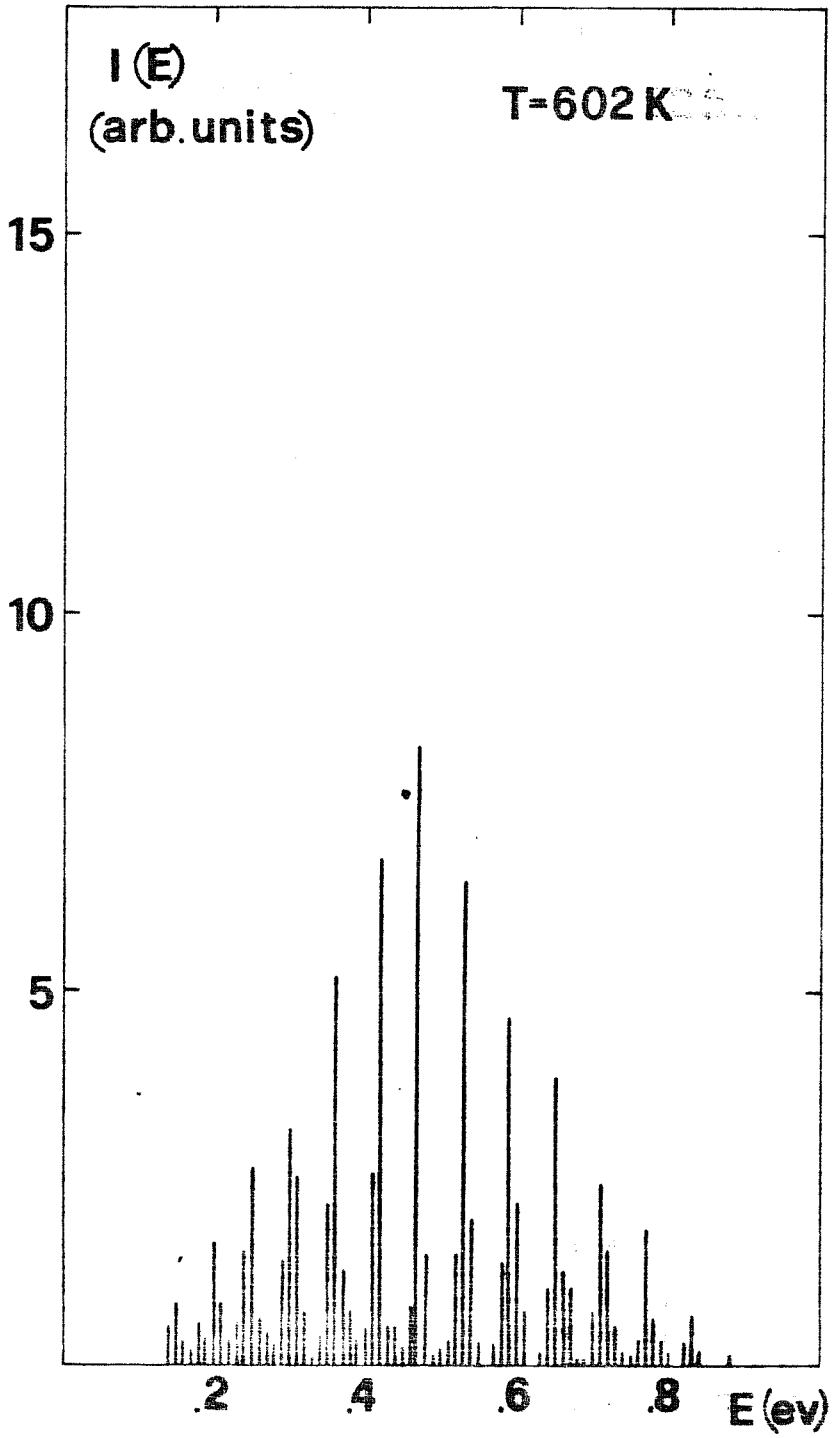

Chen, Sellers, Forsetti Fig 2.6

Chem. Letters, Japan. Fig 3 1

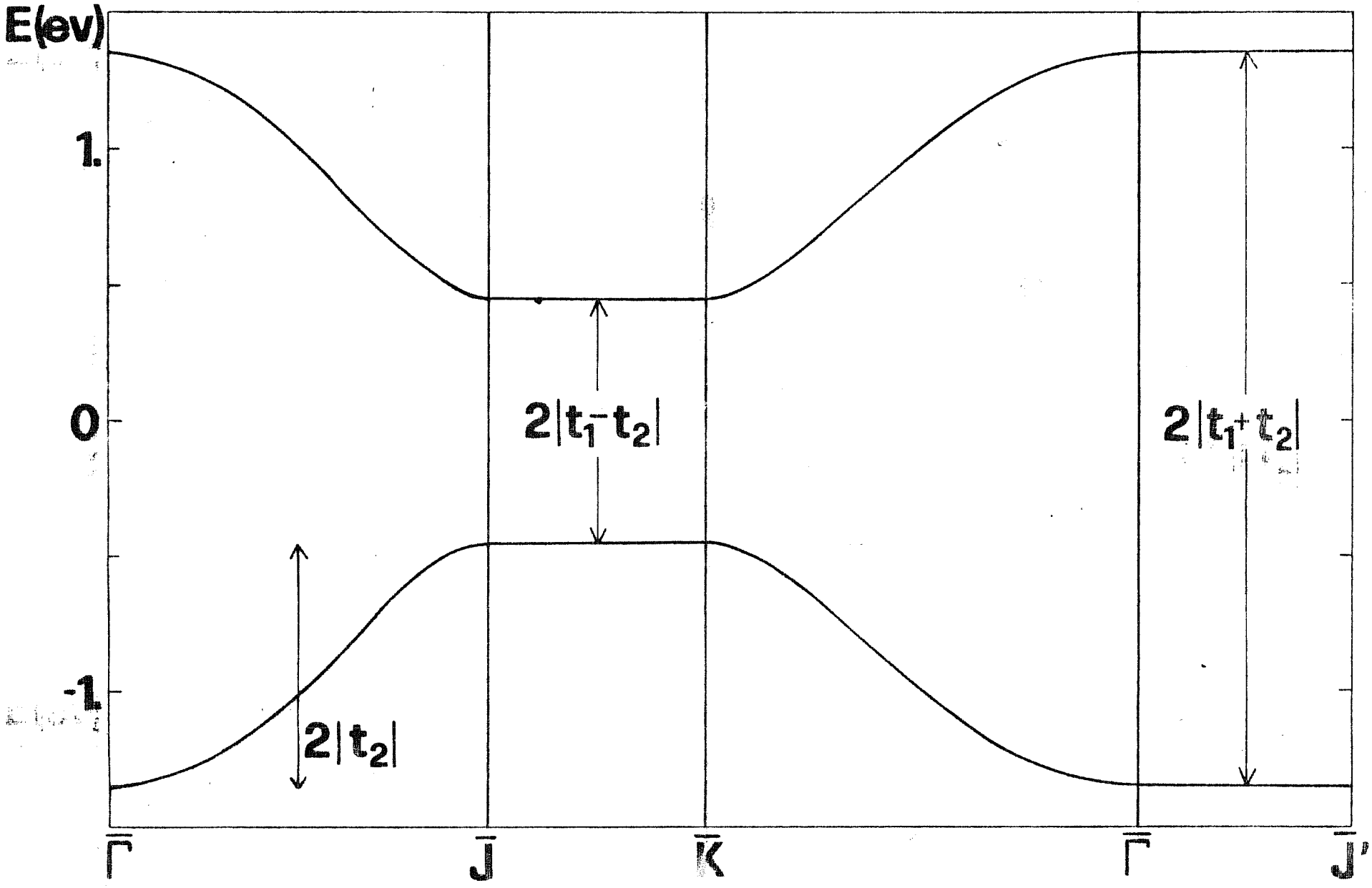
E(ev)
1.
0
-1
$2|t_1^- t_2|$
$2|t_1^+ t_2|$
$2|t_2|$
$\bar{\Gamma}$
$\bar{J}$
$\bar{K}$
$\bar{\Gamma}$
$\bar{J}'$

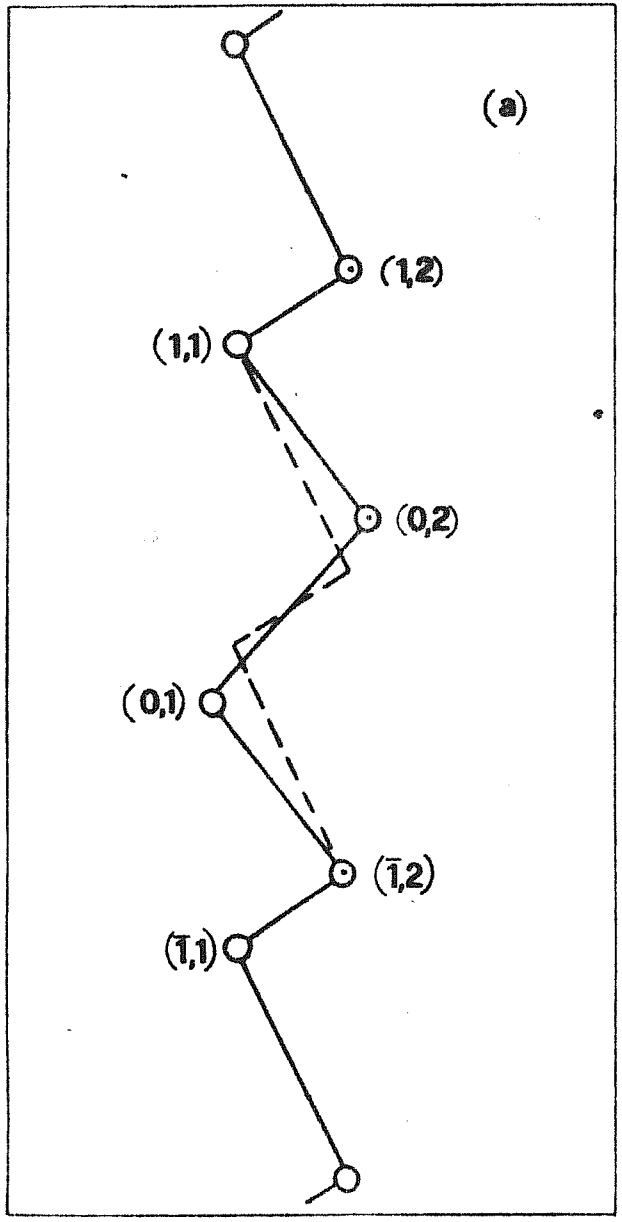

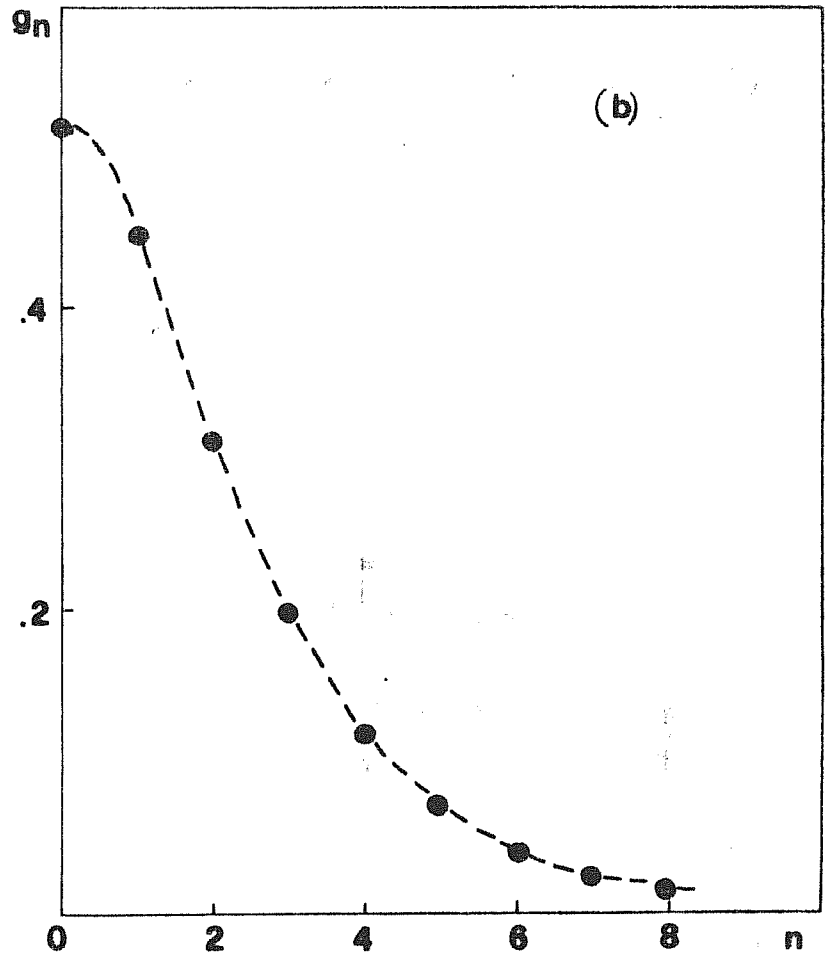

Chen, Sellom, Jozatti, Fig 3.3

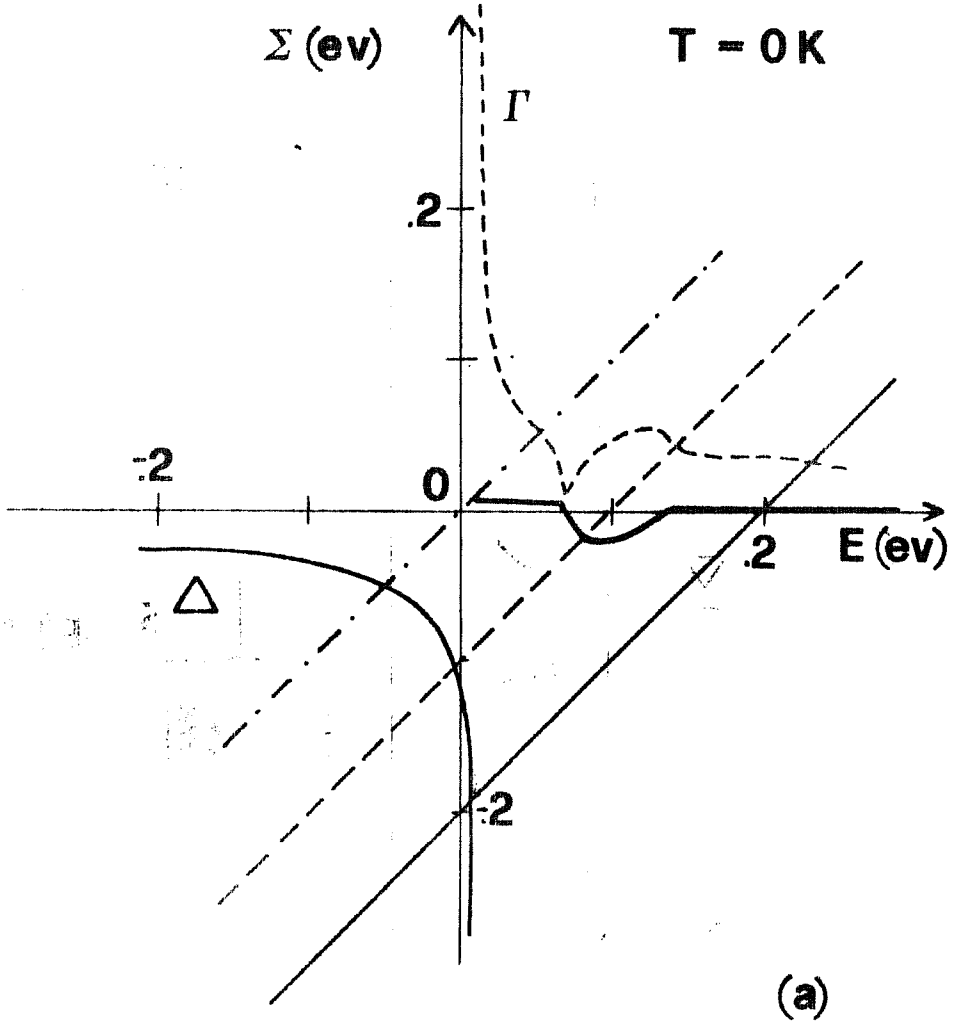

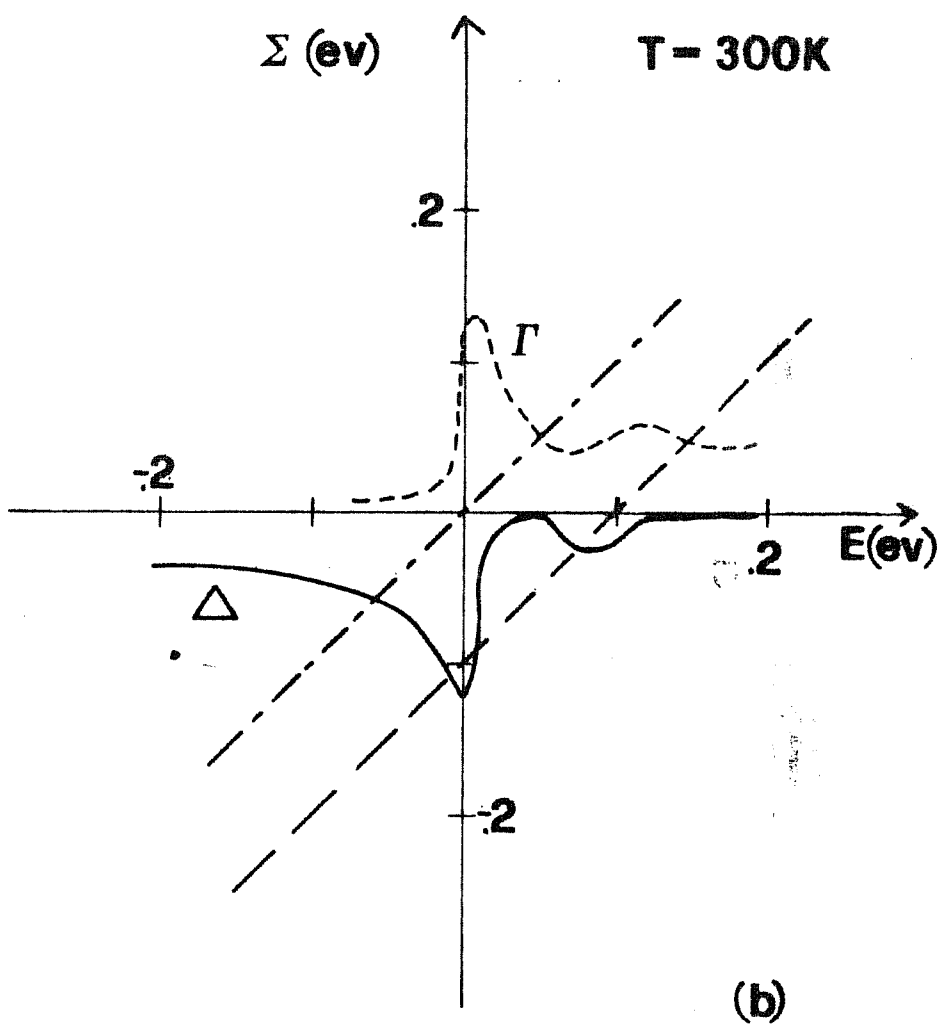

Chen. Sellon, Zaaltí Fig 3.4

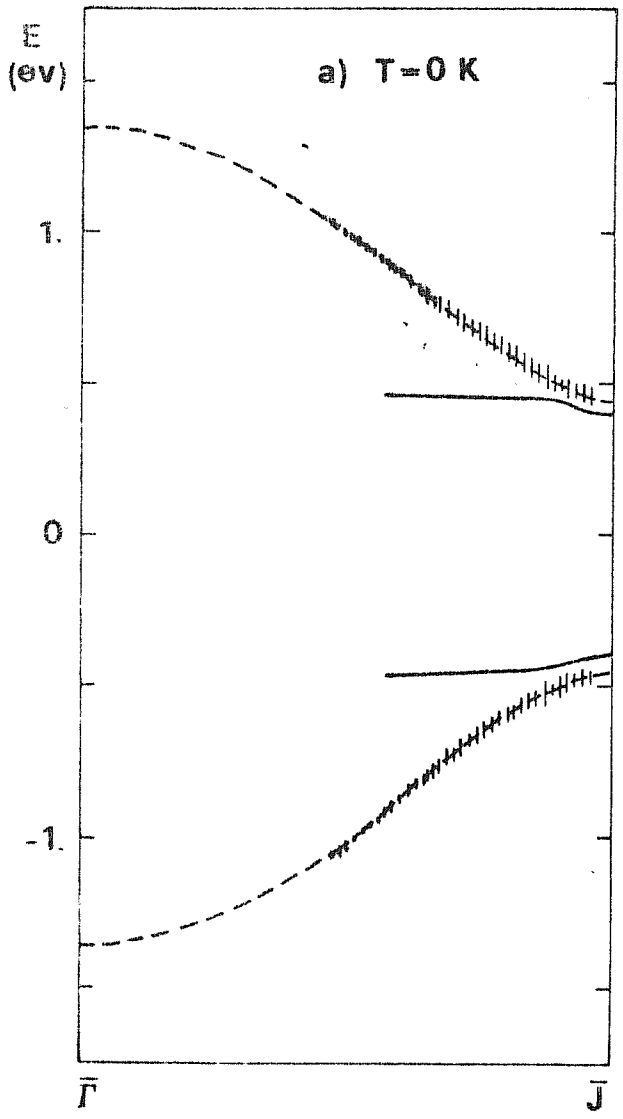

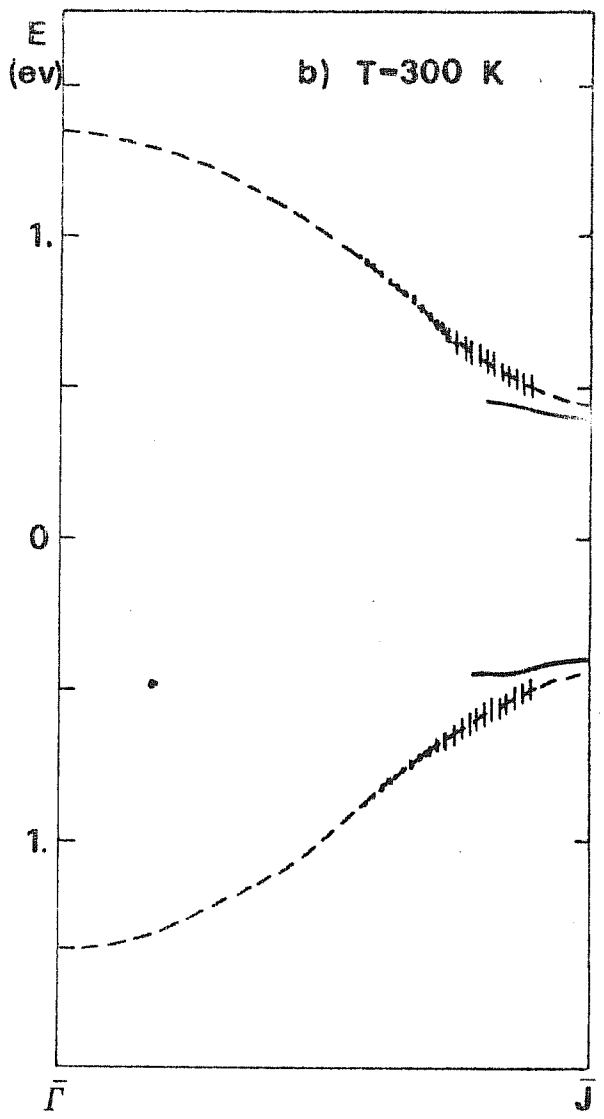

Chen . Selloni , Joannopoulos Fig. 3.5

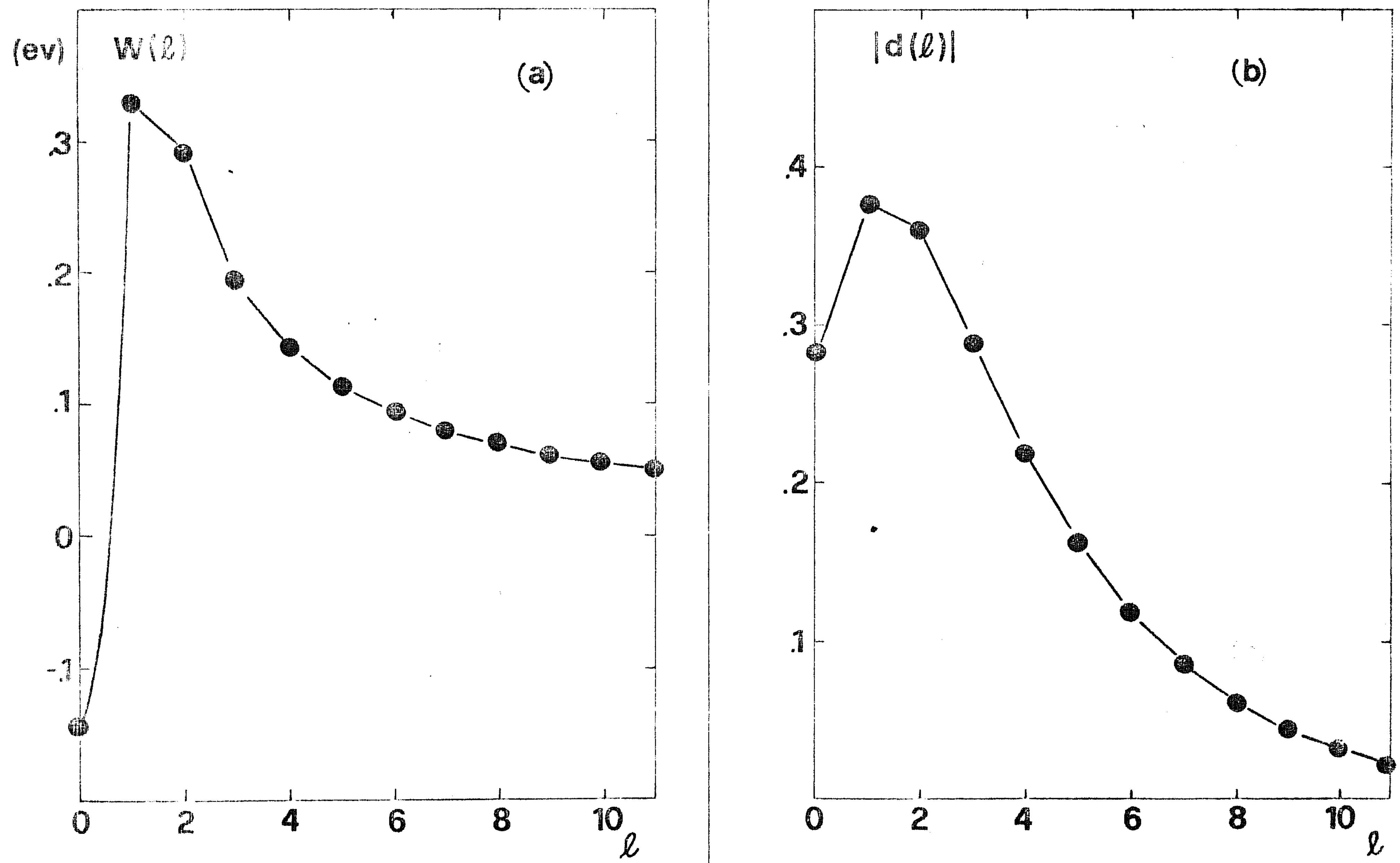

Chen, Selloni, Tosatti Fig 3.6

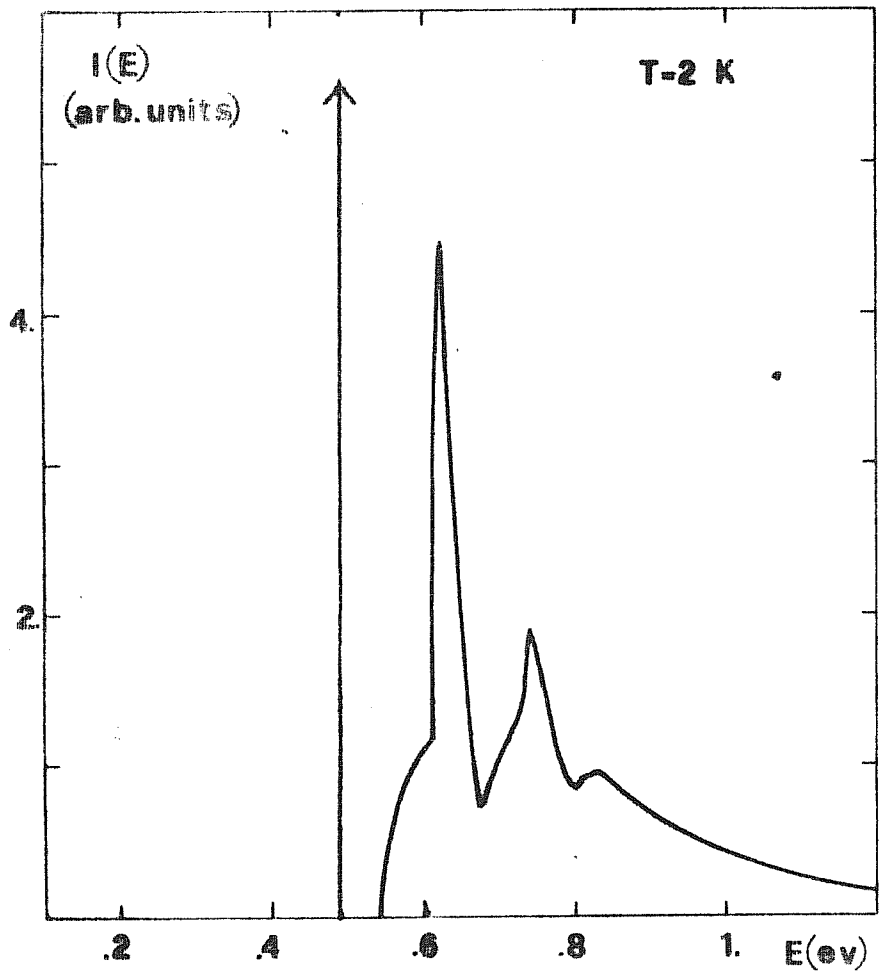

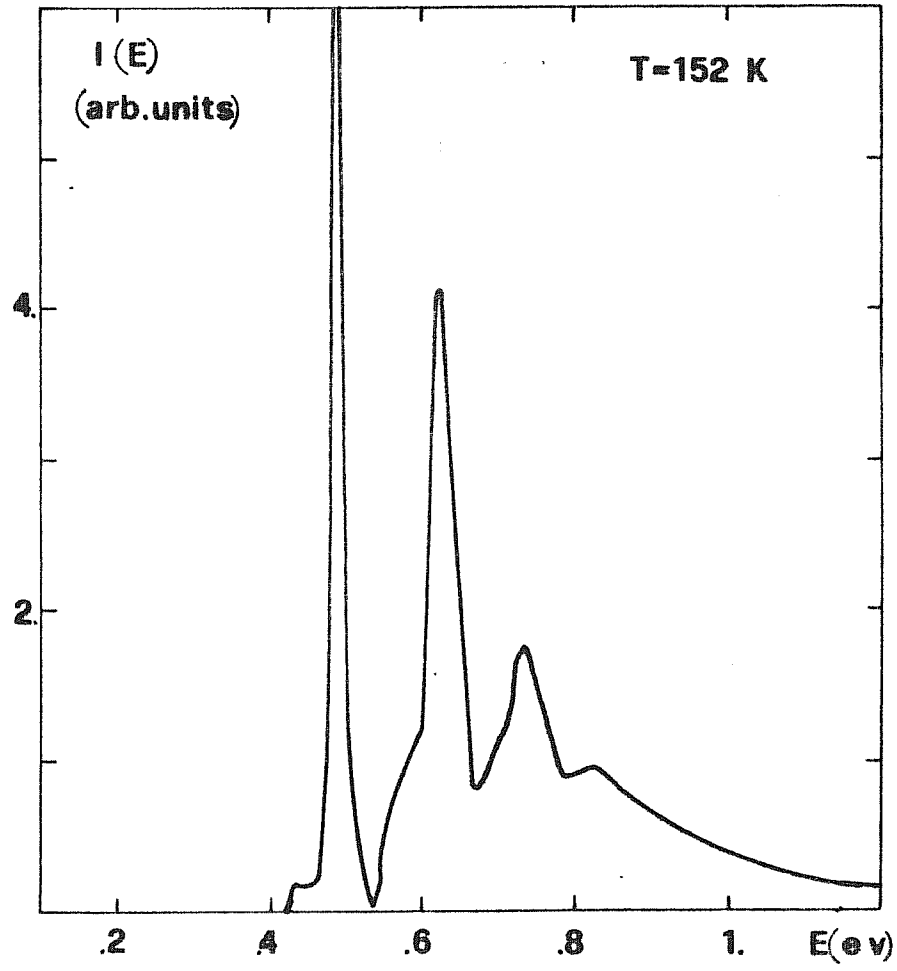

Chen. Selloni, Tosatti

Fig. 3.7 (a)

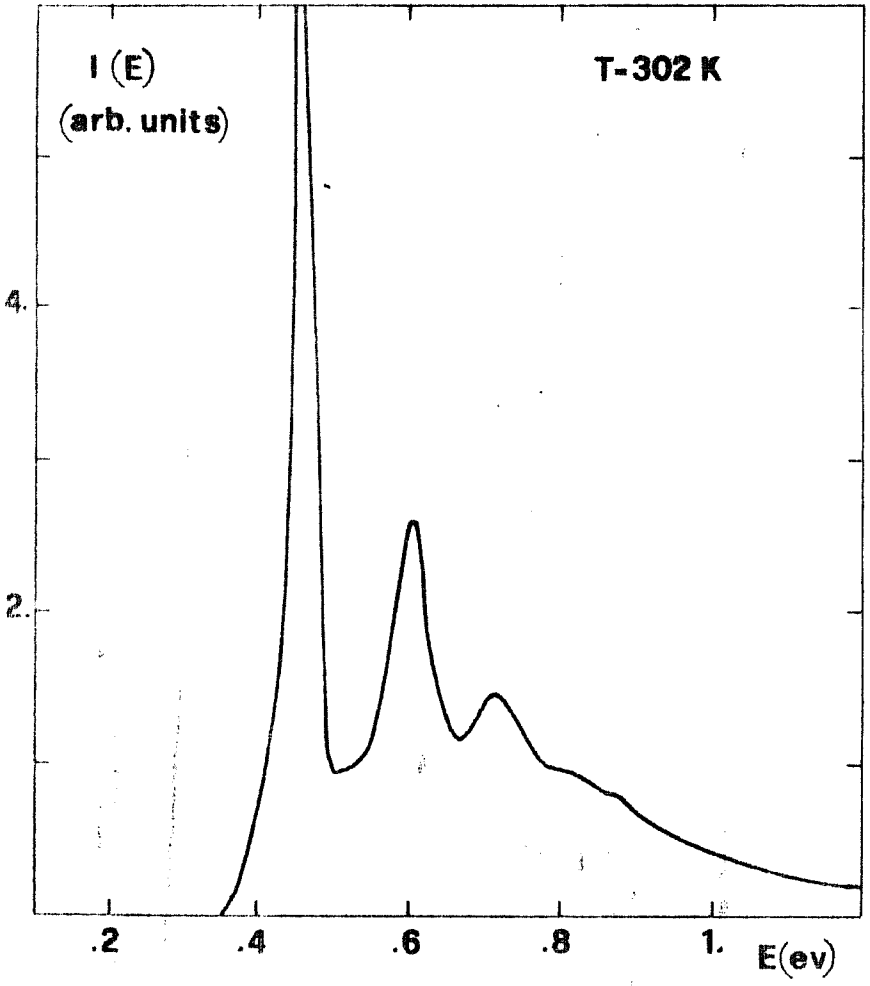

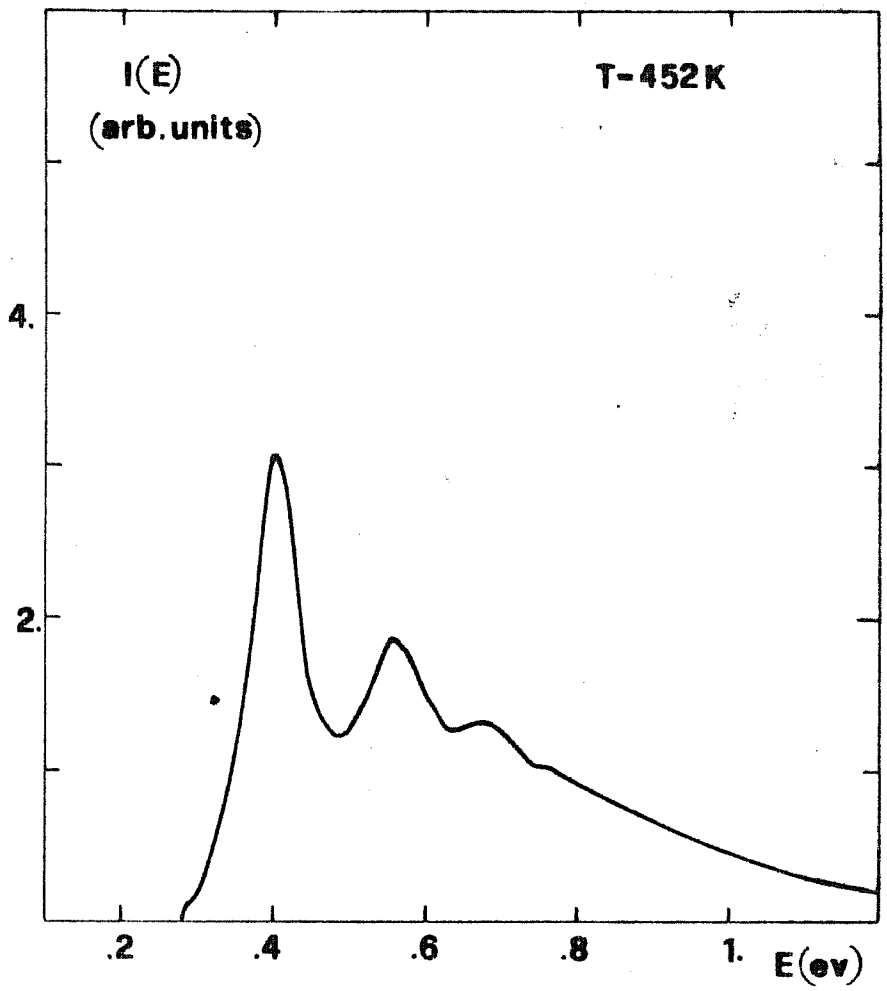

Chen, Sellon, Tozatti Fig 3.7(b)

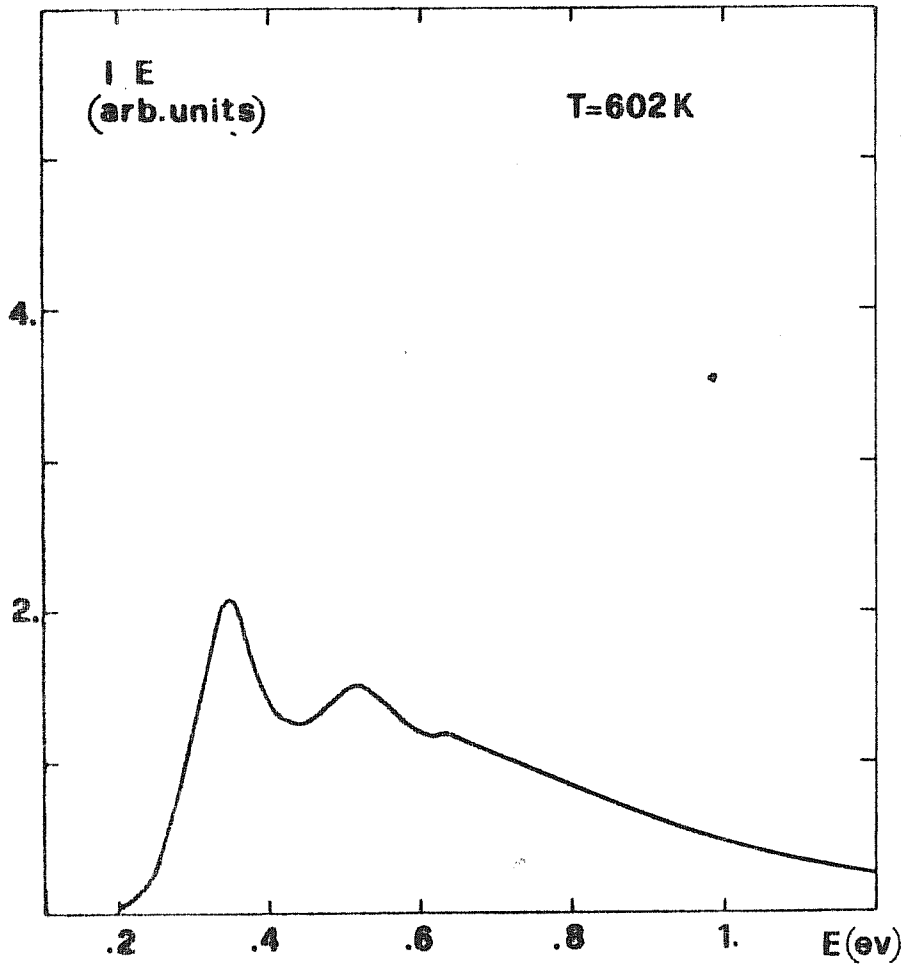

Chen. Sellioni, Tosatti Fig 3.7 (c)

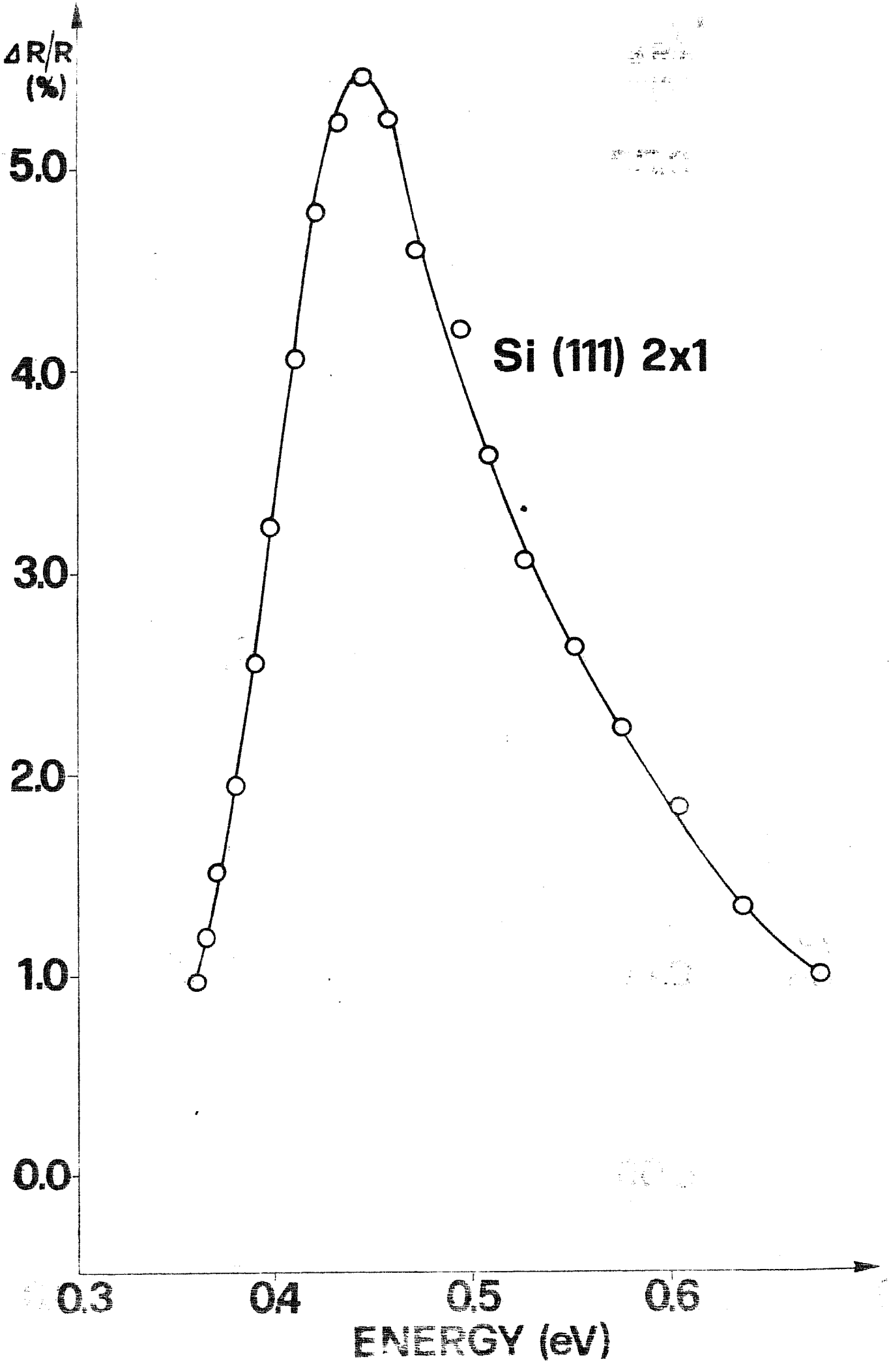
ΔR/R (%)
5.0
4.0
3.0
2.0
1.0
0.0
Si (111) 2x1
0.3
0.4
0.5
0.6
ENERGY (eV)

3. FRACTIONAL QUANTIZED HALL EFFECT.

The fractional,or anomalous,quantized Hall effect(QHE) is perhaps the most important discovery in condensed matter physics of a decade. Although the effect is seen in semiconductor devices,the physics it involves is not typical semiconductor physics,but rather more fundamental many-body physics.

In this part of my thesis,I will present first a quick survey of this new field(3.A),and then describe calculations I have done. In particular,I present a calculation of the total energy for a possible Wigner-lattice trial ground state(3.B),and exact diagonalization for a small number of electrons(up to 9),done in the symmetric gauge. These are done with two separate boundary conditions,i.e.,free(3.C)and also confined(3.D) in the attempt at learning information about the nature of the ground state.

3.A SURVEY *)

3.A.1. INTRODUCTION

Some semiconductor devices,such as MOSFETs or heterojunctions ,produce electron systems very close to being ideally two-dimensional[1]. If z=0 is the plane of confinement of the electrons, and a magnectic field B is applied along z, a Hall voltage E_y can be measured along y (open circuit direction), when a current j_x is forced along the orthogonal direction x (closed circuit direction) in the plane. The resistivity tensor for a collection of N free non-interacting two-dimensional electrons is

$$\rho_{xy} = \frac{2\pi\hbar}{e^2\nu} \qquad (1)$$

$$\rho_{xx} = \rho_{yy} = 0 \qquad (2)$$

where the "filling factor" ν, defined as $\nu = N/N_0$, is the number of filled (spin-polarized) Landau levels, each of degeneracy $N_0 = eBL^2/2\pi\hbar c$

*) Based in part on a review article by E. Tosatti, M. Parrinello, and C.D. Chen, to appear on Proceedings of The Int' School "E. Fermi" of Varenna (1983), ed. by F. Bassani, F. Fumi, and M. Tosi (to appear).

(L^2 is the system area). Hence the Hall resistivity $\rho_{xy} = E_x/j_y = \sigma_{xy}^{-1}$ is expected to simply increase linearly with B.

Experimentally however, plateaus have been observed in ρ_{xy} [3,4,5] for increasing B. There are two types of plateaus. One type of plateau occurs when ν is integer. This plateau is very remarkable, in that the value of ρ_{xy} has been shown to retain the fixed value $2\pi\hbar/e^2$ to an accuracy of perhaps one part in 10^7 for the whole range of B that constitutes the plateau [4]. This is the normal quantized Hall effect. Lest the designation "normal" should induce the readers into the false belief that all is understood about it, we immediatelly address them to what has by now become a fairly thick body of theoretical literature of newer and newer attempts at explaining it. The current belief, anyway, is that these "normal" plateaus are due to the presence of disorder in a system of otherwise essentially non-interacting electrons [6]. A very delicate and crucial role is played in this case by the existence, caused by the field itself, of at least one extended state [7]. We shall not be concerned any further with the normal plateaus here.

The second type of plateaus occurs for some fractional [5] fillings: $\nu = 1/3, 2/3, 2/5, 3/5, 2/7, 3/7, 4/7$, etc., and also $\nu = 4/3, 5/3$. The current belief is that these fractional, or "anomalous", plateaus are due to electron-electron interactions, causing new states to form at these fillings, while disorder plays a much less role. This belief is mainly due to the finding that increasing disorder tends to wipe out the fractional plateaus, while instead it makes the "normal" plateaus wider and wider [5]. The theory of the fractional Hall effect deals with attempts at explaining how and why the electron-electron interactions could produced such an effect. As of summer 1984, this theoretical body is only a collection of, at best, half-successful attempts. Nevertheless, both the facts to be explained and what theory already exists, are very fascinating, and there is little doubt that a complete explanation will soon form to constitute by itself an outstanding new chapter of many-body theory.

3.A.2. THE HAMILTONIAN

We deal with a collection of N electrons, confined along z by a strong electrostatic potential, mobile along x,y in the periodic crystal potential of a semiconductor, a neutralizing background potential $V_B(x,y)$, possibly some impurities $V_{IMP}(x,y)$. The electrons interact with one another via a screened Coulomb interaction e^{*2}/r (where $e^{*2} = e^2/\varepsilon$, with ε a background screening, and $r^2 = x^2 + y^2$) and are immersed in a strong magnetic field B parallel to z, plus an electric field E_y. The effective mass theorem are believed to hold, whereby the crystal potential can be removed, and replaced by an effective mass m*. If $\vec{A}(x,y)$ is the vector potential generating the magnetic field $\vec{B} = \nabla \times \vec{A}$, the effective hamiltonian is

$$H = \sum_{i=1}^{N} (\vec{p}_i + e\vec{A}(\vec{r}_i)/c)^2/(2m^*) + \tfrac{1}{2} \sum_{ij} e^{*2}/|\vec{r}_i - \vec{r}_j| + \sum_i (V_B(\vec{r}_i) + V_{IMP}(\vec{r}_i)) - eE_y \sum_i y_i \qquad (3)$$

In order to make progress with this formidable problem, the following approximations are customarily made:

(i)impurities are neglected, $V_{IMP}=0$, since we want to investigate first of all the effect of interactions.

(ii) the background potential $V_B(\vec{r})$ is approximated as a uniform neutralizing background of density N/L^2.

(iii) the magnetic field is taken to be so high that only the lowest Landau level is populated (quantum limit), e.g., so that $\nu \leq 1$. Then, if the cyclotron energy $\hbar\omega_c^* = \hbar eB/m^*c$ is sufficiently large in comparison with some typical electron-electron energy e^{*2}/ℓ, (where $\ell^2 = \hbar c/eB$ the Larmor radius), all higher Landau levels can be dropped from the problem.

(iv) the electric field E_y is dropped, restricting one's concern to studying the ground state problem without electric field. It is then believed that a cusp in total energy versus B at some value B* will cause "pinning" of the Hall response, yielding a plateau centered at B*[8].

With these approximation, the hamiltonian can be written as

$$H_o = \hbar\omega_c^*/2 \sum_i c_i^+ c_i + \tfrac{1}{2} \sum_{ijkl} v_{ijkl}\, c_i^+ c_j^+ c_k c_l \qquad (4)$$

where second-quantized notation is adopted, the creation operator c_i^+ spanning the lowest Landau level ($i=1,2,\ldots,N_o$). The total electron number is $N=\langle\sum_i c_i^+ c_i\rangle \leq N_o$, and

$$U_{ijkl} = \int d^2r_1\, d^2r_2\, \frac{\varphi_i^*(\vec{r}_1)\,\varphi_j^*(\vec{r}_2)\,\varphi_k(\vec{r}_2)\,\varphi_l(\vec{r}_1)}{|\vec{r}_1 - \vec{r}_2|}$$

The goal is to obtain as much insight as possible in the ground state Ψ of H_o

$$H_o \Psi(r_1 \ldots r_N) = E_o \Psi(r_1 \ldots r_N) \ , \tag{5}$$

as a function of B, or of $\nu = 2\pi\hbar cN/eBL^2$. One attractive feature of H_o is that it has no kinetic, or hopping, term any more. Hopping has been "frozen" away since the magnetic field is so high that transitions to higher Landau levels have become negligible. However, it is important to underline that this does <u>not</u> turn Eq.(5) into just a classical problem. Unless $B \to \infty$, in fact, the operators c_i^+ span only a fraction of Hilbert space which is <u>not</u> complete[9]. That is to say, one is not allowed to replace $V_o = \frac{1}{2} \sum_{ijkl} v_{ijkl}\, c_i^+ c_j^+ c_k c_l$ with $V = \frac{1}{2} \sum_{pq} e^{*2}/|\vec{r}_p - \vec{r}_q|$, unless B is infinite.

We can formalize this point by introducing a projection operator P_o, such that if Ψ is any N-particle wavefunction, then $P_o\Psi$ is its projection onto the lowest Landau level. Then we see that

$$V_o = P_o V P_o \tag{6}$$

and thus we can rewrite Eq.(4) in the form

$$P_o V P_o \Psi = (E_o - N\hbar\omega_c/2)\Psi \ . \tag{7}$$

3.A.3. CHOICE OF GAUGE, AND ONE-ELECTRON WAVEFUNCTIONS

As is well known, the vector potential $\vec{A}(x,y)$ generating the uniform magnetic field $\vec{B}=B\hat{z}$ is defined only to within a gauge transformation

$$\vec{A} \longrightarrow \vec{A} + \nabla f, \tag{8}$$

where f is an arbitrary function of coordinate and time. The single-electron Schrödinger equation

$$\hat{H}\psi = \frac{1}{2m}\left(\hat{p} + \frac{e}{c}\vec{A}\right)^2 \psi = \epsilon\psi \tag{9}$$

is satisfied if we make the gauge transformation (8) and at the same time change the wavefunction according to

$$\psi \longrightarrow \psi \exp(-ief/\hbar c) \ . \tag{10}$$

There are two, among others, most popular-used gauges: the Landau gauge

$$\vec{A} = B(-y,0,0) \tag{11}$$

which is translational invariant in the x-direction, and the symmetry gauge

$$\vec{A} = \frac{B}{2}(-y,x,0) \tag{12}$$

which is rotational invariant around the origin.

In the Landau gauge the hamiltonian takes the well-known form:

$$\hat{h} = \frac{1}{2m}\left(\hat{p}_x + \frac{e}{c}By\right)^2 + \frac{1}{2m}\hat{p}_y^2 \tag{13}$$

Here, $\left[\hat{p}_x,\hat{h}\right]=0$, e.g., the momentum along the x-direction is a good quantum number and the eigenfunction corresponding to the lowest Landau level can be expressed as

$$\psi_k(x,y) = \left(L_x \ell\sqrt{\pi}\right)^{-1/2} \exp\left[ikx - \frac{1}{2\ell^2}(y-k\ell^2)^2\right] \tag{14}$$

ψ_k is plane-wave-like along x-direction and is a Gaussian centered at $k\ell^2$ along y-direction. It is characterized by k which is quasi continuous,

$$k_j = \frac{2\pi}{L_x} j \ , \tag{15}$$

if periodic boundary condition $\psi(x+nL_x, y)=\psi(x,y)$ are applied. The degeneracy, the number of state contained in one Landau level, for a sample of area $S= L_x \cdot L_y = L^2$, equals

$$N_o = \frac{L_x \Delta k}{2\pi} = L^2/(2\pi\ell^2) \tag{16}$$

$\{\psi_k\}$ is a set of orthonormal function which span the whole lowest Landau level.

In the symmetry gauge, the hamiltonian takes the form:

$$\hat{h} = \frac{\hbar\omega_c}{2}\left(z^*\frac{\partial}{\partial z^*} - z\frac{\partial}{\partial z} + \frac{zz^*}{4\ell^2} - 4\ell^2\frac{\partial^2}{\partial z\partial z^*}\right) \tag{17}$$

if the transformation

$$\begin{aligned} z &= x+iy \\ z^* &= x-iy \end{aligned} \tag{18}$$

is made.

The angular momentum operator with respect to the origin is

$$\hat{L} = \vec{r}\times\vec{p} = -i\hbar\frac{\partial}{\partial\varphi} = \hbar\left(z^*\frac{\partial}{\partial z^*} - z\frac{\partial}{\partial z}\right) \tag{19}$$

and it commutes with $\hat{h}$, $[\hat{L},\hat{h}]= 0$. Hence, the angular momentum is a good quantum number in this gauge. Here the eigenstates of $\hat{h}$ can, if the energy scale $\hbar\omega_c=1$ and the length scale $\ell=1$ is adopted, be expressed as

$$|m,n\rangle = (2^{m+n}2\pi\cdot m!n!)^{-\frac{1}{2}}\exp(zz^*/4)\ (2\frac{\partial}{\partial z})^n\ (2\frac{\partial}{\partial z^*})^m\exp(-zz^*/2)$$

Where n labels the Landau level and m labels the angular momentum inside that Landau level. For the lowest Landau level the wavefunction takes particularly simple form

$$|m,0\rangle = |m\rangle = (2\pi 2^m\cdot m!)^{-\frac{1}{2}}z^m\exp(-zz^*/4) \qquad (20)$$

since

$$\langle m|r^2|m\rangle = 2(m+1) \quad , \qquad (21)$$

for a disk-shape sample of radius R, the number of state within one Landau level is then $(m+1)= R^2/(2\ell^2) = S/(2\pi\ell^2)$: in both gauges one single-electron state occupies on average an area of $2\pi\ell^2$.

In the following, an electron creation operator c_i^+ will create an electron either in a Landau-gauge state (whence $i\longrightarrow k_i=\frac{2\pi}{L_x}i$), or in a symmetric gauge state (whence $i\longrightarrow m$).

3.A.4. SOME SIMPLE KNOWN FACTS ABOUT H_o

Let us return to our main problem, i.e., finding the ground state of H_o, or of P_oVP_o; eqs.(5) and (7). Preliminary to that, we list here some simple known facts.

a) Exact solution at $\nu=1$

For complete filling, $\nu=1$, there is only one state (Slater determinant) one can form, namely

$$\Psi_o(\nu=1) = \prod_{q=1}^{N_o} c_q^+|0\rangle \quad , \qquad (22)$$

that is therefore automatically the exact ground state of H_o. The corresponding exact energy eigenvalue is the Hartree-Fock energy [10]

$$E_o^{(\nu=1)} = -\sqrt{\frac{\pi}{8}}\, e^{*2}/\ell = -0.6266\, e^{*2}/\ell \quad . \tag{23}$$

b) Variational lower bound for all $\nu \leq 1$

Let us suppose for a moment that the lowest Landau level states were a complete set, i.e., $P_o = 1$. Then the problem would reduce to a classical system of N classical point particles interacting via a Coulomb repulsion. The lowest energy configuration in that case is known [11] to be a "Wigner" triangular lattice, described by sites R_p

$$\Psi_W = \prod_{p=1}^{N} \psi^+_{R_p} |0\rangle \tag{24}$$

and

$$V\Psi_W = \tfrac{1}{2} \sum_{pq} \frac{e^{*2}}{|\vec{r}_p - \vec{r}_q|}\, \Psi_W = (E_W - \frac{N\hbar\omega_c^*}{2})\, \Psi_W \tag{25}$$

We can obtain a useful variational bound by using Ψ_W as a trial function in the true case, where $P_o \neq 1$, in the following manner [12]

$$\langle \Psi | P_o V P_o | \Psi \rangle = \langle P_o \Psi | V | P_o \Psi \rangle \; \rangle \langle \Psi_W | V | \Psi_W \rangle \tag{26}$$

whence the variational bound follows

$$E_o \rangle E_W \simeq -0.782\, \nu^{1/2}\, e^{*2}/\ell + N\hbar\omega_c/2 \tag{27}$$

In words, the energy of a classical triangular Wigner lattice provides an absolute lower bound for the true ground state energy E_o at all fillings.

c) Electron-hole symmetry

It is intuitively clear that, if the lowest Landau level is regarded as a (zero dimension) "band", there must be symmetry about the half-filling level. If an electron-hole transformation is introduced, so that $b_i = c_i^+$ and $b_i^+ = c_i$, then by direct inspection it can be verified that

$$H_o(c_i,\nu) + \nu^2 \frac{\sqrt{\pi}}{8} e^{*2}/\ell = H_o(b_i,1-\nu) + (1-\nu)^2 \frac{\sqrt{\pi}}{8} e^{*2}/\ell \quad (28)$$

Hence, all fillings between $\nu=1$ and $\nu=\frac{1}{2}$ need not to be discussed, since their ground state will be of the same nature as that for $1-\nu$, once the electron-hole transformation is made [13]. Therefore, one can restrict consideration to $\nu \leq \frac{1}{2}$.

This exhausts all simple "a priori" knowledge about the problem of finding the ground state of H_o, or of $P_o V P_o$, and its possible ground state energy "cusps" as a function of ν, that would explain the fractional quantized Hall effect.

In the following we shall present a quick, very qualitative and certainly incomplete review of some of the attempts that have been made at the problem.

3.A.5. HARTREE-FOCK "CHARGE DENSITY WAVES" (CDW)

Before interactions are turned on, a partly filled Landau level is a highly degenerate problem, since $N < N_o$ particles are to occupy a single level of degeneracy N_o. In analogy with Jahn-Teller systems, and perhaps even more closely with an interacting electron gas without field [14], the degeneracy may be split by some self-consistent spontaneous breaking of the translational symmetry. If the electron density is supposed to become non-uniform, let us say periodic with wavevector $\vec{Q}$, then the system may gain energy by filling all states within a certain "Brillouin Zone" whose boundaries fall at $\vec{Q}/2$, where a gap appears. The kinetic energy cost involved in this non-uniformity may be more than compensated by the potential energy gain, due to the appearance of a gap. This state of affairs has been confirmed and investigated in detail first by Fukuyama, Platzman and Anderson [15] and by Yoshioka and Fukuyama [13], and then by several authors, culminating in the very recent and complete work of Yoshioka and Lee [10]. We refer to these papers for all details. The optimal CDW wavevector Q is always found to be very close to the value dictated by inter-electron spacing, i.e., $Q^2 \sim \nu(4\pi/2\pi\ell^2)$. The ground state energies of the CDW are rather close to the variational (Wigner lattice) limit. For example, $E_o^{CDW} \simeq -0.32$ at $\nu=1/5$ ($E_w=-0.35$), and $E_o^{CDW} \simeq -0.39$ at $\nu=1/3$ ($E_w=-0.45$), all in unit of e^{*2}/ℓ. However, it has consistently been found and pointed out [10] that E_o^{CDW} displays no "cusps" as a function of ν, and therefore provides no explanation of the quantized Hall effect. Furthermore, the charge non-uniformity of the CDW state would pin onto any impurities present, preventing free drift along y for very small electric fields E_y. In the absence of such drift no Hall current can be generated at all, as is easily verified for a single Landau orbit [16].

3.A.6. MAGNETIC WIGNER COMMENSURATE SUPERLATTICE

Another attempt that is in some sense parallel to CDW's was made by Tosatti and Parrinello [16]. Based on the observation that for sufficiently high B the ground state must be close to a triangular Wigner lattice, they attempted at constructing a trial ground state for finite B in the form of a "commensurate Wigner superlattice" as

$$\Psi = \prod_{pq} c^{+}_{pq} |0\rangle \tag{29}$$

where c^{+}_{pq} creates an electron in a subset of the triangular lattice "Wannier states" constructed in the form

$$\varphi_{pq}(x,y) = \frac{\sqrt{a_1 L}}{2\pi} \int_{-(q+\frac{1}{2})2\pi/a}^{-(q-\frac{1}{2})2\pi/a} dk \, \exp(-ik\vec{R}_{pq}\cdot\hat{x}) \, \psi_k(x,y) \tag{30}$$

where $\psi_k(x,y)$ is defined in eq.14 and $\vec{R}_{pq} = p\vec{a}_1 + q\vec{a}_2$. $\vec{a}_1$ and $\vec{a}_2$ are the basis of the basic lattice and explained in (3.B). This subset can only take the optimal form of a triangular superlattice at the "commensurate" fillings

$$\nu_{st} = (s^2 + t^2 + st)^{-1} = 1/3,\ 1/4,\ 1/7,\ 1/12, \ldots \tag{31}$$

which they then interpreted as indication for a cusp of E_o at these fillings. Later ,we calculated the complete ground state energies

$$\frac{E_o}{N} = \tfrac{1}{2} \sum_{i,j} \left[\langle ij|v|ji\rangle - \langle ij|v|ij\rangle \right] + E_{e-b} + E_b \tag{32}$$

which turned out to be, as discussed in detail in (3.B) and the result shown in Table 3.2, poorer than the CDW values in the range of ν, where E_o have been calculated [10]. The wavefunction (29) is also a simplified of theirs, in that it is of the same single particle nature, but is however not variationally optimized. Hence (29) result is necessarily of

worse quality than that of a self-consistent CDW approach, and any implication of a cusp at $\nu = \nu_{st}$ is incorrect.

The present belief is that CDW, or Wigner superlattice states will actually be good for super-high magnetic fields, perhaps when ν gets to be less than 1/10 or so. For the larger ν values of experimental interest, they are probably irrelevant and they do not explain fractional Hall quantization.

3.A.7. SUPERLATTICES IN K-SPACE

Thouless and Tao[17,18] have investigated one alternative interesting route by considering wavefunctions of the form

$$\Psi = \prod_{p=1}^{N} c^{+}_{mp} |0\rangle \qquad (33)$$

where c^{+}_{k} creates an electron in a Landau state ψ_k (eq.14) and $mN=N_o$. These states have macroscopically uniform charge density, and thus do not have the difficulties with pinning that the CDW, or Wigner lattice states, have. Should they be shown to correspond to cusps of E_o, they would imply quantization at all fractional fillings $\nu = 1/m$, with m integer, both even and odd. However, Thouless and Tao produced only calculations of the single-particle energy gaps, that was found to be large at these fillings, but they did not calculate total energies. Their arguments therefore remain somewhat inconclusive. These wavefunctions remain nevertheless very interesting, since they probably share the right symmetry of the true ground state at the quantized fillings, as will be mentioned later on. Very recently, Tao[19] has produced a calculation of total energy based on Tao-Thouless states. Though his energies are apparently very low, they should be considered with suspicion, since for $\nu < 1/3$ they violate the variational bound(27).

3.A.8. CORRELATED JASTROW FUNCTIONS

In a recent crucial paper [20], Laughlin has shown that the method of correlated Jastrow functions, which had previously been successfully applied to Bose problems such as that of the He^4 by McMillan [21], can provide considerable insight also in the fractional Hall effect problem. Laughlin elects to work in the symmetric gauge, where the lowest Landau level single-particle functions is shown in eq.20. His observation is that; once higher Landau levels are neglected, the exact two-electron function is $(z_1 - z_2)^m \exp(-(|z_1|^2+|z_2|^2)/4)$,no matter how strong the electron-electron interaction is [22]. His function for N electrons is then

$$\Psi_L^{(m)} = \prod_{i<j} (z_i - z_j)^m \exp(-\sum_n |z_n|^2/4) \qquad (34)$$

where m must be odd to ensure antisymmetry. He then shows that this trial function implies the same one, two, ... n-particle correlation functions, as the two-dimensional classical one-component plasma (OCP) with logarithmic repulsive interactions, previously studied by many authors, most notably Jancovici [23]. Such a plasma is only uniform in space when it is exactly neutralized by its background, while it will segregate charge at its boundary whenever neutrality is not fulfilled. In Laughlin's case, neutrality is attained exactly only if

$$\nu = 1/m \qquad (35)$$

and not otherwise. Therefore, Laughlin's correlated functions (34) describes a uniform state only for $\nu = 1/3$, 1/5, etc. The energy of these states , as estimated by Laughlin, is $E_L(\nu=1/3) = -0.415$, $E_L(\nu=1/5) = -0.32$ and generally $E_L(\nu=1/m) = \frac{0.814}{\sqrt{m}}\left(\frac{0.23}{m^{0.64}} - 1\right)$, all in unit of e^{*2}/ℓ . This is definitely better than CDW for $\nu = 1/3$, and about the same for $\nu = 1/5$, and smaller. There are however additional strong points in favours of these wavefunctions, namely:

a) they imply a uniform state,free of pinning;

b) they imply a cusp in total energy, since on going from $\nu = 1/m$ to $\nu + \delta\nu$, a charge non-uniformity (defect) of finite energy cost must be created (This has however not been shown rigorously).

c) they involve quantization with odd denominators only, which agrees with experiment. On the other hand, the Laughlin states (34) do not represent the final solution of the problem, since

d) they do not explain quantization at fractions such as 2/5 or 2/7 and 3/7 (while of course they explain 2/3 as the electron-hole conjugate of 1/3, and 4/3, 5/3 as the replicas of 1/3, 2/3 after the lowest Landau level has been completely filled);

e) they are certainly not the exact ground state wavefunctions, even at $\nu=1/m$, as shown by Laughlin himself [22] for the case of 3 electrons, and more recently by Tao [24] by direct check that $H\Psi_L \neq \text{const} \times \Psi_L$.

3.A.9. NUMERICAL APPROACHES

Direct attack of this many body problem is somewhat simplified by the absence of a kinetic term in the hamiltonian (4). Laughlin [22] has explicitly solved the 3 electrons problem, elucidating some interesting features, that led him subsequently to propose the approximate form (34) for $N \to \infty$ electrons. Yoshioka, halperin and Lee [25] and Su [26] using a more systematic approach, have been able to extend calculations up to 6 electrons or so. They find evidence for a cusp in E_o versus ν at $\nu=1/3$, hints of one at $\nu=2/5$. Tao [24] has recently produced an explicit expansion of Laughlin's wavefunction into Slater determinants, and has been able to deal with as many as 8 electrons, by repeatedly multiplying Ψ by H_o, to yield $H_o\Psi$, $H_o^2\Psi$, ... $H_o^n\Psi \sim E_o^n\Psi$. Girvin and Jach [27], Lai et al [28] and also I (see section 3C and 3D) have carried out finite-size calculations using the symmetric gauge, and up to 9 electrons. These brute-force approaches are not easy to interpret. What seems most likely

at the moment is:

a) the ground state for $\nu = 1/3$ is a uniform fluid state [25], with qualitative features similar to that proposed by Laughlin;

b) the CDW, or Wigner-lattice states discussed earlier seem to be simply excited states rather than the ground state of the problem [25];

c) the overlap of the $\nu = 1/3$ Thouless-Tao state with the true ground state seems negligible [29];

d) the overlap of the true $\nu = 1/3$ ground state with a Laughlin state is large for $N \lesssim 4$ electrons, but then it tends to drop to figures of the order of 0.2 for $N = 8$ [24].

While all of this is quite useful information, it does not in itself shed much light on the qualitative physics of what may be going on, which still calls for a separate investigation.

3.A.10. FRACTIONAL CHARGE EXCITATIONS

Laughlin [20] showed first, with arguments based on the specific form (34) of his wavefunction for $\nu = 1/m$, that addition (subtraction) of a flux quantum $\delta\Phi = 2\pi\hbar c/e$ (which is the smallest change of magnetic field one can make, and therefore leads to the nearest configuration to $\nu = 1/m$), is equivalent to a fractional charge $\delta q = \pm 1/m$. Alternatively, it takes m extra (or missing) flux quanta to make up for one full missing (extra) electron. The simplest way to envisage such an excitation is to build it upon a Thouless-Tao state, rather than a Laughlin state [30]. Once constructed in the symmetric gauge, these states have the same symmetry as Laughlin's states, and presumably of the true ground state for ν not too small. Being simple Slater determinents, they are much easier to handle for all counting purposes such as we need here. One starts by occupying fermion states $z^p \exp(-|z|^2/4)$ with $p = p_o, p_o+m, p_o+2m$, etc. Since p_o can take any integer value from 0 to (m-1) there are actually m such states, all macroscopically degenerate. This is again a general feature of the problem, as stressed by Thouless [31] as well as by Anderson

[32] and Yoshioka [29]. By adding one flux quantum, one creates a "defect" leading to occupation p_o, p_o+m, p_o+2m,...,p_o+nm+1, $p_o+(n+1)m+1$, $p_o+(n+2)m+1$, ...

The arbitrariness of the integer n, underlying the arbitrariness in the placement of the extra flux quantum, i.e. of the defect. Such a state with defect has a slight charge non-uniformity at $r = \sqrt{2(n+1)}\ell$. The change of filling caused by m such defects is of one electron, whence the fractional charge 1/m attached to one defect alone, mentioned earlier. The energy of one defect has been estimated by Laughlin [20,33] to be in the order of $0.03\ e^{*2}/\ell$ .Very recently, Arovas, Schrieffer and Wilczek [34] have given an interesting discussion of new aspects implied by fractional excitations in the QHE.

3.A.11 THE 2/5 AND 2/7 STATES

Recently, some ideas [32,33,35,36] have been put forward to explain the states such as $\nu = 2/5$ and 2/7, in terms of correlated states of defects themselves. The basic concept is that, starting from $\nu=1/m$, where the ground state might be qualitatively similar to a Laughlin state ,one can create in it a macroscopically large density of fractional charge excitations, by taking the system from ν to $\nu' \neq \nu$. The defects interact with one another just in the same way as the original particle did, since they consist of a charge excess (defect) in the form of a ring, superposed onto an otherwise uniform state. They have been described as bosons by Haldane [35], an alternative of fermions by Laughlin [33]. If we take the view that they are bosons, we can start with a Thouless-Tao state $\Psi_o(\nu=1/m) = (p_o, p_o+m, p_o+2m,...)$, with m odd, and arrange the defects in an <u>even</u> [30] superlattice, i.e.

$$\Psi_o(\nu=1/m\mp\Delta) = (p_o,\ p_o+m\pm1,\ p_o+2m\pm1,\ p_o+3m\pm2,\ p_o+4m\pm2,\ p_o+5m\pm3,\ p_o+6m\pm3,\ \ldots) \qquad (36)$$

Anderson's [32] parent functions, constructed in an apparently different way, turn out to be the same as those generated in this way, provided the defects are arranged in even sequence. For m=3 the fillings of the states

are, with simple counting:

$$\nu = 1/3 \mp \Delta\nu = 1/3 \begin{cases} -1/21 \\ +1/15 \end{cases} = \begin{cases} 2/7 \\ 2/5 \end{cases} \qquad (37)$$

which are just the mysterious fillings at which quantization appears.

The general formula for all these fillings has been given by Haldane[35] and also by Laughlin[33], and is easy to understand in terms of the above counting. The alternative view that the defects should take a Thouless-Tao configuration with odd spacings would lead, starting from 1/3, to the fillings 7/24 and 8/21, where nothing is observed.

We conclude this section by the following remarks:

1. The fact that one gets the observed quantized fillings by constructing successive super-superlattices in angular momentum space suggest that this problem has a fascinating "Chinese box" structure, of successive defect condensates one into the other.
2. Except for a crude attempt by Halperin[8] and by Laughlin[33], no explicit wavefunction of the same quality as Laughlin's functions for $\nu=1/m$ is yet available for $\nu \neq 1/m$.

3.A.12. CONCLUSIONS

We can summarize this quick survey of the present state of affairs of the theory of FQHE making again the main points:

1. The effective hamiltonian of this problem appears to be extremely simple. In particular, as shown by eq.4, there is no kinetic energy left in the problem, since all kinetic degrees of freedom are frozen out by the magnetic field.
2. The CDW, or Wigner lattice states, that had received some attention in the earlier attacks to the problem, appear to be just excited state, rather than the true ground state, which is a correlated fluid at least for fillings that are not too small.
3. A handy and clever approximation available for the ground state wavefunction for $\nu = 1/m$ is provided by Laughlin's correlated Jastrow-

type function (20).

4. Though undoubtedly of worse quality than Laughlin's functions, the single Slater determinant functions of Thouless and Tao are quite useful in providing qualitative insight in the state of affairs away from $\nu = 1/m$, where the physics can be usefully cast in terms of fractional charge excitations.

5. Quantization at fillings such as 2/5 and 2/7 can perhaps be understood as a successive phenomenon of condensation of excitations. No wavefunction of quantitative relevance is however available as yet for these states.

3.B. ENERGY CALCULATION FOR A MODEL WIGNER LATTICE

In this section we calculate the energy (eq.32) of the "commensurate triangular Wigner lattice" defined in eq.29 and introduced by Tosatti and Parrinello [16]. The basic lattice is assumed to have basis $\vec{a}_1$ and $\vec{a}_2$, whose total number of site $L_x L_y / |\vec{a}_1 \times \vec{a}_2|$ equals N_ϕ, the number of state contained in one Landau level. Hence

$$|\vec{a}_1 \times \vec{a}_2| = \frac{\sqrt{3}}{2} a^2 = 2\pi\ell^2 \tag{38}$$

a is the length of both $\vec{a}_1$ and $\vec{a}_2$.

If the x-direction is chosen along $\vec{a}_1$, then

$$\vec{a}_1 = a(1,0) \quad , \quad \vec{a}_2 = a\left(\frac{1}{2} \, , \, \frac{3}{2}\right) \tag{39}$$

and the corresponding reciprocal lattice has basis $\vec{h}_1$ and $\vec{h}_2$,

$$\vec{h}_1 = \frac{2\pi}{a}\left(1 \, , \, -\frac{1}{\sqrt{3}}\right) \quad , \quad \vec{h}_2 = \frac{2\pi}{a}\left(0 \, , \, \frac{2}{\sqrt{3}}\right) \quad . \tag{40}$$

A triangular Wigner lattice which is <u>commensurate</u> with the basis (39) should have a unit cell defined by

$$\begin{aligned} \vec{b}_1 &= s\vec{a}_1 + t\vec{a}_2 = a\left(s + \frac{t}{2} \, , \, \frac{\sqrt{3}}{2} t\right) \\ \vec{b}_2 &= -t\vec{a}_1 + (s+t)\vec{a}_2 = a\left(\frac{s-t}{2} \, , \, \frac{\sqrt{3}}{2}(s+t)\right) \end{aligned} \tag{41}$$

with s,t integers. The basis of the corresponding reciprocal lattice are

$$\vec{G}_1 = \nu_{st} \frac{2\pi}{a}\left(s+t , \frac{t-s}{\sqrt{3}} \right)$$
$$\vec{G}_2 = \nu_{st} \frac{2\pi}{a}\left(-t , \frac{2s+t}{\sqrt{3}} \right) \qquad (42)$$

Where ν_{st} is the corresponding fractional filling factor defined in eq.31.

Each function $\varphi_{\vec{R}_i}(x,y)$ of the orthonormal set (30) has a charge density centered around $\vec{R}_i = i_1\vec{a}_1 + i_2\vec{a}_2$. The decay is Gaussian along the y-direction but roughly as 1/r along the x-direction. Its translational properties are also peculiar

$$\varphi_{\vec{R}_i}(\vec{r}) = \varphi_o(\vec{r} - \vec{R}_i) \exp(-iR_{iy}(x - R_{ix})/\ell^2) \qquad (43)$$

The wavefunction of the commensurate Wigner lattice on this basis set can be written as

$$\Psi = \prod_{j=1}^{N} c^{+}_{\vec{R}_j} |0\rangle \qquad (44)$$

where $c^{+}_{\vec{R}_j}$ is the creation operator corresponding to the $\varphi_{\vec{R}_j}(\vec{r})$, $\vec{R}_j$ runs over all Wigner lattice site

$$\vec{R}_j = j_1\vec{b}_1 + j_2\vec{b}_2 = (j_1 s - j_2 t)\vec{a}_1 + (j_1 t + j_2(s+t))\vec{a}_2$$
$$= a(j_1(s+t/2) + j_2(s-t)/2 , \sqrt{3}j_1 t/2 + \sqrt{3}j_2(s+t)/2) \qquad (45)$$

and N is the number of electron in our system

$$N = \nu_{st} N_o \qquad (46)$$

The energy of Ψ can be expressed as

$$(E - N\hbar\omega_c/2) = E_{ee} + E_{eb} + E_{bb} \qquad (47)$$

Where E_{ee}, E_{eb}, and E_{bb} are the electron-electron, electron-background and background-background interaction energy, respectively.

As well known in the infinite system with uniform neutralizing background, $E_{bb} = -E_{eb}/2$, and hence

$$E_{eb} + E_{bb} = \tfrac{1}{2} E_{eb} \quad . \tag{48}$$

Denoting the positive background density by n_o ,

$$n_o = \nu \frac{1}{2\pi\ell^2} \quad , \tag{49}$$

the density of the single-electron state centered at origin $\vec{R}_i = (0,0)$

$$\rho_{oo}(\vec{r}) = |\varphi_o(\vec{r})|^2 \tag{50}$$

and its Fourier transform

$$\rho_{oo}(\vec{q}) = \int d^2r \exp(-i\vec{q}\cdot\vec{r})\, \rho_{oo}(\vec{r}) \tag{51}$$

$$= \frac{a}{\pi\ell^2} \exp(-\ell^2 q^2/4)\, \theta(2\pi/a - |q_x|)\, \sin(\ell^2 q_y (\frac{\pi}{a} - \frac{|q_x|}{2}))/q_y$$

E_{eb} can be calculated in a straightforward way,

$$E_{eb} = -Ne^{*2} \int d^2r \int d^2R\, \rho_{oo}(r) n_o / |r-R|$$

$$= -Ne^{*2} n_o \int d^2q\, \rho_{oo}(q)\, (2\pi)^2\, \delta(\vec{q})/(2\pi q)$$

$$= -N\nu \frac{e^{*2}}{\ell^2} \lim_{q\to o}(1/q) \tag{52}$$

The electron-electron energy E_{ee} is the expectation value of $P_o V P_o$ (eq. 6) , in the present case is just the Hartree-Fock energy

$$E_{ee} = \tfrac{1}{2} \sum_{i\neq j} (I_{ij} - J_{ij}) = \frac{N}{2} \sum_{j\neq o} (I_{o,j} - J_{o,j})$$

$$= N(I - J) \tag{53}$$

Where i,j, are a simplified notation for sites $\vec{R}_i$, $\vec{R}_j$, and the summation runs over Wigner lattice site. $I_{i,j}$ and $J_{i,j}$ are the Coulomb and exchange interaction, respectively, between electrons in state $\varphi_{\vec{R}_i}(\vec{r})$ and $\varphi_{\vec{R}_j}(\vec{r})$,

$$I_{i,j} = e^{*2} \int d^2r_1 \int d^2r_2\, \rho_{ii}(\vec{r}_1)\, \rho_{jj}(\vec{r}_2)/|\vec{r}_1 - \vec{r}_2|$$

$$= e^{*2} \int d^2q\ \rho_{\vec{R}_i}(\vec{q})\, \rho_{\vec{R}_j}(-\vec{q})/(2\pi q) \tag{54}$$

$$J_{i,j} = e^{*2} \int d^2r_1 \int d^2r_2\, \rho_{ij}(\vec{r}_1)\, \rho_{ji}(\vec{r}_2)/|\vec{r}_1 - \vec{r}_2|$$

$$= e^{*2} \int d^2q\, \rho_{ij}(\vec{q})\, \rho_{ji}(-\vec{q})/(2\pi q) \tag{55}$$

Here, $\rho_{oo}(\vec{q})$ is given by (51), and more generally

$$\rho_{ij}(\vec{q}) = \frac{a}{\pi\ell^2}\frac{\exp(-\ell^2 q^2/4)}{\beta}\left(\frac{2\pi}{a} - |\alpha|\right)\sin(\ell^2\beta\left(\frac{\pi}{a} - |\alpha|/2\right))$$

$$\exp\left(-\frac{i}{2}(q_x(R_{ix}+R_{jx}) + q_y(R_{iy}+R_{jy}) - (R_{ix}-R_{jx})(R_{iy}+R_{jy})/\ell^2\right) \tag{56}$$

where $\Theta(x) = \begin{cases} 1 & x>0 \\ 0 & x<0 \end{cases}$

is a step function, and

$$\alpha = q_x + (R_{iy} - R_{jy})/\ell^2$$
$$\beta = q_y - (R_{ix} - R_{jx})/\ell^2 \tag{57}$$

Note that $\rho_{ij}(\vec{q}) = \rho^*_{ji}(-\vec{q})$, as it should be.

The Coulomb and exchange energy I,J can then be written as

$$I = \tfrac{1}{2}\sum_{j(\neq o)} I_{oj} = \tfrac{1}{2}\sum_{j(\neq o)}(e^{*2}/\ell)a^2/(4\pi^3\ell^3)\int d^2q\ \exp(i\vec{q}\vec{R}_j - \ell^2q^2/2)$$
$$(2\pi/a - |q_x|)(1-\cos(\ell^2 q_y(2\pi/a - |q_x|)))/(q\cdot q_y^2) \tag{58}$$

$$J = \tfrac{1}{2}\sum_{j(\neq o)} J_{oj} = \tfrac{1}{2}(e^{*2}/\ell)\sum_{j(\neq o)} a^2/(4\ell^3\pi^3)\int d^2q\ \exp(-\ell^2q^2/2)$$
$$(2\pi/a - |\alpha_j|)(1-\cos(\ell^2\beta_j(2\pi/a - |\alpha_j|)))/(q\beta_j^2) \tag{59}$$

with $\alpha_j = q_x - R_{jy}/\ell^2$, $\beta_j = q_y - R_{jx}/\ell^2$.

For some particular fractional filling of the lowest Landau level ν_{st} (31), the summation in (58) and in (59) is to be done over the corresponding Wigner lattice sites $\vec{R}_j$ (45). If the periodic boundary condition is implied, then

$$\sum_j \exp(i\vec{q}\vec{R}_j) = \nu_{st} N_o \sum_{m,n} \delta_{q,Q_{m,n}} \tag{60}$$

$$\int d^2q \longrightarrow (2\pi)^2/S\sum_{q_i} = 2\pi/(N_o\ell^2)\sum_{q_i} \tag{61}$$

where

$$\vec{Q}_{m,n} = m\vec{G}_1 + n\vec{G}_2 \tag{62}$$

is the reciprocal lattice vector corresponding to the Wigner lattice. Therefore the Coulomb interaction energy I, for filling factor ν , can be written as

$$I = (e^{*2}/\ell)\ \tfrac{1}{2}\nu a^2/(2\pi^2\ell^5)\sum_{m,n}\exp(-\ell^2 Q_{mn}^2/2)\,\theta(2\pi/a - |Q_{mn,x}|)$$
$$(1 - \cos(Q_{mn,y}\ell^2(2\pi/a - |Q_{mn,x}|)))/(Q_{mn}\cdot Q_{mn,y}^2) - \tfrac{1}{2}I_{o,o}$$
$$\doteq (e^{*2}/\ell)\ \tfrac{1}{2}\nu 2(1/\sqrt{3}\pi)^{5/2}\sum_{m,n}\exp(-\sqrt{3}\pi(X_{mn}^2 + Y_{mn}^2)/2)\,\theta(1-|X_{mn}|)$$
$$(1 - \cos(\sqrt{3}\pi Y_{mn}(1-|X_{mn}|)))/(Y_{mn}^2(X_{mn}^2 + Y_{mn}^2)^{1/2}) - \tfrac{1}{2}I_{o,o} \qquad (63)$$

Where eq.38 has been used and

$$X_{mn} = \nu_{st}(m(s+t) - t\cdot n)$$
$$Y_{mn} = (\nu_{st}/3)\,(m(t-s) + n(2s+t)) \qquad (64)$$

Note that the (m=0, n=0) term in eq.63. just cancels $E_{eb} + E_{ee}$ exactly (both are divergent). Therefore we can exclude the (m=0, n=0) term, and the summation converges rapidly. For $\nu_{10} = \nu_{01} = 1$, the summation (excludes m=0, n=0 term) over m,n vanishes, hence $I^{(10)} = -\tfrac{1}{2}I_{o,o}$.

Whereas J (eq.59) is computed straightforwardly. Some of $J_{o,\vec{R}}$ is tabulated in Table 3.1 .

Table 3.1 Exchange energy $J_{o,\vec{R}}$ between electrons centered at origin $\varphi_o(\vec{r})$ and that centered at $\vec{R}$, $\varphi_{\vec{R}}(\vec{r})$.

$\vec{R}$ (X,Y) in unit of a	(0, 0)	(1,0)	(2,0)	(3,0)	(4,0)	(5,0)
$J_{o,\vec{R}}$ (e^{*2}/ℓ)	0.736522	0.083426	0.015082	0.006612	0.003742	0.002411

(6,0)	(7,0)	(8,0)	(1/2,3/2)	(3/2,3/2)	(0, 3)	(1, 3)
0.001684	0.001243	0.000955	0.040624	0.012485	0.000109	0.000075

It can be seen from Table 3.1 that $J_{o,\vec{R}}$ decreases very rapidly as $\vec{R}$ moves away along y-direction, while it is roughly decreases as $1/R^2$ along the x-direction. This just reflects the fact that our basis function $\varphi_{\vec{R}}(\vec{r})$ does not decay exponentially along x-direction.

We have done the calculations for a first few filling factors and the result is given in Table 3.2 and also shown in Fig. 3.1 together with other people's results for the purpose of comparation.

Table 3.2 Expectation energy of the model Wigner lattice at various filling factor ν.

ν	1	3	4	7	12
$\epsilon - \frac{1}{2}\hbar\omega_c/2$ (e^{*2}/ℓ)	-0.626	-0.364	-0.325	-0.257	-0.204

The exact result $E(\nu=1) = -0.6266\ e^{*2}/\ell$ is well recovered, and the variational bound (27) is obviously respected. As expected the energy is slightly higher than the true Hartree-Fock CDW values, which should represent the best single Slater determinant. In view of the simplicity of the present calculation as compared to the full CDW's, we can consider the result satisfactory. The present method is however unsuitable for a calculation of Wigner lattice energies at a general "incommensurate" filling $\nu \neq \nu_{st}$, since then no suitable basis can be constructed via eq.(31). However, this does not mean, contrary to the earlier surmise of Ref. 16, that a stable perfect Wigner lattice will not exist in HF for a general filling .

3.C. CONFIGURATION INTERACTION FOR FEW ELECTRONS IN THE SYMMETRIC GAUGE

3.C.1. Introduction

Laughlin [22] showed first that the exact study of few electrons in the symmetric gauge could yield interesting information, for the subsequent construction of a trial ground state wavefunction of the N-electron problem. Girvin and Jach [27], who performed calculations for 3,4 and 5 electrons, have found interesting oscillations of both ground state energy

, and energy gap Δ to the first excited state, as a function of the total angular momentum L ,which in turn is connected, for a very large homogeneous system, to the filling, in the form

$$\nu = N(N-1)/(2L) \qquad (65)$$

These authors did not provide an insight into these oscillation.

From a direct expansion of Laughlin's approximate wavefunction , it is however clear that the most important single Slater determinant of N electrons is that one where all of them are "lumped" together, i.e., they occupy a whole compact block of single-particle states.

If this can be extrapolated to few-electron systems, one finds that such an arrangement is possible only for total angular momentum L of the form

$$L_s = N(N-1)/2 + sN \quad , s= 0, 1, 2 \ldots \qquad (66)$$

This turns out to be precisely where the minima of Girvin and Jach's [27] energy fall.

Lai et al [28], who performed again similar calculations find precisely the same fact, and observe that their ground state wavefunctions are indeed dominated by component where all electrons are "lumped" together.

We have undertaken similar calculations with the following goals:

1. To study carefully total energies and gaps, for variable N and variable L, to gain more understanding to be extrapolated to larger N's.
2. To study the effect of a neutralizing background, which was not included by Girvin and Jach [27], and treated approximately by Lai et al [28].
3. To look for new quantum numbers in the problem. In the absence of background, we find that the center of mass angular momentum M is indeed a good quantum number, separate from the total angular momentum L.
4. To compare exact calculations in the symmetric gauge with those done

in the Landau gauge [25,26,29]. While of course physics should be gauge-invariant, the boundary conditions turn out to be quite different in the two cases.

5. To probe into the open question of whether the true infinite ground state for $\nu=1/m$ is, or is not, m-fold degenerate. This has been claimed to occur Anderson, Thouless, and not to occur Laughlin, and it stands as an open issue.

6. To extend existing calculations to higher number of electrons. Our present limit is of 9 electrons and $L= 55$, corresponding to $\nu\simeq 2/3$.

3.C.2. Outline of the calculation

Here, the energy scale and the length scale are set, so that $\hbar\omega_c = \ell = 1$. We consider an N-electron system where N is small, with the goal of solving exactly eq.7, we will do that with and without uniform neutralizing positive background, taken of disk shape with radius R and surface density of $n_o = N/(\pi R^2)$.

The hamiltonian H_o without background is that of eq.4. Using the basis set of function $\varphi_m(\vec{r})$ defined in eq.20, we can rewrite H_o in the symmetric gauge as

$$H_o = \tfrac{1}{2}\sum_{i=1}^{N}\left(z_i^*\frac{\partial}{\partial z_i^*} - z_i\frac{\partial}{\partial z_i} + z_i z_i^*/4 - 4\frac{\partial^2}{\partial z_i \partial z_i^*}\right) + \tfrac{1}{2}(e^{*2}/\ell)\sum_{i\neq j} 1/|z_i - z_j| \qquad (67)$$

If the positive background is included, then

$$H = H_o + V_B \qquad (68)$$

where
$$V_B = \sum_m v_m c_m^+ c_m + V_{bb} \qquad (69)$$

and v_m is the interaction of an electron in state $\varphi_m(\vec{r})$ with the background

$$v_m = -e^{*2}\int dr\, r\int_0^{\ell} dr'\, r'\int_0^{2\pi} d\theta\int_0^{2\pi} d\theta'\, |\varphi_m(\vec{r})|^2\, n_o/|\vec{r}-\vec{r}'|$$
$$= -N(e^{*2}/\ell)\int dk\, \exp(-k^2/2)\, L_m(k^2/2)\, 2\, J_1(kR)/(kR) \qquad (70)$$

where $L_m(x)$ is the Laguerre polynomial of order m and $J_1(x)$ is the Bessel function of order 1.

V_{bb} is the positive background self-energy,

$$V_{bb} = (e^{*2}/\ell)\ \tfrac{1}{2}\int_0^R dr\ r \int_0^{2\pi} d\theta \int_0^R dr'\ r' \int_0^{2\pi} d \quad n_o^2/|\vec{r}-\vec{r}'|$$

$$= (e^{*2}/\ell)\ \frac{8}{3\pi} N^2/R \tag{71}$$

The total angular momentum of the electrons $\hat{L}$, defined as

$$\hat{L} = \sum_{i=1}^{N} (\vec{r}_i \times \vec{p}_i) = \hbar \sum_i \left(z_i^* \frac{\partial}{\partial z_i^*} - z_i \frac{\partial}{\partial z_i}\right) = \sum_i \left(-i\hbar \frac{\partial}{\partial \theta_i}\right)$$

$$= \sum_m m\hbar\, c_m^+ c_m \tag{72}$$

$\hat{L}$ commutes both with H_o, $\left[H_o, \hat{L}\right] = 0$, and with H, $\left[H, \hat{L}\right] = 0$, because of the circular form assumed. Hence $\hat{L}$ is a good quantum number both for system with and without background.

The wavefunction of the N-electron system of angular momentum L can be written as a linear combination of Slater determinant with the same L,

$$\Psi_L(\vec{r}_1, \vec{r}_2, \ldots, \vec{r}_N) = \sum_{\sum m_i = L} C_{m_1, m_2, \ldots, m_N} |m_1, m_2, \ldots, m_N\rangle \tag{73}$$

$m_1, m_2, \ldots$ are non-negative integer, and $|m_1, m_2, \ldots, m_N\rangle$ is a Slater determinant with electrons in states $\varphi_{m_1}, \varphi_{m_2}, \ldots \varphi_{m_N}$ $(m_1+m_2+\ldots+m_N = L)$,

$$|m_1, m_2, \ldots, m_N\rangle = \frac{1}{\sqrt{N!}} \det(\varphi_{m_i}(\vec{r}_j)) \ . \tag{74}$$

The coulomb matrix $\langle m_1, \ldots, m_N |\ H_o\ | m_1', \ldots, m_N' \rangle$ can be evaluated knowing the matrix element of the Coulomb potential[28,37]

$$M(J,I,k) = \int d^2 r_1 \int d^2 r_2\, \varphi^*_{J+k}(\vec{r}_1)\ \varphi^*_{I-k}(\vec{r}_2)(e^{*2}/r_{12})\ \varphi_I(\vec{r}_2)\ \varphi_J(\vec{r}_1)$$

$$= (e^{*2}/\ell)\frac{\sqrt{\pi}}{2} \left(\binom{I}{I-k} \binom{J+k}{J} \right)^{-\frac{1}{2}} \sum_{m=0}^{I-k} \sum_{n=0}^{J} \left((-1)^{m+n}/2^{3(m+n+k)}\right)$$

$$\binom{I}{I-k-m} \binom{J+k}{J-n} \binom{2(k+m+n)}{k+m+n} \binom{k+m+n}{m+n} \binom{m+n}{m} \tag{75}$$

and the corresponding exchange matrix element

$$M_x(J,I,k) = M(J,I,I-J-k) \tag{76}$$

The matrix element of V_B is clearly diagonal,

$$V_B |m_1,\ldots,m_N\rangle = \left(\sum_{i=1}^{N} v_{m_i} + V_{bb} \right) |m_1,\ldots,m_N\rangle \qquad (77)$$

For a fixed L, there is a maximun single-electron angular momentum L_{Max},

$$L_{Max} = L - (N-1)(N-2)/2 \qquad (78)$$

which defines the radius R of positive background disk by the following relation:

$$R^2 = \langle L_{Max} | r^2 | L_{Max} \rangle = 2(L_{Max} + 1) \quad . \qquad (79)$$

3.C.3. Center of mass angular momentum: a good quantum number?

In the absence of background, $V_B = 0$, one important point that emerges is that the center of mass angular momentum (CMA) is another good quantum number. CMA is defined as

$$\hat{M} = \left(\left(\frac{1}{N} \sum_i \vec{r}_i \right) \times \sum_i \vec{p}_i \right) \hat{z} = \hbar \sum_i \left(Z \frac{\partial}{\partial z_i} - Z^* \frac{\partial}{\partial z_i^*} \right)$$

$$= \frac{\hbar}{N} \sum_{i,j} \left(z_j \frac{\partial}{\partial z_i} - z_j^* \frac{\partial}{\partial z_i^*} \right) \qquad (80)$$

where $Z = \frac{1}{N} \sum_i z_i$ is the center of mass coordinate.

It can easily be proved that

$$\left[H_o, \hat{M} \right] = 0 \qquad (81)$$

and also

$$\left[\hat{L}, \hat{M} \right] = 0 \quad . \qquad (82)$$

When only the lowest Landau level is of concern, as is the case here, operating with $\hat{M}$ on a single-electron wavefunction

$$\varphi_m(z_i) = c_m z_i^m \exp(-z_i z_i^*/4) \qquad (83)$$

has a simple form

$$\hat{M} \varphi_m(z_i) = c_m \exp(-z_i z_i^*/4) \left(\frac{\hbar}{N} \sum_{i,j} z_j \frac{\partial}{\partial z_i} \right) z_i^m \qquad (84)$$

Dropping the Gaussian factor, which appears everywhere in the problem, we can consider the reduced function

$$\exp(z_i z_i^*/4) \varphi_m(z_i) = f_m(z_i) = z_i^m / (2\pi 2^m m!)^{1/2} \qquad (85)$$

Defining ladder operators [38]

$$a_i^+ = z_i/\sqrt{2} \quad ; \quad a_i = \sqrt{2}\,\frac{d}{dz_i} \tag{86}$$

then
$$a_i^+ f_m(z_i) = \sqrt{m+1}\, f_{m+1}(z_i)$$
$$a_i f_m(z_i) = \sqrt{m}\, f_{m-1}(z_i) \tag{87}$$

and $\hat{M}$, $\hat{L}$ can be expressed as

$$\hat{M} = \frac{\hbar}{N} \sum_{i,j} a_i^+ a_j \tag{88}$$

$$L = \hbar \sum_i a_i^+ a_i \tag{89}$$

The background destroys clearly CMA invariance, since $\left[\hat{M}, V_B\right] \neq 0$.

3.C.4. Results, and discussion

The ground state energy as well as the first excited state energy for 7,8, and 9 electron systems are shown in Fig.3.2 versus total angular momentum. For $V_B = 0$, also the M-value is indicated. The results for 3,4, and 5 electrons without background, and for 5, 6, and 7 electrons with background all look like the previous results of Girvin and Jach [27] and of Lai et al [28].

We have also calculated the average number of electron having specific angular momentum m, $\langle c_m^+ c_m \rangle$, which for several case is shown in Fig. 3.3 .

There are some comments can be made from our calculation:

1) Cusps seem connected with electrons wanting to go all together and hence gaining more exchange energy, which Lai et al [28] have noticed too. The loss in energy in connection with the inhomogeneity of our system seems not big enough to discourage electrons being close to each other at least for small system. This feature, we believe, cannot persist in really large systems. This means that the present systems are still far too small to simulate the real ones.

2) Gaps (the first excited state energy minus the ground state energy) seem large when $\nu = N(N-1)/(2L) = p/q$, where q are both even and odd integers.

3) On the shape of $\langle c_m^+ c_m \rangle$, which brings information about the ground state, we notice that there is no oscillations of period 3, when $\nu = 2/3$. The presence of oscillations might have been expected, after the work of Su [26], in the Landau gauge with periodic boundary condition, who found large oscillations. At the moment it is not yet clear how to interpret this finding. Tentatively, one may advance the following two alternatives:

(i) the true infinite ground state is <u>not</u> m-fold degenerate, and there was no reason to expect oscillations of period m in $\langle c_m^+ c_m \rangle$. The oscillations in Su's calculation [26] are entirely an artifact due to the periodic boundary condition in his Landau gauge calculation.

(ii) the finite-size calculations for $N \leq 9$ electrons are totally inadequate to get any understanding of the large N-behavior. In particular, the "lumping" together of electrons, which dominates over 50% of the ground state, should decrease in relative importance, to become an infinitesimal component for $N \longrightarrow \infty$, since otherwise one would get macroscopic charge segregation. The true $N \longrightarrow \infty$ ground state is of a different character altogether.

3.D. N ELECTRONS CONFINED ONTO A DISK

In this final Section on FQHE we describe briefly some very preliminary results on a recent investigation conducted within the symmetric gauge formulation.

One defect of the calculations described in the previous section was to have a very ill-defined filling factor ν. In fact, although the wavefunctions could in principle extend out of $R^2 \sim 2(L_{Max} + 1)$, they usually fall to zero much sooner. A clearer way to handle the filling

problem, for few electrons, which has been suggested to us by F. Iachello, is to choose a circular box, and put 1, 2, 3,... N electrons into it. If the box contains N_o orbitals, the filling is then $1/N_o$, $2/N_o$,..., N/N_o without ambiguity.

Such a box is easy to produce by simply limiting the single-particle basis functions to those below a maximum L_o,

$$m_i = 0,1,2,\ldots,L_o. \qquad (90)$$

whence $N_o = L_o + 1$.

The questions that can be asked of an exact configuration interaction calculation done in this way are:

1. Does the ground state energy show cusps with variable filling?
2. If the electron number is varied, what does the total energy per particle do? Are there any oscillations indicating tendencies to form pairings, triplets, etc?
3. What does the total angular momentum of the ground state do, as the filling changes?

Some preliminary results are shown in Fig. 3.4 . They suggest the following comments:

1) The ground state energy per particle decreases with filling, which was to be expected, but no cusps are found.
2) The ground state energy does not have, at least for as few electrons as we have studied, any oscillations that would indicate pairing. The only clustering phenomenon is that, already discussed in the previous section, of "lumping" all the electrons together.
3) The total angular momentum decreases by quantum jumps as the filling increases (i.e. L_o decreases with N fixed), pretty much as was found by Laughlin in his study of 3 electrons system.

We are planning to continue and extend this type of calculations , to gain more insight into the physics of this fascinating phenomenon.

REFERENCES

1. A very comprehensive review of the general properties of such systems is given in ref.(2).
2. T. Ando, A.B. fowler and F. Stern, Revs. Mod. Phys., 54, 437(1982).
3. For early references, consult ref.(2).
4. K. von Klitzing, G. Dorda and M. pepper, Phys. Rev. Lett. 45, 494 (1980).
5. H.L. Störmer, A.M. Chang, D.C. Tsui, J.C.M. Huang, A.C. Gossard and W. Wiegmann, Phys. Rev. Lett. 50, 1953(1983).
6. R.B. Laughlin, Phys. Rev. B23, 5622 (1981).
7. G.F. Giuliani, J.J. Quinn and S.C. Ying, Phys. Rev. B28, 2969 (1983).
8. See e.g. B.I. Halperin, Helv. Physica Acta 56, 75 (1983).
9. We thank Dr. G. Baskaran for his lucidly pointing onto this fact to us.
10. D. Yoshioka and P.A. Lee, Phys. Rev. B27,4986 (1983).
11. L. Bonsall and A.A. Maradudin, Phys. Rev. B15,1459 (1977).
12. We thank Prof. G. Fano for suggesting this derivation.
13. See, e.g., F. Yoshioka and H. Fukuyama, J. Phys. Soc. Japan, 47, 394 (1979).
14. A.W. Overhauser, Phys. Rev. 167, 691 (1968).
15. H. Fukuyama, P.M. Platzman and P.W. Anderson, Phys. Rev. B19, 5211 (1979).
16. E. Tosatti and M. Parrinello, Lett. Nuovo Cimento, 36, 289 (1983).
17. R. Tao and D.J. Thouless, Phys. Rev. B28, 1142 (1983).
18. R. Tao, Phys. Rev. B29, 636 (1984).
19. R. Tao, preprint.
20. R.B. Laughlin, Phys. Rev. Lett. 50, 1395 (1983).
21. W.L. McMillan, Phys. Rev. 138, A442 (1965).
22. R.B. Laughlin,Phys. Rev. B27, 3383 (1983).
23. B. Jancovici, Phys. Rev. Lett. 46, 386 (1981).
24. R. Tao, preprint.

25. D. Yoshioka, B.I. Halperin and P.A. Lee, Phys. Rev. Lett. 50, 1219 (1983).

26. W.P. Su, Phys. Rev. B30, 1069 (1984).

27. S.M. Girvin and Terrence Jach, Phys. Rev. B28, 4506 (1983).

28. Wuyan Lai, Kun Yu, Zhaobin Su and Lu Yu, Preprint.

29. D.Yoshioka, Surface Science, to appear and private communication.

30. J.J. Quinn and S.C. Ying, private communication.

31. D.J. Thouless, Surface Science, to appear.

32. P.W. Anderson, Phys. Rev. B28, 2264 (1983).

33. R.B. Laughlin, Surface Science, to appear.

34. D. Arovas, J.R. Schrieffer and F. Wilczek, Phys. Rev. Lett. 53, 722(1984).

35. F.D.M. Haldane, Phys. Rev. Lett. 51, 605 (1983).

36. R. Tao, preprint.

37. G. Fano, "Comments on the mathematical structure of the Laughlin's wavefunction for the anomalous quantum Hall effect. A pedagogical exposition" . Lectures given at the International School for Advanced Studies, Trieste (1984).

38. S.M. Girvin and Terrence Jach, in Phys. Rev. B29, 5617 (1984), have also defined the same operators a and a^+ .

FIGURE CAPTIONS

Fig. 3.1 Ground state energy per particle versus the inverse fractional filling of the lowest Landau level, $m = 1/\nu$. Dot points are our results for the "commensurate" Wigner lattice. Also shown are results of Yoshioka, and Lee [10] (square points), Laughlin [20] (crosses) and Bonsall and Maradudin [11] (solid line). The dashed line drawn through crosses is a guide to the eye only.

Fig. 3.2

a) The ground state energy (solid line) as well as the first excited state energy (dash line), both for per particle, versus total angular momentum for 7, 8, and 9 electron systems with uniform positive baclground.

b) The ground state energy versus total angular momentum for 7, 8, and 9 electron systems without background. The integers above each point are the corresponding center of mass angular momentum.

c) Energy gap (the first excited energy minus the ground state energy) versus total angular momentum for 8 and 9 electron systems without background.

Fig. 3.3 The average number of electron having specific angular momentum m, $\langle c_m^+ c_m \rangle$, for 8-electron system (a) and 9-electron system (b), with (dash line) and without (solid line) background, at total angular momentum L= 36, 42 and 49, respectively.

Fig. 3.4

a) The ground state energy (solid line) and the first excited state energy (dash line), both for per particle, versus the inverse fractional filling, $1/\nu$, for 3, 4 and 5 electron systems confined onto a disk. Below also shown are the corresponding total angular momentum of the system.

b) The ground state (solid) and the first excited state (dash line) energies, both for per particle, versus electron number (N) for systems confined onto a disk having N_o= 5, 6,..., 16 single-particle states, respectively. And thus the filling factor equals N/N_o.

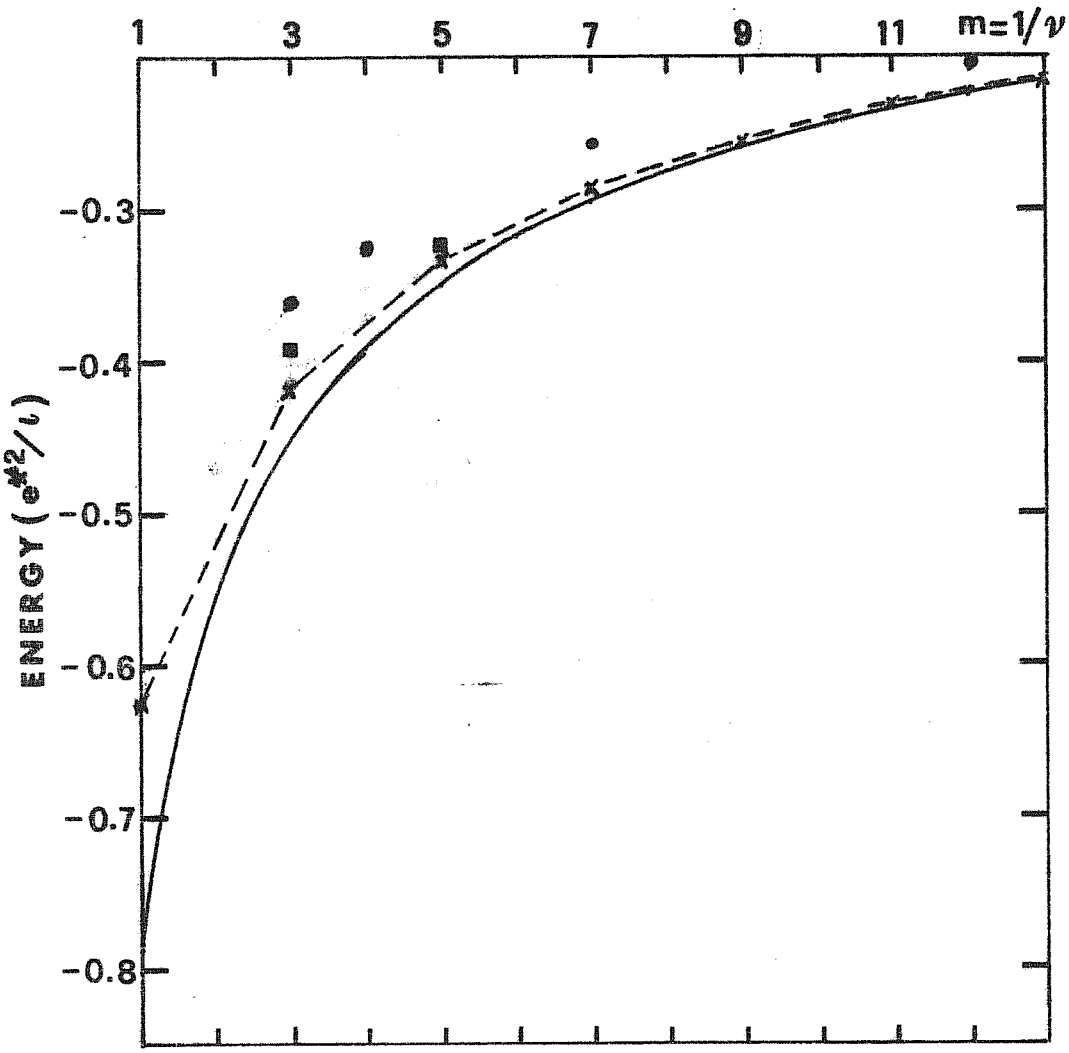

Fig. 3.1

Fig 3.2.1

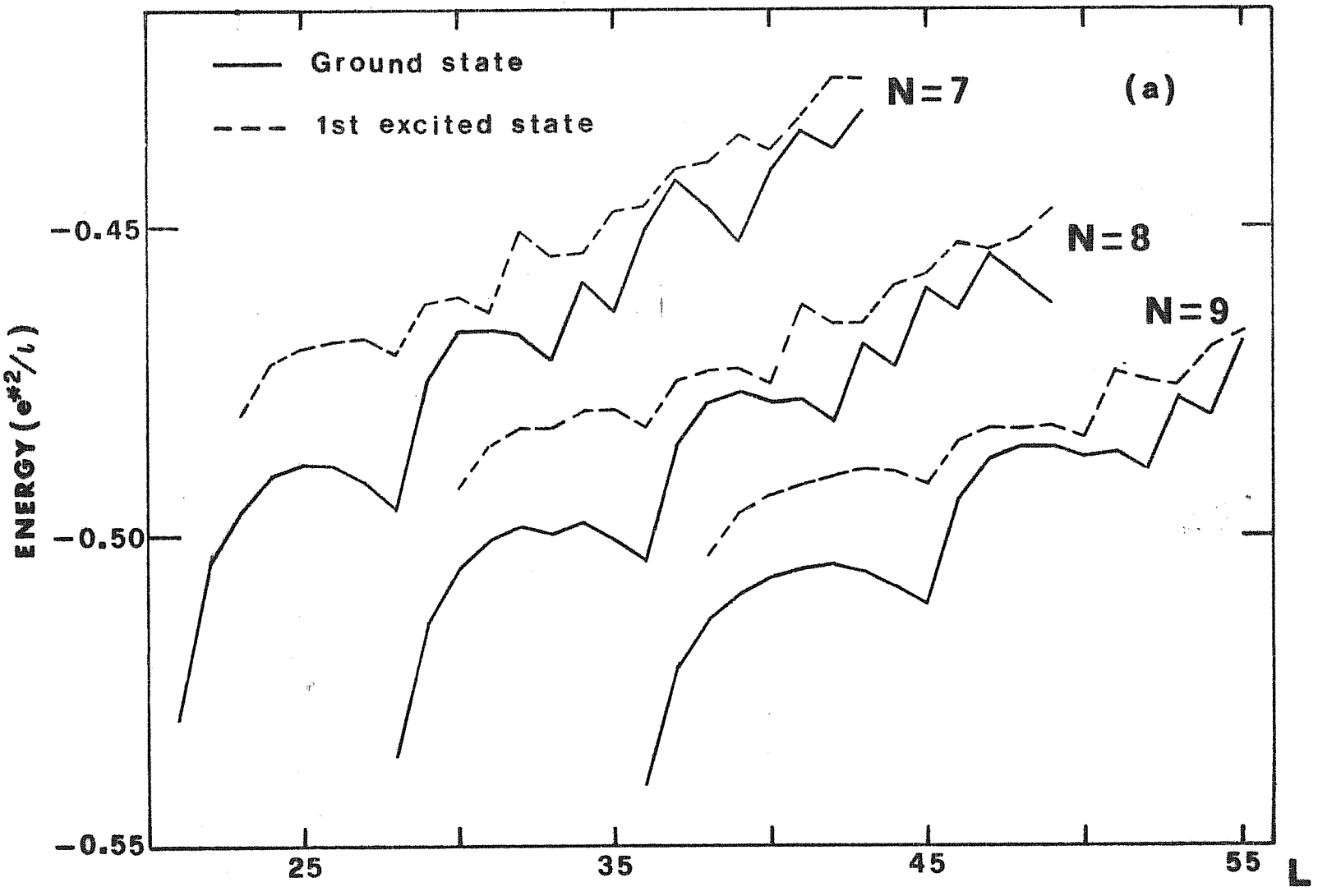
Ground state
1st excited state
N=7
(a)
N=8
N=9
−0.45
−0.50
−0.55
ENERGY (e^{*2}/L)
25
35
45
55
L

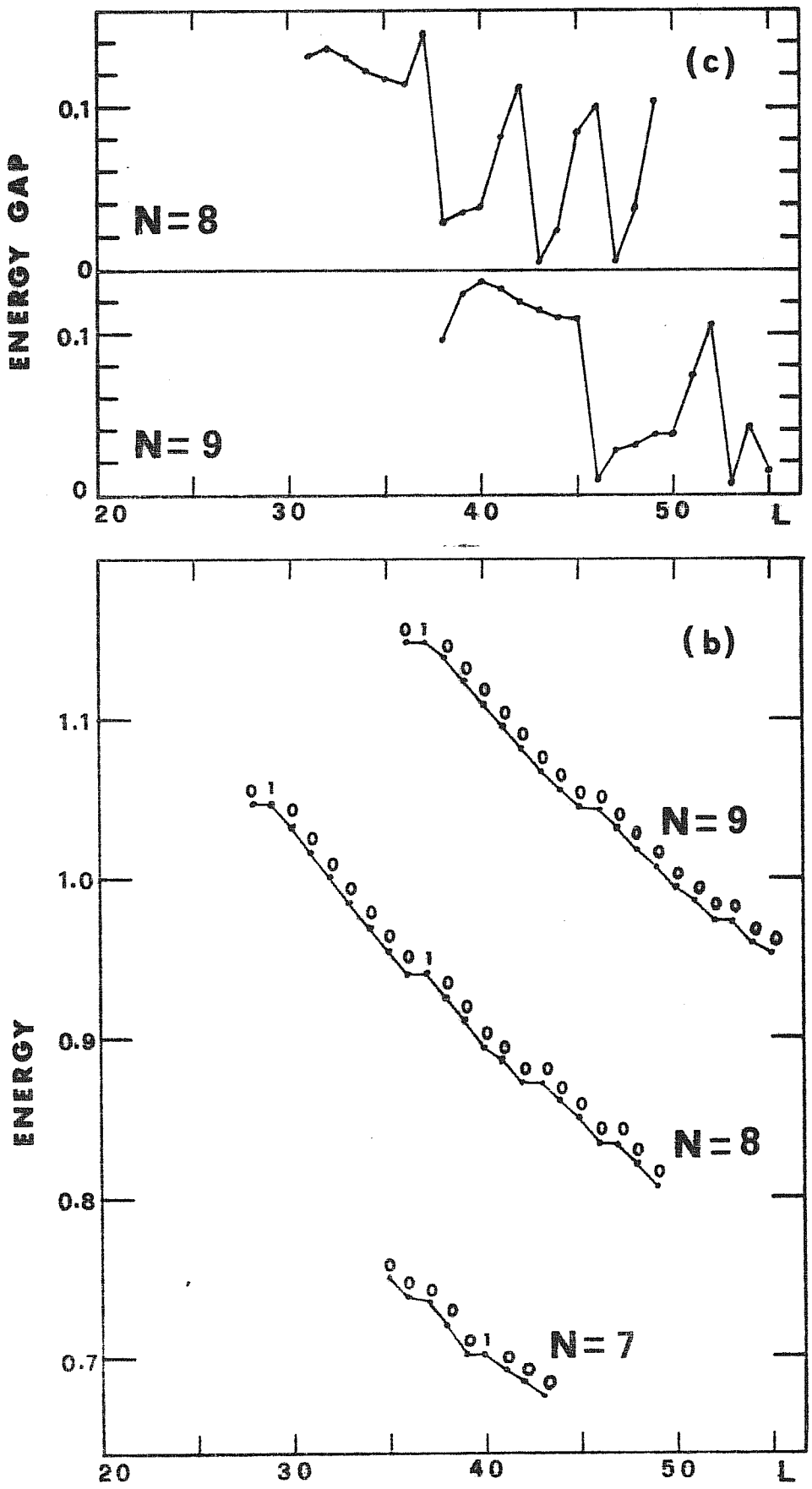
(c)
ENERGY GAP
0.1
0
N=8
0.1
0
N=9
20
30
40
50
L
(b)
ENERGY
1.1
1.0
0.9
0.8
0.7
N=9
N=8
N=7
20
30
40
50
L

Fig 3 a B & C

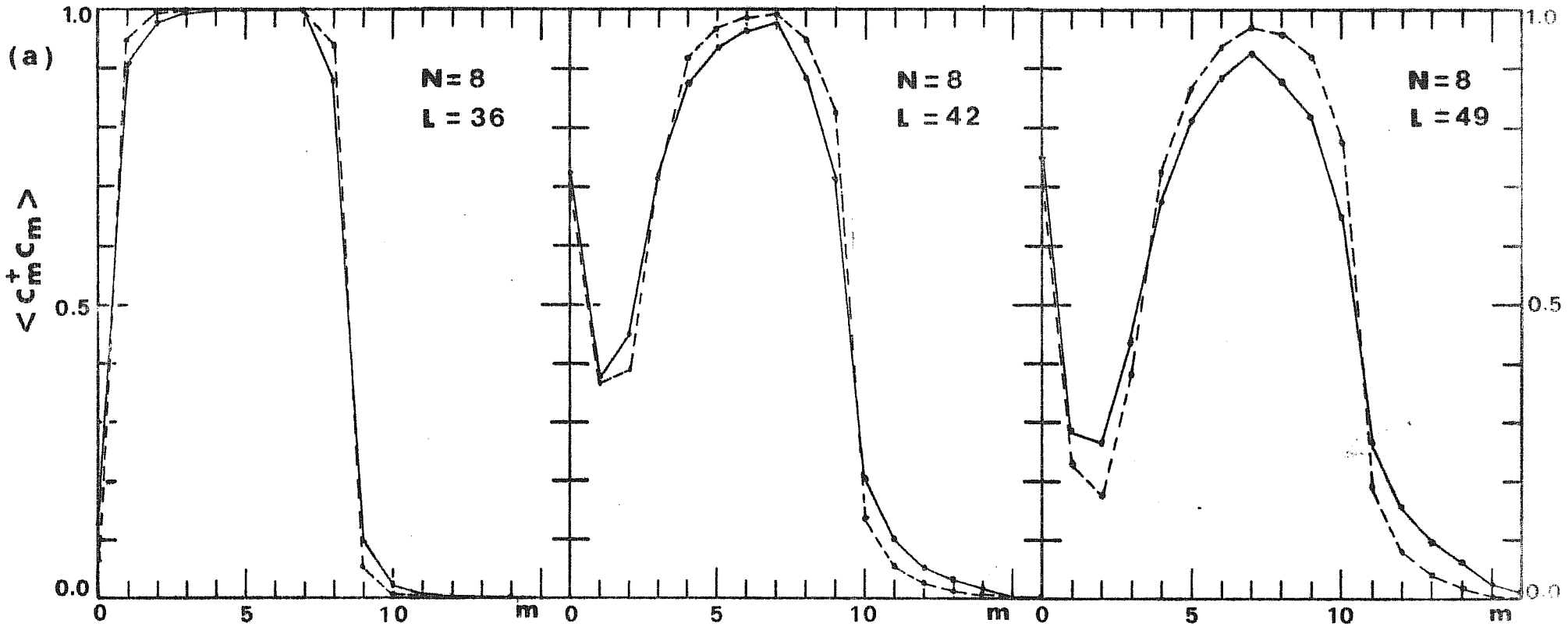

Fig 3.3

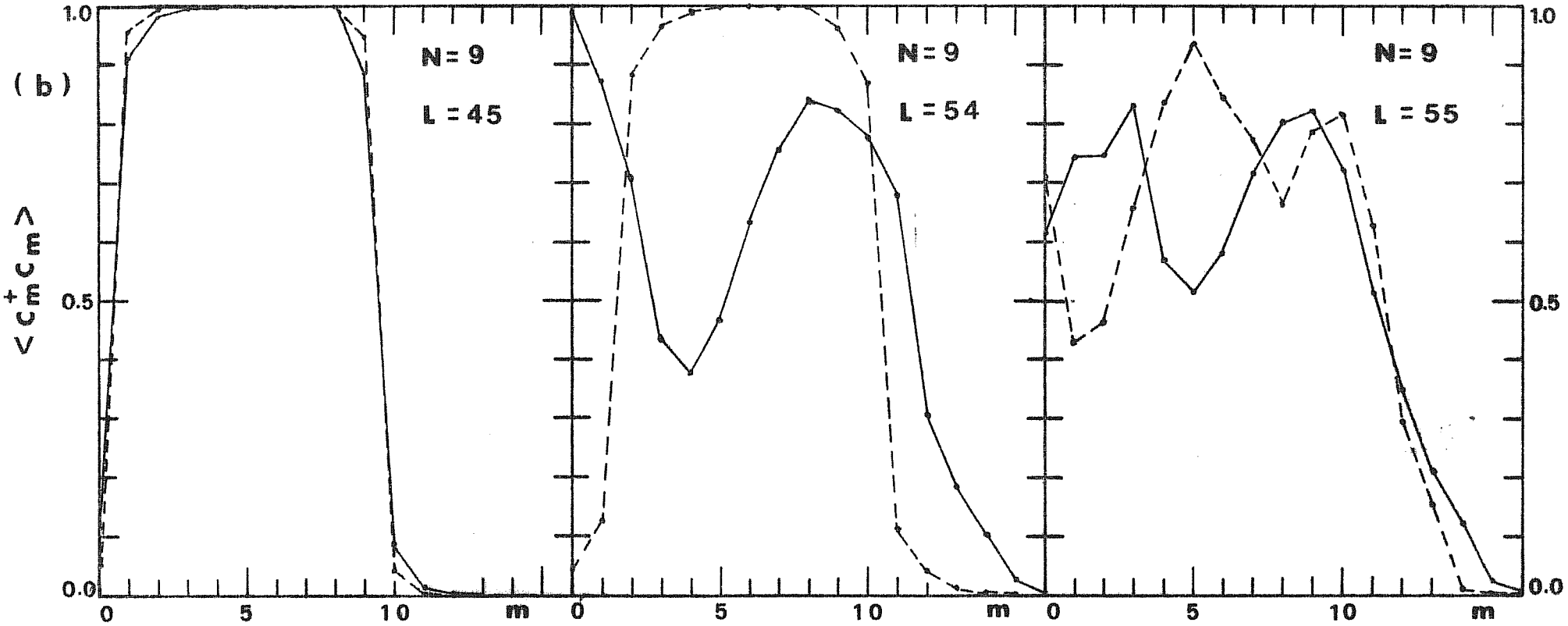
(b)
1.0
0.5
0.0
$\langle C_E C_E^+ \rangle_V$
N = 9
L = 45
N = 9
L = 54
N = 9
L = 55
0
5
10
m

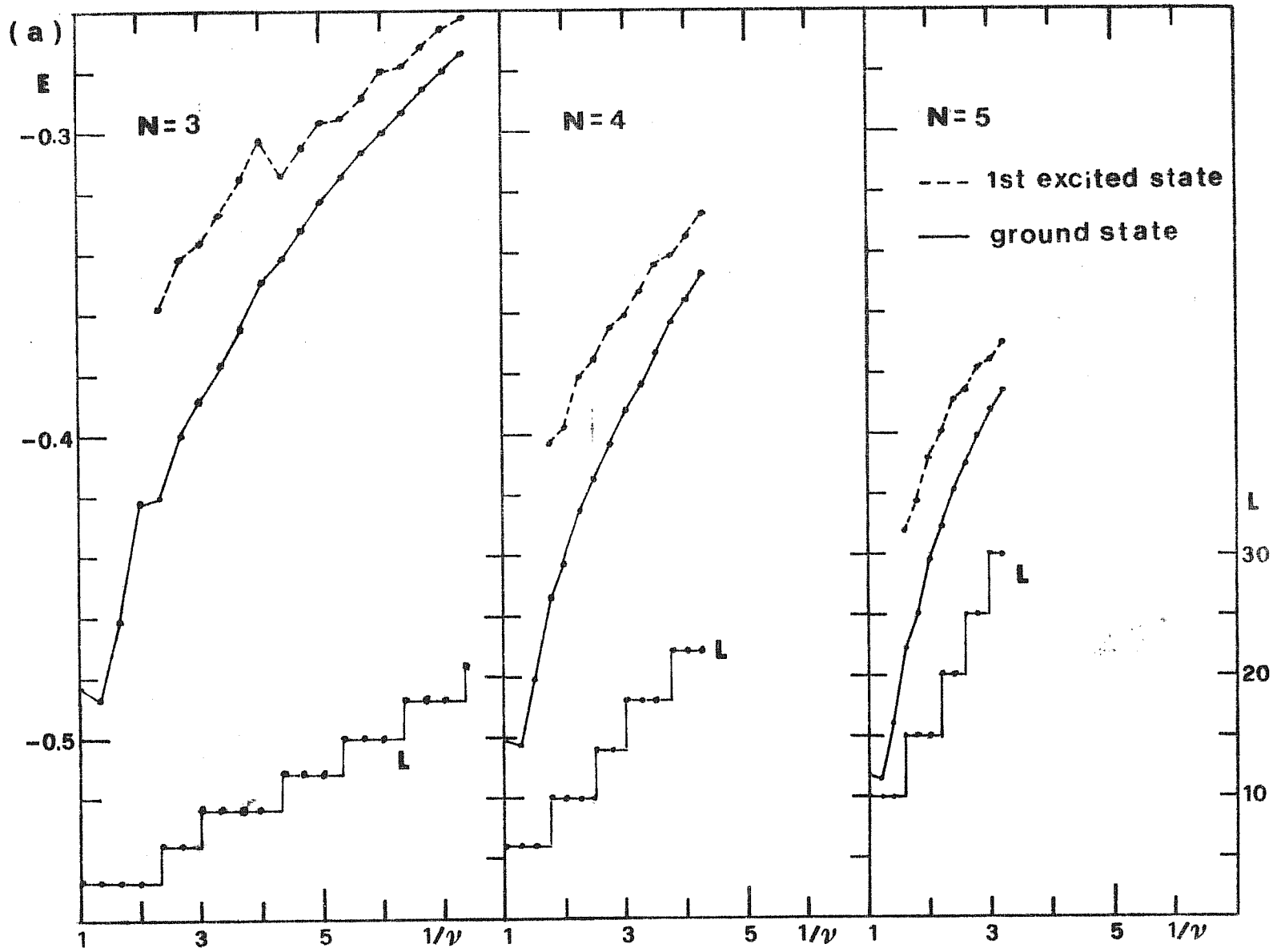
(a)
E
−0.3
−0.4
−0.5
N = 3
N = 4
N = 5
--- 1st excited state
—— ground state
L
L
L
L
30
20
10
1
3
5
1/ν
1
3
5
1/ν
1
3
5
1/ν

Fig 3.4.6

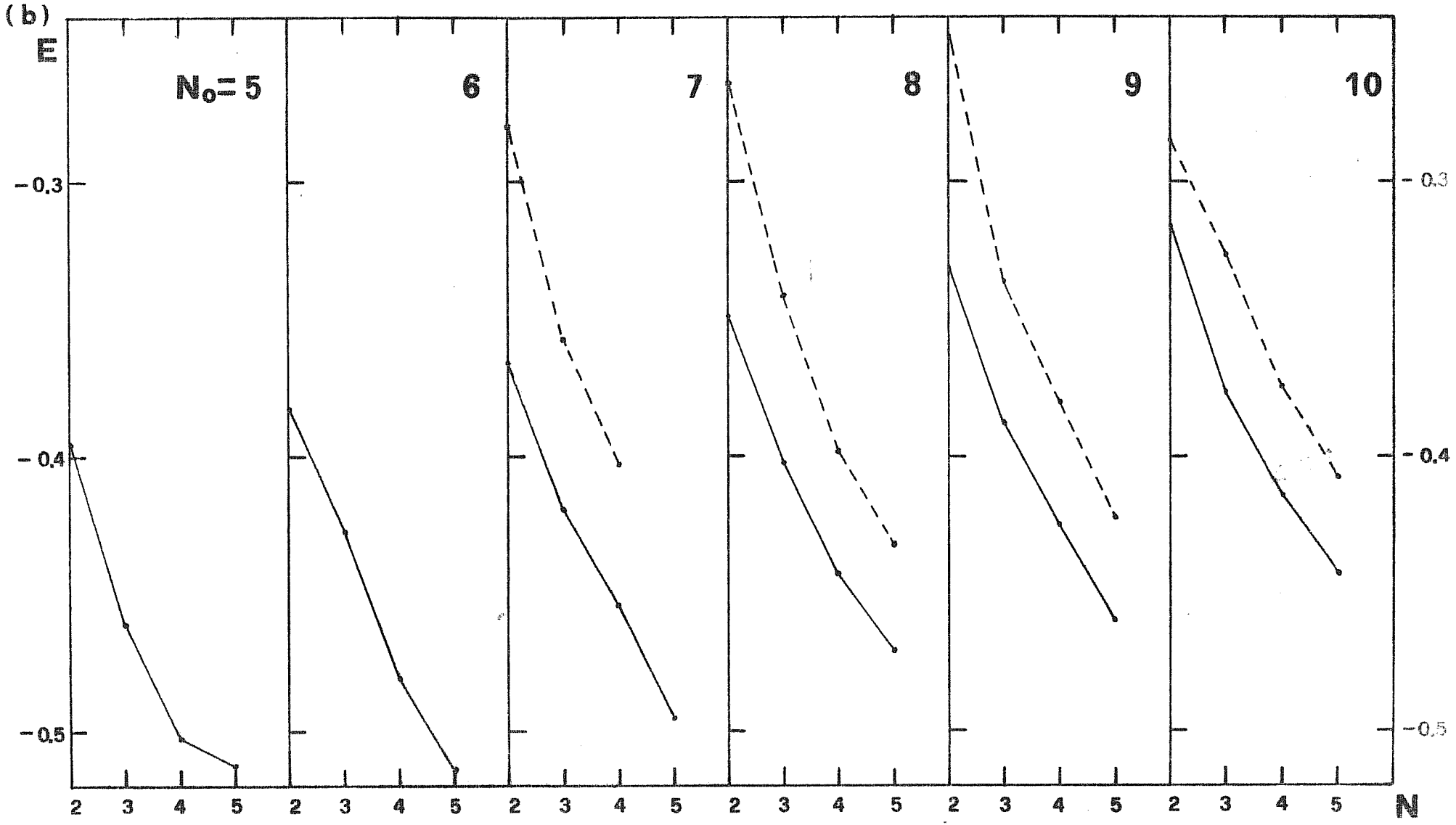

Fig 3.4 b)